Universitat Autònoma de Barcelona

Assessing spatio-temporal impacts of pine processionary moth defoliation on Mediterranean forest dynamics using UAV remote sensing

Kaori Otsu

ADVERTIMENT. L'accés als continguts d'aquesta tesi doctoral i la seva utilització ha de respectar els drets de la persona autora. Pot ser utilitzada per a consulta o estudi personal, així com en activitats o materials d'investigació i docència en els termes establerts a l'art. 32 del Text Refós de la Llei de Propietat Intel·lectual (RDL 1/1996). Per altres utilitzacions es requereix l'autorització prèvia i expressa de la persona autora. En qualsevol cas, en la utilització dels seus continguts caldrà indicar de forma clara el nom i cognoms de la persona autora i el títol de la tesi doctoral. No s'autoritza la seva reproducció o altres formes d'explotació efectuades amb finalitats de lucre ni la seva comunicació pública des d'un lloc aliè al servei TDX. Tampoc s'autoritza la presentació del seu contingut en una finestra o marc aliè a TDX (framing). Aquesta reserva de drets afecta tant als continguts de la tesi com als seus resums i índexs.

ADVERTENCIA. El acceso a los contenidos de esta tesis doctoral y su utilización debe respetar los derechos de la persona autora. Puede ser utilizada para consulta o estudio personal, así como en actividades o materiales de investigación y docencia en los términos establecidos en el art. 32 del Texto Refundido de la Ley de Propiedad Intelectual (RDL 1/1996). Para otros usos se requiere la autorización previa y expresa de la persona autora. En cualquier caso, en la utilización de sus contenidos se deberá indicar de forma clara el nombre y apellidos de la persona autora y el título de la tesis doctoral. No se autoriza su reproducción u otras formas de explotación efectuadas con fines lucrativos ni su comunicación pública desde un sitio ajeno al servicio TDR. Tampoco se autoriza la presentación de su contenido en una ventana o marco ajeno a TDR (framing). Esta reserva de derechos afecta tanto al contenido de la tesis como a sus resúmenes e índices.

WARNING. The access to the contents of this doctoral thesis and its use must respect the rights of the author. It can be used for reference or private study, as well as research and learning activities or materials in the terms established by the 32nd article of the Spanish Consolidated Copyright Act (RDL 1/1996). Express and previous authorization of the author is required for any other uses. In any case, when using its content, full name of the author and title of the thesis must be clearly indicated. Reproduction or other forms of for profit use or public communication from outside TDX service is not allowed. Presentation of its content in a window or frame external to TDX (framing) is not authorized either. These rights affect both the content of the thesis and its abstracts and indexes.

Assessing spatio-temporal impacts of pine processionary moth defoliation on Mediterranean forest dynamics using UAV remote sensing

Doctoral thesis submitted by

Kaori Otsu

for the degree of PhD in Terrestrial Ecology

Director:
Dr. Lluís Brotons Alabau
CSIC - CREAF

Tutor:
Dr. Javier Retana Alumbreros
Universitat Autònoma de Barcelona - CREAF

Centre de Recerca Ecològia i Aplicacions Forestals (CREAF)
Universitat Autònoma de Barcelona

February 2020

Acknowledgements

I feel very fortunate that I was given research opportunities funded for the projects INFORMED by FORESTERRA and Boscos i Salut by La Caixa. I thank my PhD academic committee (Prof. Joan Pino, Prof. Miquel Ninyerola and Dr. Arnald Marcer) for their annual review and guidance on my thesis work. I owe special thanks to my thesis supervisor Dr. Lluís Brotons for his significant contributions, insightful advices, and editorial time. He kindly referred me to various contact persons in Catalonia, Spain, and Europe to obtain the information and data necessary to complete my thesis.

I also appreciate co-author contributions and collaborations by Forest Science and Technology Centre of Catalonia (Ms Magda Pla, Dr. Alejandra Morán-Ordóñez, Dr. Andrea Duane, Mr. Jaume Balagué at CTFC), Centre for Ecological Research and Forestry Applications (Prof. Jordi Vayreda, Dr. Jose Roces-Díaz, Dr. Roberto Molowny, Dr. Víctor Granda, Ms Mireia Banqué, Ms Anabel Sanchez at CREAF), and Dr. Adrián Cardil from the University of Lleida, for providing technical support and requested data as well as consulting the data content and analysis regarding forest cover and disturbances. In addition, at the Cartographic and Geological Institute of Catalonia (ICGC), Ms Anna Tardà and Mr. Jordi Corbera kindly invited me to their workshop as a speaker to present one of my thesis projects.

Lastly, I am deeply grateful that all my family, friends, and colleagues who have encouraged me in many ways throughout my doctoral program. I include many thanks to the CREAF, director Prof. Joan Pino and the former director Prof. Javier Retana, coordinator Dr. Anna Avila, secretaries Ms Marta Barceló and Ms Magda Pujol, and administrators for assisting with my stay as an international student researcher for four years I have spent at the CREAF-UAB.

Abstract

Natural disturbances are driven by a range of biotic or abiotic factors that may occur independently or interactively from each factor. Such disturbances induce a series of changes in forest structure and composition, leading to interrupting forest succession and altering forest ecosystem dynamics. Consequently, the forest disturbances may continue to increase with the future trend of climate change scenarios and may affect global forest ecosystems. While pest outbreaks can be triggered by climate change in terms of altering their distributions and population dynamics, stressed trees due to climate change can become more susceptible to pests, which may accelerate reducing tree growth and forest production. Currently, crucial limitations to predict impact of natural disturbances on forest ecosystems are due to the complex interactions among trees, pests and climate. Especially, effects of climate change such as decreased precipitations and increased temperatures under drier and warmer conditions and extreme weather events on the Mediterranean forests have increased frequency and intensity of outbreaks, shifting and expanding the pest distribution to higher latitudes as well as altitudes. Since biotic disturbances driven by defoliators are known as major causes of forest decline in the Mediterranean region, my approach in this thesis focuses on evaluating defoliation damages for their visible detection.

With this research interest, my thesis starts with a systematic literature review on tree defoliation caused by insects worldwide at any spatial scale, assessing the past and present impact of defoliation on forest ecosystem dynamics during the period of 1996-2016. This review presents spatial and temporal distributions of defoliation by each pest-host tree relationship to evaluate change dynamics, associated detection methods, and observed quantitative indicators over time in relation to ecosystem services. Three case studies are then demonstrated on defoliations caused by *Thaumetopoea pityocampa* in Catalonia, Spain, in Mediterranean forests where I aim to quantify the levels of defoliation damage using vegetation indices (VIs) derived from remote sensing techniques, in particular UAV (unmanned aerial vehicle), for data calibration and validation purposes. In the first case study, UAV-derived RGB colour images are used as observed data for quantifying defoliation and are calibrated with Landsat-based VIs. The second study applies UAV-RGB imagery as referenced data to generate canopy height model (CHM) and automatically detect individual trees while the normalized difference vegetation index (NDVI) derived from UAV multispectral imagery is obtained to detect defoliation at the high-resolution pixel level. In the third study, four different NDVIs obtained from UAV multispectral imagery are tested in additional study areas to estimate the average threshold of detection on tree defoliation and discrimination of host species in various pine-oak mixed stands. Finally, all VIs used are further classified by thresholding and validated in each confusion matrix with referenced UAV-derived RGB

imagery.

Main findings in the thesis include that calibrating UAV-RGB data with the Landsat-based VIs may contribute to filling temporal data gaps for monitoring and detecting defoliations since satellite images are provided at a regular interval due to orbit scheduling. In addition, automated image processing techniques applied to UAV imagery, enabling to identify and delineate individual trees, may enhance the accuracy of defoliation estimations at tree and stand level. Further advancements with the use of UAV multispectral imagery include that some VIs are more suitable for predicting the health of trees, depending on whether the species is coniferous or deciduous. Moreover, the threshold values of detecting defoliation with those VIs are sought for establishing robust classification techniques, which may require increasing the number of sample study areas and should be tested on a large number of pine dominated stands in the Mediterranean region.

Overall, this thesis highlights that the latest modelling and remote sensing techniques, including UAV as an alternative 3D technology, are currently available to be combined with conventional ground surveys and statistical analyses according to the spatial and temporal scales and types of defoliation. The use of UAV images may also hold great potential as an alternative cost-effective method to other conventional ground-truth data for monitoring forest health. I conclude that optimal detection and monitoring methods are often specific to each pest agent associated with host tree species. Therefore, the advancement in prediction models linked to ecosystem services in pest and disease control would be promising for mitigating the future damage to our forests under climate change.

Chapter References

- Chapter 2
  Otsu, K. and L. Brotons. A review of the past and present impacts of insect defoliation on forest dynamics. In preparation to be submitted in Forests.

- Chapter 3
  Otsu, K., M. Pla, J. Vayreda, and L. Brotons 2018. Calibrating the severity of forest defoliation by pine processionary moth with landsat and UAV imagery. Sensors, 18(10):1-14. doi: 10.3390/s18103278.

- Chapter 4
  Cardil, A., K. Otsu, M. Pla, C. A. Silva, and L. Brotons 2019. Quantifying pine processionary moth defoliation in a pine-oak mixed forest using unmanned aerial systems and multispectral imagery. PLoS One, 14(3):1-19. doi: 10.5281/zenodo.2539199.

- Chapter 5
  Otsu, K., M. Pla, A. Duane, A. Cardil, and L. Brotons 2019. Estimating the Threshold of Detection on Tree Crown Defoliation Using Vegetation Indices from UAS Multispectral Imagery. Drones, 3(4). doi: 10.3390/drones3040080.

List of Figures

List of Tables

Contents

Chapter 1

General introduction

1.1 Forest disturbance drivers

Natural disturbances are driven by a range of biotic or abiotic factors that may occur independently or interactively from each factor. Such disturbances induce a series of changes in forest structure and composition, leading to interrupting forest succession and altering forest ecosystem dynamics (Flower and Gonzalez-Meler, 2015). Consequently, forest disturbances are predicted to increase with the future trend of climate change scenarios and may affect global forest ecosystems serving timber production and carbon sequestration (Boyd et al., 2013; Roques, 2015). As disturbance factors are categorized in Figure 1.1, biotic disturbances caused by insects, pathogens and wildlife browsing are generally specific to host tree species, therefore, their recovery patterns may be more difficult to model predictions than the abiotic ones such as fires, droughts, floods, windthrows and volcanoes (Flower and Gonzalez-Meler, 2015; Kautz et al., 2017).

While pest outbreaks can be triggered by climate change in terms of altering their distributions and population dynamics, stressed trees due to climate change or anthropogenic malpractice can become more susceptible to pests, which may consequently reduce tree growth and forest production (FAO, 2009; Ramsfield et al., 2016; Linnakoski et al., 2019). Effective means to mitigate increased pest damage have been explored since both climate change and forest management can affect the level of risks, with a combination of the frequency of pest, the vulnerability of the forest stand to pest, and the socio-economic impact on standing volume (Ramsfield et al., 2016). Since the importance of provisioning forest disturbance impacts combined with future climate change on ecosystems is increasing, it requires integrating their effects on the carbon cycle such as net ecosystem production (NEP) in ecosystem services (Flower and Gonzalez-Meler, 2015).

Currently, crucial limitations to predict impact of natural disturbances on forest ecosystems are due to the complex interactions among trees, pests and climate (Linnakoski et al., 2019) as shown in Figure 1.2. A monitoring study on these interactions (Whipple et al., 2019) revealed that chronically stressed and pest-susceptible trees have better adapted to poor environments, therefore, healthy trees resulted to be more sensitive to extreme events such as drought and outbreak with a higher mortality (Linnakoski et al., 2019). Hentschel et al. (2018) also analyzed relationships between past outbreaks caused by three different defoliators and other disturbance drivers, depending on the surrounding landuse type adjacent to the tree stand,

climate parameters, or a combination of climate and stand structure parameters (Linnakoski et al., 2019).

Thus, scientific communities and societies are more interested than ever before in predicting the effects of global change on ecosystems to maintain forest as well as human health (Morán-Ordóñez et al., 2018). In particular, effects of climate change such as decreased precipitations and increased temperatures under drier and warmer conditions and extreme weather events on the Mediterranean forests (FAO, 2018) have been observed as changes in tree growth and phenology, vegetation pattern and distribution, wildfires, and pest outbreaks. Warmer winter temperatures have increased frequency and intensity of outbreaks, shifting and expanding the pest distribution to higher latitudes as well as altitudes. In general, the scientific communities agreed that climate change would favor forest pest species in that the survival of many insects depends on low temperature limits while pathogens benefit from dry conditions (Jactel et al., 2012; FAO, 2018). Moreover, how this general pattern will apply to specific cases is uncertain, which makes the predictions more difficult.

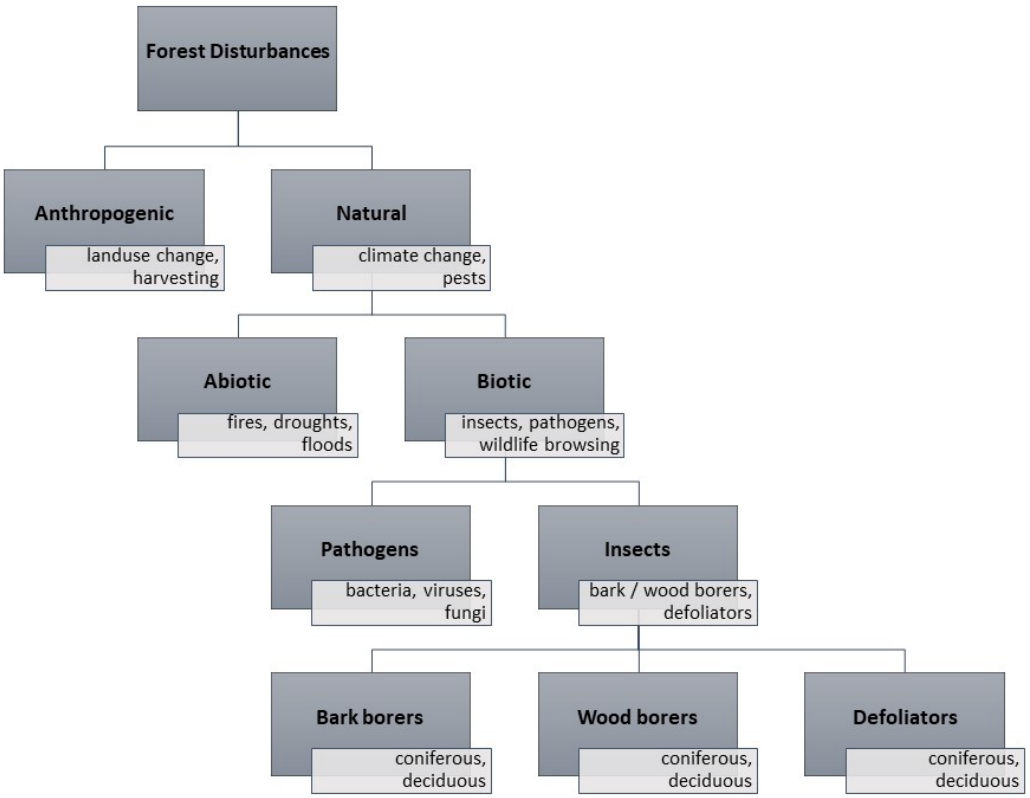

Figure 1.1: Breakdown of forest disturbance drivers by causal factor.

1.2 Biotic disturbances under climate change

Kautz et al. (2017) reviewed past published studies and concluded that annual percentages of forest areas affected by biotic disturbances vary spatially and temporally and are significantly higher than those caused by abiotic disturbances. Biotic dis-

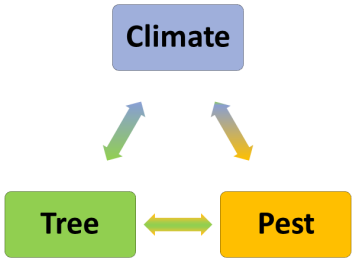

Figure 1.2: Interactions and associations among tree, pest and climate.

turbances can cause both ecological and economic impacts including tree damage such as growth reduction or even tree mortality, degraded timber quality, alteration on biodiversity, and loss of ecosystem services (flood mitigation, water purification, recreational and cultural values) (Ramsfield et al., 2016; Haines-Young and Potschin, 2018).

Among biotic disturbance drivers, insects and pathogens are considered to be more susceptible to climate change than browsing wildlife animals, due to their dependency on their host trees' resilience (Tiberi et al., 2016). Insect and pathogen drivers can impact species composition, structure, and function in forest ecosystems, which may even affect their resilience to extreme events and outbreaks (Flower and Gonzalez-Meler, 2015). According to the global review of forest pests and diseases reported by FAO (2009), the majority of the pests worldwide, accounting for 77%, were insects followed by pathogens (16%). In general, it is easier to trap insects and visually detect the damage bored or defoliated by them than other pest types in such that the pathogenic impact on tree growth can be subtle or delayed.

1.2.1 Insect type

In the Mediterranean region, defoliators can be harmful to tree growth and mortality while boring insects can cause serious damage more rapidly (Paine and Lieutier, 2016). On the contrary, phloem-feeding insects are not usually considered harmful to trees for their survival, yet, damage is rather aesthetically significant for the chlorosis, leaf deformity, and twig distortion (Paine and Lieutier, 2016). The optimal host habitat and the time of the year for detection as well as damage type are specific to each pest species (Hall et al., 2016). The following sections differentiate three most harmful insect types focusing on the Mediterranean region.

Bark borers

Insects as small as less than one centimeter in length feed on the cambium, making the first impact toward wood decomposition (Flower and Gonzalez-Meler, 2015). After bark borers infest the host trees by a sudden and massive attack, the infested canopy may start to turn yellow within a few weeks, continue to reddish and fall completely (Paine and Lieutier, 2016).

Their attacks on the cambium for reproduction are dependent on the physiological tree conditions, following the molecules released by stressed trees to select the suitable host tree. For this reason, they are known as secondary pests for attacking weakened trees by pioneer pests while they can even attack healthy trees during epidemic outbreaks (Paine and Lieutier, 2016). While some species can feed on both coniferous and deciduous trees, the majority of bark colonization occur on conifers where larger size species tend to infest the lower part of large trees with thick bark and smaller size species on the contrary colonize in the upper part of young trees with thin bark (Paine and Lieutier, 2016).

Bark beetles have been mostly studied in temperate forests (Senf et al., 2017), which can result in degraded timber quality and eventually tree mortality within a few years (Wulder et al., 2006; Meigs et al., 2011). As bark beetles are particularly susceptible to temperature changes, the population dynamics have been already affected on the background of the climate change. Moreover, with simulations of future climate scenarios the Mediterranean region is predicted more vulnerable to global change than temperate and boreal regions (Paine and Lieutier, 2016).

Wood borers

Insects in larval or adult forms that consume wood are known as one of the most important threats to both coniferous and deciduous forests worldwide, causing serious ecological and economic consequences and leading to the longest recovery time (Brockerhoff et al., 2006; Flower and Gonzalez-Meler, 2015; Paine and Lieutier, 2016).

While some species can be primary pests infesting healthy trees, other species bore galleries into the wood of weakened trees, causing tree death, which can be the secondary driver damaging those trees stressed by abiotic factors and/or defoliators (Tiberi et al., 2016). These secondary species may take advantage of greater quantities of stressed trees, suitable for colonization, allowing further extended network of galleries and an accumulation of dead wood on decaying trees (Paine and Lieutier, 2016).

Outbreaks of wood-boring insects, especially beetles, following the fires may also further negatively affect such stressed stands (Tiberi et al., 2016). Thus, increased wildfire frequency due to drought and global warming may negatively affect post-fire survival of trees (FAO, 2018).

Defoliators

Defoliators are defined as larval or adult forms that consume leaf or needle material (Flower and Gonzalez-Meler, 2015). Defoliation can cause severe damage often associated with outbreaks of insect populations over subsequent years, leading to intensive and extensive defoliation and even tree mortality (Paine and Lieutier, 2016; Tiberi et al., 2016). Completely defoliated trees decrease the following growth without photosynthesis, in consequence, the stressed trees start to reduce the vigor (Paine and Lieutier, 2016; Tiberi et al., 2016), which may be even more susceptible to any other disturbance factors (FAO, 2018). Some pest insects prefer to feed on young leaves (needles) while others can defoliate all age classes (Hall et al., 2016). Regardless of the defoliation patterns, cumulative defoliation over subsequent years may lead to tree mortality.

Deciduous defoliators have been mostly studied in temperate forests while coniferous defoliators were more commonly observed in boreal forests (Senf et al., 2017). In the Mediterranean region, while the foliage loss may be detected within one year with most deciduous defoliators on oaks, the process of coniferous defoliation on pines is usually gradual over a long period of time, which may take several years to be measured (Vogelmann et al., 2009; Paine and Lieutier, 2016). Recent increased winter temperatures have been favorable for overwintering larvae to feed and therefore increasing their survival (Battisti et al., 2005).

1.2.2 Host type

Coniferous vs. deciduous

On a global scale the majority of pests were observed on deciduous (broadleaf) tree species (62%) while the pests on conifer species account for 30%. Variability in forest responses to biotic disturbance is likely a function of host type (coniferous or deciduous) as well as insect type (Flower and Gonzalez-Meler, 2015).

In the Mediterranean region, dominant native conifers are pines while common deciduous species include oaks, which can be evergreen and deciduous, poplars and willows (Paine and Lieutier, 2016). Depending on the Mediterranean tree species, adaptation to drought which is typical abiotic disturbance in this region can vary due to differences in morphology and phenology according to host species (Tiberi et al., 2016). Thus, mixed Mediterranean forests (e.g. pine-oak stands) may benefit from this species diversity that contributes to a stand-level efficient use of scarce water resource allocated by the ecosystem.

Planted vs. natural

The trend in forest type was reported (FAO, 2009) that pests were more dominantly recorded in planted forests with single tree species than natural forests where the species composition and stand structure are diverse. While there has been a numerous studies on forest health assessment and monitoring of natural (unmanaged) stands, much fewer studies have focused specifically on plantations. Planted forests are typically single-species stands such as *Pinus* spp. and *Eucalyptus* spp., which are poorer in species diversity and stand structure, and consequently more susceptible to pest attacks despite the importance of containing economic resources and providing various ecosystem services (Wingfield et al., 2015). In forest management, it is important that the selected tree species is adapted to the site conditions (Ramsfield et al., 2016). Moreover, silviculture systems such as single-tree or group selection would play an important role to increase stand structural diversity, leading to recover the tree vigour and thus resistance to pests, which would also reduce the risk of affecting the timber value (Ramsfield et al., 2016).

Nevertheless, if not natural forests, increased species and genetic diversity at a landscape level is one of the most effective and efficient methods to maintain healthy plantations under climate change (Jactel and Brockerhoff, 2007; Miller and Thode, 2007; O'Neill et al., 2008). Promoting the right tree species composition in mixed plantations (e.g. fast-growing deciduous species associated with host pines against the pine processionary moth) would provide an opportunity to increase stand resistance and reduce vulnerability to forest pests since most of them are species specific

and their damage potentials are dependent on the species composition (Wingfield et al., 2015; Damien et al., 2016).

Exotic vs. native

Both exotic and native forest stands in the Mediterranean region are subject to the threats of climate change and anthropogenic activities as well as the introduction of exotic pests (Paine and Lieutier, 2016). While native tree species can be vulnerable to introduced pests, exotic trees in plantations can be successful when they are separated from their natural enemies (Wingfield et al., 2015). On the other hand, when those trees can coevolve with introduced or native pests to which they are not resistant, damage can be severe. The longer exotic trees are planted in an area, the more threatened they become by native pests (Wingfield et al., 2015).

Pest problems are often specific to the Mediterranean forests rather than in common with other forest regions. While the forests are subject to both native and introduced insects, they are also at risk from intensive plantation forestry using exotic timber species from outside of its native range, in addition to native pines and oaks (Paine and Lieutier, 2016). In particular, plantations of introduced pine and eucalyptus have been established for the production of wood fiber and structural timber (Paine and Lieutier, 2016). These newly established stands are highly susceptible to pests and may trigger insect outbreaks over large areas, remaining a challenging issue to forest management (Jactel et al., 2012).

1.2.3 Monitoring and detection

Conventional data

In most of the regions worldwide, monitoring and detection methods are informal, involving field surveys by forest practitioners, which are often targeted to specific pests. Conventional forest health surveys include aerial mapping, ground measurements and sampling, and pheromone traps while additional surveys are conducted in commercially valuable planted forests than in natural forests (FAO, 2009). As much as conventional data on forest health are qualitative in nature, quantitative data are limited, varied in format and difficult to access online in many regions. Since data are often collected after visual symptoms have been observed and significant damage has been caused, time-series data for monitoring on the impacts of forest pests are not available for most regions (FAO, 2009).

As the need for monitoring forest pests is increasing, agreement on quantitative parameters to standardize data, in particular, common definitions on how the data are to be collected (FAO, 2009). Conducting worldwide surveys to better understand forest ecosystems on a global scale remains challenging when new pests are still unknown or undetected in numerous developing countries (Wingfield et al., 2015). Those pest problems are typically managed at small scales to deal with local damage, of which information should be shared and funded for collaborations through global networks of forest scientists such as European Union, International Union of Forest Research Organizations, and United Nations (Wingfield et al., 2015). Moreover, such local information should be linked to a compatible central database system and integrated internationally.

Remote sensing data

Due to limitations such as lack of reliable and timely data, and inconsistency in temporal trends across regions, it was suggested that future forest monitoring should improve by providing accessible, precise and consistent data harmonized across regions (Kautz et al., 2017). With the use of worldwide satellite images at a medium spatial resolution (e.g. Landsat, MODIS, Sentinel) which are available to the public, remote sensing of insect disturbances has gained so much attention for its ability to monitor spatial and temporal distributions and dynamics. Such remote sensing technologies should be integrated into operational forest management to improve quantifying spatial and temporal disturbances included in regional and global ecosystem models (Hall et al., 2016; Senf et al., 2017). While pest prevention approaches are currently only effective in some developed wealthy countries with advanced technologies, they are not available elsewhere, yet affecting global impacts on the long-term forest sustainability worldwide (Wingfield et al., 2015). Therefore, continuous improvements in monitoring and prevention techniques should be made on forest health issues by a variety of international working groups, research organizations and networks, which are currently initiated by the National Aeronautics and Space Administration (NASA) and European Space Agency (ESA).

Remote sensing information regarding the areal extent, location, and severity of insect damage is also effective for a range of forest pest management planning and modelling purposes (Hall et al., 2016), with the aim to quantify and understand their consequences on the wide range of ecosystem services that forests provide (Hicke et al., 2012; Boyd et al., 2013). Widely used forest monitoring models include TIMESAT with MODIS images and LandTrendr with Landsat, at different spatial resolutions, for effectively monitoring phenological trends and detecting disturbance and recovery processes with time-series analysis.

UAV data

Most recently, one of remote sensing technologies, UAV (Unmanned Aerial Vehicle) in particular, has advanced as a low-cost time-efficient tool to acquire both hyperspectral and multispectral data that are effective for detecting specific vegetation properties in small-scale forestry applications (Adão et al., 2017; Torresan et al., 2017; Barbedo, 2019). This latest remote sensing technology is capable of capturing 3D imagery at a high spatial resolution in centimeter using airborne sensors to detect individual tree crowns as well as flying much closer to the ground surface than spaceborne satellites, without significantly being influenced by cloud effects (Näsi et al., 2015; Dash et al., 2017; Cardil et al., 2019). In addition to such advanced spatial resolution, temporal resolution may be improved with more flexible scheduling for UAV flights under clear weather conditions than fixed satellite orbit scheduling (Näsi et al., 2015; Dash et al., 2017; Torresan et al., 2017). Moreover, it is suitable for quantifying acquired data in image processing and analysis such as target detection, classification, and vegetation indices (VIs), which may further enable to assess the impacts of various disturbances on forest health (Adão et al., 2017; Barbedo, 2019).

In the Mediterranean region, forests are continuous in nature across administrative boundaries of European or North African countries. At European Union level (Torresan et al., 2017), research activities using UAV are increasing in forestry appli-

cations, however, current regulations for forest monitoring purposes fall under each member state and thus lack common rules for cross-boundary operations within Europe, except large UAV operations used by the military and defense forces. While small-scale forest monitoring activities increase within the Mediterranean region and Europe, it would require harmonizing such regulations at a common framework to promote mobility and exchange opportunities for regular monitoring operations across different countries (Torresan et al., 2017).

1.3 Thesis objectives

Biotic disturbances driven by defoliators are major causes of forest decline in the Mediterranean region; furthermore, climate change suggests increasing impact in the future (FAO, 2018; Muller et al., 2018). Thus, I decided to focus on evaluating defoliation damages for their visible detection. In this thesis I started with an overview of all the past published studies on pest defoliation throughout the world, identifying spatial and temporal distribution of defoliations by each pest-host tree relationship to evaluate change dynamics, associated detection methods and observed quantitative indicators over time in relation to ecosystem services. Then three case studies are demonstrated on defoliations caused by the pine processionary moth (*Thaumetopoea pityocampa*) in Catalonia, Spain, in Mediterranean forests where I have involved in quantifying the levels of defoliation damage with various remote sensing techniques, in particular UAV (unmanned aerial vehicle), to be further incorporated into forecasting models and ecosystem services. According to the review in **Chapter 2** that addressed the issue of existing data gaps, the main objective of the thesis is to conduct analyses on forest defoliation using the detection methods specific to pest-host tree relationships between *T. pityocampa* and *Pinus* spp. (**Chapters 3, 4 and 5**). The specific objectives are as follows:

- To assess the past and present impact of insect defoliation worldwide on forest ecosystem dynamics as a state-of-the-art review (**Chapter 2**).
- To calibrate the severity of forest defoliation due to *T. pityocampa* in Mediterranean pine-dominated stands observed by UAV imagery with Landsat-based VIs (**Chapter 3**).
- To automatically detect individual trees and quantify defoliation on host tree species in a pine-oak mixed stand using Normalized Difference Vegetation Index (NDVI) derived from UAV multispectral imagery (**Chapter 4**).
- To estimate the average threshold of detection on tree defoliation and discrimination of host species in various pine-oak mixed stands using different UAV-derived NDVIs (**Chapter 5**).

Chapter 2

I focused on damage caused by defoliators for their visible detection and visual impact on the forest health as well as aesthetic. While systematically reviewing studies published over the past two decades associated with the world's forest defoliations without limiting to geographical regions or types of detection methods, I

mainly considered quantifying the levels of defoliation damage to be incorporated into forecasting models and ecosystem services. I also aimed to identify spatial and temporal distributions of defoliation by each pest-host tree relationship to evaluate change dynamics, associated detection methods and observed quantitative indicators over time in relation to ecosystem services.

Chapter 3

For quantifying forest response to infestation by defoliators in Mediterranean pine-dominated stands, I used Landsat-derived VIs to predict the defoliation levels. In this study, I aimed to evaluate the spatiotemporal degree of defoliation during a recent outbreak of *T. pityocampa* in Catalonia, by change detection analysis using a combination of satellite (multispectral) and UAV (RGB) imagery. I mainly examined regression models between VIs derived from medium-resolution Landsat imagery and defoliation degrees interpreted by high-resolution UAV imagery for data calibration so that defoliation classes based on the best-fit VI model can be mapped to assess classification accuracy.

Chapter 4

I aimed at applying UAV multispectral imagery to calculate NDVI and quantitatively assess defoliation due to *T. pityocampa* on a pine-oak mixed stand in Catalonia and potentially identify host tree species. The UAV-derived RGB imagery was also used to generate digital surface model (DSM) and canopy height model (CHM) for delineating individual trees. The multispectral imagery was further analyzed to develop a method of unsupervised classification by thresholding to objectively quantify defoliation and distinguish tree species for automatically detected individual trees.

Chapter 5

In addition to the study area analyzed in Chapter 4, I analyzed three additional areas in seeking to develop a simple and robust method applicable to similar pine-oak mixed stands, for forest practitioners to obtain timely information and monitor forest defoliation at the operational level. Specifically, I explored simple histogram thresholding classification tools to detect defoliation of host pine trees affected by *T. pityocampa* using UAV multispectral imagery. I further attempted to estimate the threshold values of different NDVIs averaged over four study areas, for detecting defoliation and distinguishing pine species at the pixel level to examine the robustness at a larger scale.

Chapter 2

Background: A review of the past and present impacts of insect defoliation on forest dynamics

Abstract
Currently, pest insects are one of the major driver to cause disturbances threatening the world's forests in a combination with abiotic factors. In a systematic review of literature on detecting pest disturbances, we identified specific methods for quantifying the defoliation degrees derived by insects. Recent improvements in detection and monitoring methods over the past 20 years and potential future improvements were discussed. Following the systematic literature review by keyword search (Web of Science), selected study cases associated with forest defoliation were sorted into the database to summarize the parameters such as pest drivers, tree effects, defoliation scales, detection methods, and ecosystem service types studied in each case. We used articles published during the period of 1996-2016 in various countries and regions in the world's forests. A summary of the time-series studies assessing quantitative impacts of forest defoliation was presented in both temporal and spatial scales. It is noted that the effort on improving methods for pest detection and monitoring has been significantly increased over the past decade. Depending on the spatial and temporal scales and types of defoliation in concern, the latest modelling and remote sensing techniques, including an emerging UAV (unmanned aerial vehicle) technology, are currently available to be combined with conventional ground surveys and statistical analyses. As we conclude that optimal methods recommended are specific to each pest agent associated with host tree species, the advancement in pest detection and monitoring methods is promising for mitigating the future damage to forests with high ecological, social and economic values. Thus, predictive models based on those monitoring methods may be linked to ecosystem services as pest and disease control with the future trend of climate change scenarios.

2.1 Introduction

Currently, pest insects are the principal biotic drivers for disturbances threatening the world's forests (Muller et al., 2018) in addition to abiotic factors such as droughts, fires, floods and climate change (Rullan-Silva et al., 2013; Sangüesa-Barreda et al., 2014). Some of the major pest insects have been considered by the Intergovernmen-

tal Panel on Climate Change (IPCC) as indicator of global warming (Rosenzweig et al., 2007) for being recorded in the expanded biogeographical range of host distribution, mainly in Europe and North America, towards northern latitudes and higher elevations over the past twenty years (Battisti et al., 2005; Roques, 2015). Consequently, the disturbances derived from those insects may continue to increase with the future trend of climate change scenarios and may affect global forest ecosystems serving timber production and carbon sequestration (Boyd et al., 2013; Roques, 2015).

Most recently, several reviews have summarized the studies measuring and monitoring forest damages due to various biotic and abiotic disturbance drivers. Morán-Ordóñez et al. (2018) focused on the studies within the Mediterranean basin, assessing the modelling approaches used to predict the trends of biodiversity and ecosystem services under the future scenarios of global change, including the associated biotic and abiotic disturbance drivers and indicators of change. They found that in general scenario forecasting makes relatively little use of modelling approaches based on ecological processes. Kautz et al. (2017) expanded the spatial extent of their review to Northern Hemisphere forests, evaluating annual percentages of forest areas affected according to data sets of large-scale, multi-year biotic disturbances, without detailing the detection methods. The main findings showed that the percentages affected by biotic disturbances vary spatially and temporally and are significantly higher than those caused by abiotic disturbances such as fire. Due to limitations such as absence of reliable and timely data, inconsistency in temporal trends across regions and inherent uncertainties, it was suggested that future forest monitoring should improve by providing accessible, precise and consistent data harmonized across regions.

As impacts of the climate change on forests have been concerned in recent years, the increasing number of infestation problems caused by insects have been reported. Therefore, this combination of biotic and abiotic factors causing forest infestations is more complex than ever before for modelling spatiotemporal forest dynamics. While being a source of aesthetic problems in cultural values, forest infestations are most commonly ecological and economic problems leading to tree growth reduction or mortality caused by various feeding behaviors such as leaf chewing, sap sucking, stem boring, and root pruning (Kautz et al., 2017). Due to defoliators, in particular, trees lose the capability of continuing photosynthesis, leading to nutrient deficiencies and a stress factor to the leaf water content in the following years if host trees are attacked repeatedly or intensively (Cooke et al., 2007).

With the aim to quantify infestations and understand their consequences on the wide range of ecosystem services that forests provide, information regarding the areal extent, location, and severity of insect damage is required for forest pest management planning and modelling purposes (Hicke et al., 2012; Boyd et al., 2013; Hall et al., 2016). Senf et al. (2017) reviewed worldwide studies without limiting geographic extents, but with a focus on forest insect disturbances detected by the use of remote sensing. By comparing sensors and methods used for mapping disturbances by insect types (pest as borers vs. defoliators, host as coniferous vs. deciduous), they found significant differences among the methods used across insect types. In their conclusions, remote sensing of insect disturbances has gained so much attention for its ability to monitor spatial and temporal distributions and dynamics that it should be integrated into operational forest management and that the improvement

in quantifying spatial and temporal disturbances should be included into regional and global ecosystem models. Hall et al. (2016) also reviewed studies associated with insect disturbances monitored by remote sensing, highlighting Canadian case studies in more details. They compared the monitoring methods, involving field and aerial surveys combined with sensors by incorporating change detection techniques, in relation to major pest species and the damage. While relatively cost-effective aerial surveys may not be consistent or sufficient for detailed monitoring continuous vast forests at a national scale, remote sensing may provide greater extent and increased precision, even at a lower cost as sensor developments advance. They emphasized the importance of resolving data gaps with the development of integrated monitoring systems that combine aerial survey and remote sensing for mapping and monitoring.

The focus of above reviews was narrowed down to certain regions or detection techniques while the type of forest disturbances was amplified. To fill the information gap among above reviews on forest disturbances, differentiated by geographical extent, disturbance type and detection method, we systematically reviewed on studies over the past two decades associated with the world's forest defoliations without limiting to regions or types of detection method. In addition to that biotic disturbances driven by defoliators are major causes of forest decline in many regions, climate change suggests increasing impact in the future (Muller et al., 2018). Thus, we decided to focus on defoliation damages for their visible detection and visual impact on the forest aesthetic and health. Mainly we considered quantifying the levels of defoliation damage to be incorporated into forecasting models and ecosystem services. We also aimed to identify spatial and temporal distribution of defoliations by each pest-host tree relationship to evaluate change dynamics, associated detection methods, and observed quantitative indicators over time in relation to ecosystem services.

2.2 Materials and methods

2.2.1 Selection of case studies

Our systematic literature review selected articles published in English during the period of 1996-2016 in various countries and regions throughout the world. Specifically, we searched articles using the topic search (TS) by Web of Science: TS = (defoliation* AND (pest* OR insect*) AND (forest* OR tree*) AND (manage* OR monitor* OR detect*)). Based on this search the total of 490 articles were initially included. Furthermore, filtering by the title and abstract excluded irrelevant articles such as experimental and DNA studies, biological controls, plantations of exotic species, orchards, and generic studies (not specific to pest or host species), and reduced the final number to 160 articles with 183 studies in total. The criteria selected in those articles are as follows:

- Forest defoliation affected by insects must be natural disturbance. No manipulation or experiment (artificially caused defoliation);
- Spatial and temporal scales must be defined;
- Pest driver and host tree must be defined;
- Damage must be evaluated quantitatively;

- There must be some methods or models for detecting and/or monitoring defoliations;
- Whether the model can predict future scenarios and/or provide ecosystem services.

Following to extracting necessary information from above case studies, we summarized the parameters in the database, such as pest drivers, tree effects, damage scales, detection methods, and ecosystem service types studied in each case. The description of each parameter is shown in Table 2.1.

Table 2.1: A summary of parameters extracted into the database from articles associated with forest defoliation.

Parameter	Data type	Description
ID	Numeric	selection indexed by keyword search on the Web of Science database
Published year	Numeric	the year of publication in journals and books
Title	Character	the article title
Study area	Character	the name and location of study area
Spatial scale	Discrete	local/subnational/national/regional/global
Temporal scale	Numeric	specific year(s) or a period of consecutive years
Method/model	Character	damage assessment methods and models including aerial and field surveys, sampling, measurements, statistical analysis, GIS, remote sensing, algorithms, simulations
Pest driver	Character	scientific name of pest insect
Host tree	Character	scientific name of host tree
Stand group	Discrete	coniferous (C), deciduous (D), mixed (M)
Indicator	Character	damage indicator assessed quantitatively
Prediction	Discrete	yes/no whether method/model is capable of predicting future conditions
Ecosystem Service (ES)	Discrete	yes/no whether method/model is associated with Ecosystem Services
ES category	Discrete	if applicable, category of Ecosystem Services defined by Common International Classification of Ecosystem Services (CICES) V5.1 (Haines-Young and Potschin, 2018)

2.3 Results

2.3.1 Geographical distribution and spatial scale

The geographic locations of case studies are mostly concentrated in North America with 87 studies (Figure 2.1), counting for 47 percent of the total studies, where substantial studies were conducted across the national border between Canada and

United States as vast forests are often continuous rather than fragmented by administrative boundaries. The central Europe including Mediterranean areas resulted in 39 studies (21%), followed by Scandinavia and Russia with 38 studies (21%). In Europe, the trend of outbreaks across countries was found especially in Fennoscandia (Finland, Norway and Sweden) and Alps regions where the majority of forests are concentrated. The rest of studies were mainly found in Iran, China and Japan from Asia and in Chile from South America.

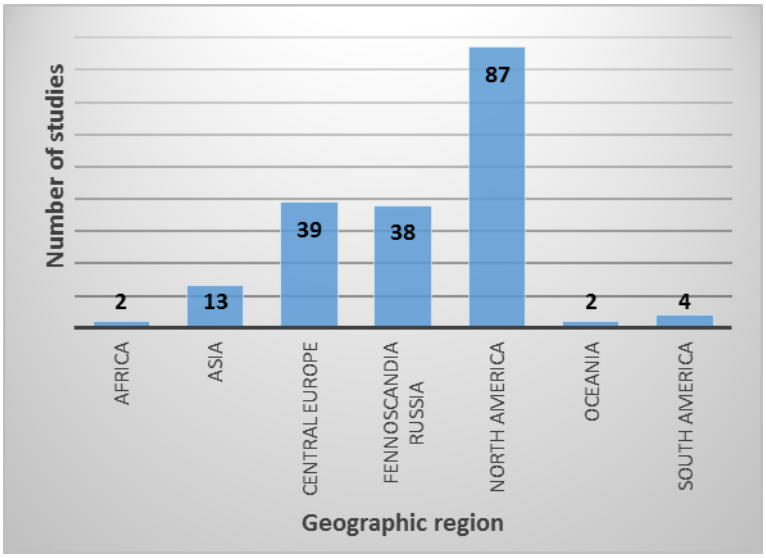

Figure 2.1: The number of studies on forest defoliation categorized by geographic distribution.

2.3.2 Spatial and temporal scales

Spatial scale is the key parameter to success in damage detection, which depends on the spatial resolution required for the nature of the defoliation and the indicator in question (Hall et al., 2016).

At the tree level, submetric imagery, which is less than 1 m spatial resolution, enables to assess individual trees and their health conditions (Hall et al., 2016). Metric imagery at 1-9 m spatial resolution is suitable for mapping dispersed stands that have been damaged by endemic or incipient infestations (Hall et al., 2016). In addition, there are some advantages of applying appropriate silviculture practices to stand management against forest pests (Ramsfield et al., 2016). For larger epidemic infestations at the landscape level, decametric imagery up to 100 m spatial resolution is appropriate for damage mapping (Hall et al., 2016). The landscape scale can be as small as local (135 studies), extending to larger landscapes defined by administrative boundaries on subnational (28 studies), national (12 studies), regional (7 studies) mainly in Europe and North America, and global (1) scales, as summarized in Figure 2.2. On a global scale, Martin et al. (2008) attempted to develop a generalized calibration model for predicting canopy nitrogen concentration, based on field survey and remote sensing data combined from North America, Central American and Australia.

We also quantified the temporal scale parameter over a period of time in each study. As shown in Figure 2.3, most of which conducted their survey once in sin-

gle year (26 studies) or repeated it for two years (13 studies) to three years (19 studies). While some studies focused on change detection among multiple years or decades comparing the current and past satellite images, other studies applied a dendrochronological method such as tree ring analysis enabling to trace back up over 300 years.

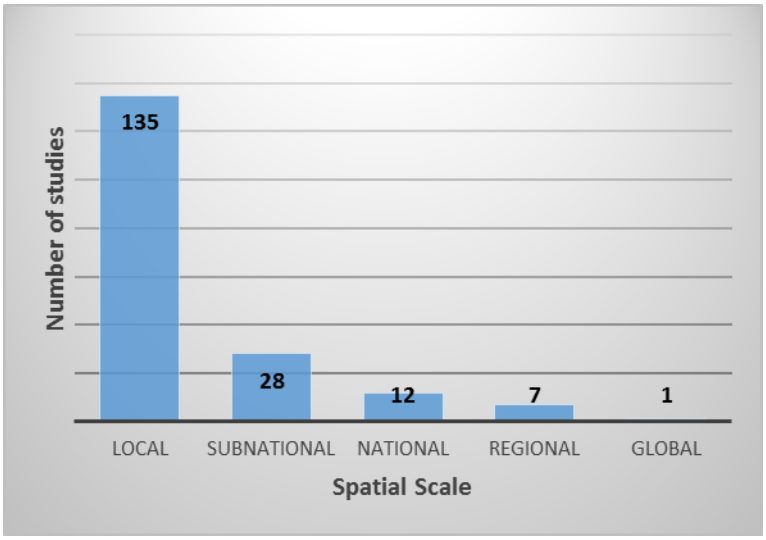

Figure 2.2: The number of studies on forest defoliation categorized by spatial scale.

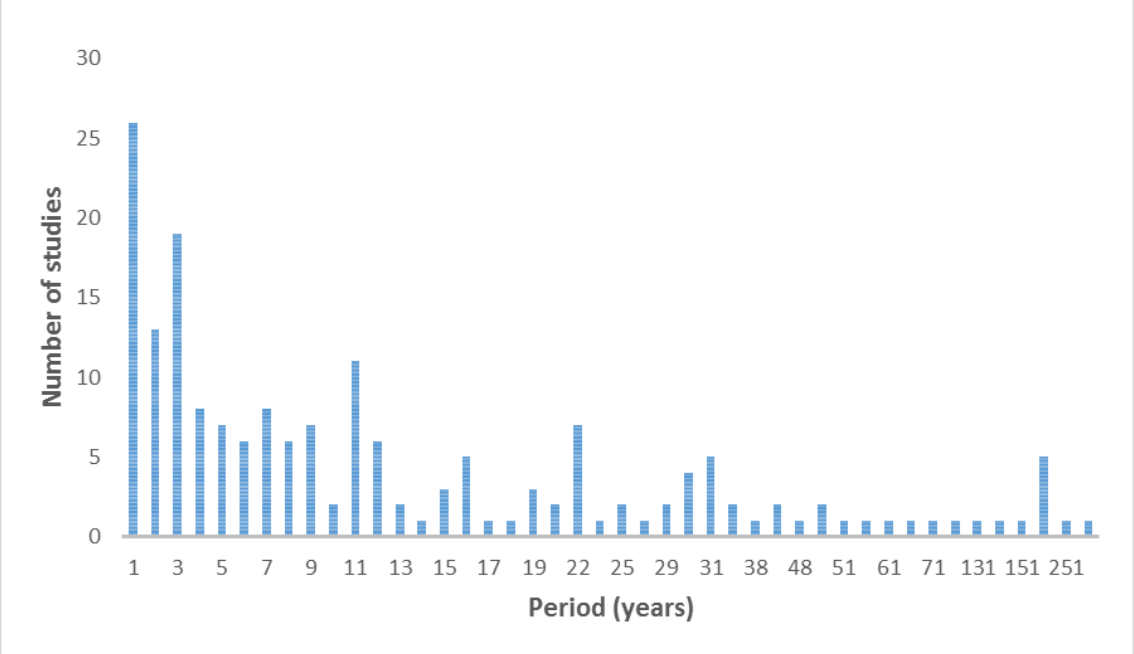

Figure 2.3: The number of studies on forest defoliation categorized by temporal scale for the study period.

2.3.3 Pest drivers and host trees

Knowledge of how trees are manifested by their pest agents is important as it leads to the impacts on the host tree in terms of changes in morphology and/or physiology

(Hall et al., 2016). The damage patterns are associated with the life cycle of their different pests, and the damage types can vary from defoliation to tree mortality (Hall et al., 2016). Table 2.2 shows 18 major defoliators, of which seven were defoliators on deciduous trees, as well as associated host trees with their geographical distribution.

2.3.4 Damage assessment methods and indicators

Symptoms of defoliation include foliage yellowing or reddening, and loss of foliage (Murtha, 1972; Hall et al., 2016). Defoliators cause moderate to severe short-term reductions in photosynthesis and associated carbon sequestration, however, it may not affect the following growing season as leaves can re-flush for photosynthesis (Kramer and Kozlowski, 1979; Cook et al., 2008; Dymond et al., 2010; Flower and Gonzalez-Meler, 2015). Damage assessment involves assigning severity classes or quantitatively estimating values to each tree parameter and spatial unit (polygon or pixel) (Hall et al., 2016). Table 2.3 shows trends of such assessment methods used and combined in 1990s, 2000s and 2010s by decade.

Aerial survey

As the primary tool for mapping the location and severity of pest damage, aerial survey has been widely used for reporting on forest health conditions locally and nationally (Hall et al., 2016). Mapping polygons and grid cells of defoliated areas is an example of sketch maps from the air. In general, accuracy is not high enough for damage mapping with aerial surveys due to the subjectivity of surveyors, limited to monitoring the outbreak frequency of those defoliated areas (Kautz et al., 2017).

Field survey

During the 90's, field measurements including tree-ring analysis were the main means to detect and assess the tree growth associated with defoliations. The field data were used for further statistical analysis to assess the relationship between the insect population density, damage degree and tree growth reduction. Some statistical models also enabled to estimate the cyclic trends of outbreaks. However, since it is quite time-consuming to apply field surveys to a large area, it is not efficient to deal with the rate of pest outbreaks.

Typically, the average of pest damage within a fixed-area plot with the Global Positioning System (GPS) coordinates was assigned to percent intervals based on visual assessment (Royle and Lathrop, 2002; Hall et al., 2003; Hall and Skakun, 2006; Hall et al., 2016). In the 2000s, Leaf Area Index (LAI) and canopy foliar nitrogen concentration started to be measured in some Permanent Sample Plots (PSPs) for monitoring forest health. Routine field surveys are recommended for assessing forest health conditions and reporting to the province, country or region in a standardized manner. However, when sampling procedures are different and specific to tree species, the methods are not standardized or consistent (Hall et al., 2016). Therefore, sampling results can be biased by the surveyor's experience, time available, season, weather, and illumination (Hall et al., 2016).

Table 2.2: A list of major defoliators and host trees with their geographical extent.

Common name	Scientific name	Host tree	Study area	Study count
Eastern Spruce budworm	*Choristoneura fumiferana*	*Abies balsamea, Picea mariana, P. glauca*	Eastern North America	14
European pine sawfly	*Neodiprion sertifer*	*Pinus sylvestris*	Fennoscandia	10
Common pine sawfly	*Diprion pini*	*Pinus sylvestris*	Europe	6
Jack pine budworm	*Choristoneura pinus*	*Pinus banksiana*	Eastern North America	8
Siberian silk moth	*Dendrolimus superans sibiricus*	*Abies sibirica, Pinus sibirica*	Russia	6
Mountain pine beetle	*Dendroctonus ponderosae*	*Pinus ponderosa, P. contorta*	Northwest Canada-USA	4
Douglas-fir tussock moth	*Orgyia pseudotsugata*	*Pseudotsuga menziesii, Abies grandis, A. concolor*	Northwest USA	5
Pine processionary moth	*Thaumetopoea pityocampa*	*Pinus nigra, P. sylvestris, P. pinaster, P. halepensis*	Mediterranean	5
Western spruce budworm	*Choristoneura occidentalis*	*Pseudotsuga menziesii, Abies* spp.	Northwest USA	4
Hemlock woolly adelgid	*Adelges tsugae*	*Tsuga canadensis*	Northwest USA	4
European spruce bark beetle	*Ips typographus*	*Picea abies*	Northern Europe	3
Gypsy moth	*Lymantria dispar*	*Quercus* spp.	USA, Japan, Italy	22
Autumnal moth	*Epirrita autumnata*	*Betula pubescens*	Fennoscandia, Russia	7
Winter moth	*Operophtera brumata*	*Betula pubescens*	Fennoscandia, Russia	8
Forest tent caterpillar	*Malacosoma distria*	*Populus tremuloides*	Eastern North America	7
Larch budmoth	*Zeiraphera diniana*	*Larix decidua*	Alps	5
Green oak tortrix	*Tortrix viridana*	*Quercus robur, Quercus* spp.	Russia, UK, Iran	5
Large aspen tortrix	*Choristoneura conflictana*	*Populus tremuloides*	Western Canada	4

Trap sampling

Three types of trapping methods were found: pheromone, yellow sticky and burlap. Pheromone traps (Sharov et al., 1996; Lyytikäinen-saarenmaa et al., 2001; Lyytikäinen-

Table 2.3: Type of methods used for damage assessment by decade.

Assessment method	1990s	2000s	2010s
Aerial sketch-map	x	x	
Field Measurement	x	x	x
Trap sampling	x	x	x
Tree ring	x	x	x
Statistics	x	x	x
Remote sensing	x	x	x
GIS		x	x
Algorithm		x	x
Prediction model			x
Ecosystem service			x

Saarenmaa et al., 2006; Augustin et al., 2009; Chenchouni et al., 2010) and yellow sticky traps (Battisti and Rodeghiero, 1998) capturing pest insects were used to assess emergence dates of adults and local population density in relation to defoliation risks for monitoring future outbreaks. On the other hand, burlap traps (Liang et al., 1998) were mainly designed to sample pupae on host trees to estimate the population density of pest insects in relation to defoliation levels. Combined with geostatistical analysis, trapping methods in general can quantify the spatial distribution of insect populations associated with defoliation degrees.

Tree-ring analysis

Using an increment borer, sample cores were analyzed for visually cross-dating for long time series over the past hundreds of years by the program such as COFECHA (Holmes, 1983) . In the 1990s, tree-ring widths were measured to the nearest 0.01mm as an indicator to quantify radial growth changes in basal area of defoliated trees (Oberhuber et al., 1999). Moreover, since 2000s the trend of tree-ring analysis has been shifted to reconstruct historical cyclic insect outbreaks and their spatiotemporal dynamics by comparing the dendrochronology of host and non-host stands for the same tree species (Ryerson et al., 2003; Avcí and Carus, 2005; Carus and Avci, 2005; Paritsis et al., 2009; Babst et al., 2010; Bouchard and Pothier, 2010; Sangüesa-Barreda et al., 2014; Leland et al., 2016).

Statistical analysis

Statistics has been the most fundamental tool for quantitatively assessing the relationship among variables in all decades, whether manually calculated or automatically computed. Most commonly, simple and generalized linear regressions were analyzed, as well as linear fixed or mixed regression, multiple regression, logistic regression and logarithmic regression. For assessing the fit of regression models, various coefficients were used such as ANOVA, ANCOVA, AIC, PCA, Pearson's, kappa, etc., using software applications (e.g. SAS, SPSS, R, Minitab, Matlab, GenStat, Statgraphics, Statistica, StatSoft and BMDP). The shift is notable that SAS has been most commonly used (24 articles) from the 1990s (Sharov et al., 1996; Coli et al., 1997; Koukl et al., 1997; Liebhold et al., 1998), the 2000s (Alonso et al.,

2000; Royle and Lathrop, 2002; Brandt et al., 2003; Halldórsson et al., 2003; Solberg et al., 2006; Eisenbies et al., 2007; Hanssen and Solberg, 2007; Weiskittel and Maguire, 2007; Barron and Patterson, 2008; Kozlov, 2008; Man et al., 2008; Tobin and Whitmire, 2009; Wolter et al., 2009) up to the 2010s (Cocco et al., 2010; Nevalainen et al., 2010; Sikström et al., 2011; Krause et al., 2012; Simmons et al., 2014; Gómez et al., 2015; Rullán-Silva et al., 2015) while the use of R (20 articles) (Candau and Fleming, 2005; Cooke and Roland, 2007; James et al., 2010; Kantola et al., 2010; Thayn, 2013; Vastaranta et al., 2013; Adelabu et al., 2014; Cayuela et al., 2014; Fisichelli et al., 2014; Haynes et al., 2014; Kretchun et al., 2014; Rozendaal and Kobe, 2014; Sangüesa-Barreda et al., 2014; Simmons et al., 2014; Li et al., 2015; Nakajima, 2015; Walter et al., 2016; Bognounou et al., 2017; Popa et al., 2017) has increased and become more common in the 2010s. Some software applications, in particular, R functions hold the advantage of generating geostatistics including spatial analysis without any license fee.

Remote sensing analysis

There were 62 studies associated with remote sensing analysis, accounting for 34% of the total studies reviewed. In the 1990s satellite-based sensors at low spatial resolution such as AVHRR and SPOT VEGETATION were already launched, however, their resolution was as coarse as 1 km, typically used for mapping cloud and surface (land, water, snow and ice). Imagery at medium spatial resolution from MODIS, providing most commonly used vegetation indices (VIs) such as Normalized Difference Vegetation Index (NDVI) and LAI, has proved to be useful for detecting defoliation over a large area of interest at regional scale while the 250 m spatial resolution was not fine enough for estimating the damage severity (Van Der Sanden et al., 2006; Eklundh et al., 2009; Rullan-Silva et al., 2013; Hall et al., 2016). On the other hand, Landsat-derived NDVI, most frequently used since 1990s at a 30 m spatial resolution, became available for free of charge from the United States Geological Survey (USGS). It has been found sufficient for mapping damage at the stand level in various studies as a general method to assess percent defoliation and calculate the change in VIs (Hall and Skakun, 2006; Wulder et al., 2006; Rullan-Silva et al., 2013; Hall et al., 2016). This method allows for continuous spectrum across defoliation values, rather than discrete defoliation classes (Rullan-Silva et al., 2013). More recently in 2015, Sentinel-2 imagery of the 10-20 m spatial resolution became freely downloadable from the European Space Agency (ESA). For spaceborne sensors at high spatial resolution (<10 m), the private industry continued to launch satellites such as RapidEye, SPOT-5, IKONOS and QuickBird. With further advancements, the sensor's spatial resolution nowadays can be as high as 0.3 m (WorldView-4), in addition, temporal and spectral resolutions continue to enhance.

Apart from spaceborne remote sensing, the focus of airborne Light Detection and Ranging (LiDAR) technology in the 2000s provided three-dimensional (3D) parameters such as tree height as well as more advanced canopy height model (CHM) and individual tree detection (ITD) based on the tree-level crown structure. Furthermore, the emergence of airborne laser scanning (ALS), characterized by the spatial resolution higher than any spaceborne technology, complemented point clouds in the 3D structure (Rullan-Silva et al., 2013; Roncat et al., 2014). Using ALS metrics, classification of defoliated Scots pines at the individual tree level was demonstrated by Kantola et al. (2013). Moreover, new 3D technologies in the 2010s featuring

cost-effective UAVs (unmanned aerial vehicles) have been used to predict defoliation classes for small operational areas, which may bridge gaps between field and satellite scales by offering data for image calibration and validation of satellite-based monitoring (Hall et al., 2016). A total of 19% of the studies with remote sensing analysis included the use of airborne sensors.

GIS

In the 2000s the use of Geographic Information System (GIS) has increased for generating defoliation maps to show spatial patterns of insect outbreaks (Liebhold et al., 1998; Eshleman et al., 2000; MacLean et al., 2000; Peltonen et al., 2002; Eshleman et al., 2004; Tobin and Whitmire, 2009; Cocco et al., 2010). Using a geostatistical tool, predicting or interpreting the spread rate and frequency probability became effective. At the operational level, Decision Support System (DSS) was implemented for assisting forest managers to predict outbreak effects on forest structure and productivity, forecast forest growing stock and sustainable harvest levels, and use silviculture and harvest scheduling to restructure forests to reduce future damage (MacLean et al., 2000). Towards 2010s, integrating GIS and remote sensing techniques has become more effective for monitoring insect defoliations (Radeloff et al., 2000; Allen and Kupfer, 2001; Gilichinsky et al., 2013; Kirschbaum et al., 2016).

Algorithm

In the 2000s algorithms such as Markov Chain Monte Carlo (MCMC) were performed for simulations by random variables to map probability distribution for defoliation severity and frequency and consider uncertainty in prediction models (James et al., 2010). In addition, with MODIS time-series images, TIMESAT was developed by Jönsson and Eklundh (2002) using different smoothing functions (asymmetric Gaussian (AG), double logistic (DL) and adaptive Savitzky–Golay (SG) filtering) to fit the time-series data and fill the gaps for computing phenological metrics. It was also applied as a damage mapping method for identifying pixels that represent areas containing forest damage.

In the 2010s Random Forest (RF) algorithm was commonly used due to the robust and flexible non-parametric method, enabling to handle both categorical and continuous independent variables. RF is based on model aggregation that can be used for both regression and classification problems. This method consists of a set of random decision trees in a sequence of rules that are constructed from sets of samples taken randomly with replacement from the original training set. Measurement of nearness in RF is defined based on observations of the probability of ending up in the same terminal node in classification (Kantola et al., 2010; Vastaranta et al., 2013), with each tree contributing to the final classification outcome (Adelabu et al., 2014). With Landsat time-series images, LandTrendr was developed using statistical algorithms to separate trends from noise, on a per-pixel basis (30 m resolution), to describe a time series of spectral reflectance values and the shape of the curve such as phenological condition or sun angle at the time of image acquisition. As a detection method for trends in disturbance and recovery, LandTrendr has been effective to identify periods of spectral stability and instability (Kirschbaum et al., 2016).

Prediction model

A model of predicting future scenarios was found in only 5 articles (Mason, 1996; MacLean et al., 2000; Kapeller et al., 2011; Fisichelli et al., 2014; Kretchun et al., 2014) among 160 reviewed. In the 1990s some models were based on statistical analysis to predict pest density change (Mason, 1996). As the computer technology advances in spatiotemporal modelling, GIS-based DSS (MacLean et al., 2000) and cellular automaton (Kapeller et al., 2011) simulations were developed for estimating future conditions such as volume loss (m^3/ha) and population dynamics. Finally, in compliance with the IPCC climate change scenarios, some models developed in 2010s predicted tree habitat suitability (Fisichelli et al., 2014) and carbon-related indicators such as Net Primary Production (NPP) (g C/m^2/year), carbon (g Cm^2), biomass (g Cm^2) (Kretchun et al., 2014). The associated study areas were mostly in USA and Canada followed by some Mediterranean countries such as Spain and France. The spatial scale was mainly local as it is often less robust to apply a complex of predictable variables at a large scale across country. On the contrary, temporal scales were generally long enough (10-30 years) to make inferences or simulate the future conditions. While there was no major defoliator species modelled in common, most of the host trees were coniferous such as pines and firs.

Ecosystem service

The studies associated with ecosystem services (ES) were found in 15 articles and categorized into provisioning or regulation & maintenance according to Common International Classification of Ecosystem Services (CICES) (Haines-Young and Potschin, 2018). The indicators in provisioning (MacLean et al., 2000; Cook et al., 2008; Catal, 2011; Sikström et al., 2011; Fisichelli et al., 2014; Kretchun et al., 2014; Rozendaal and Kobe, 2014; Sangüesa-Barreda et al., 2014; Olsson et al., 2017) included LAI, basal area growth, radial increment, volume loss or growth, NPP and habitat suitability. In regulation & maintenance category (Eshleman et al., 2004; Fischer et al., 2007; McNeil et al., 2007; Pitman et al., 2010; Scanlon et al., 2010; Fernández et al., 2011), physical, chemical and biological conditions in water and soil, such as nutrient concentration and nitrate export derived from defoliation, were quantified as indicators. These articles were all published posterior to year 2000, focusing on study areas at various spatial scales ranging from local, subnational, national to regional in European or North American countries. The range of temporal scales was wide, depending on whether the model is capable of forecasting the future conditions (ES: provisioning category) which would require a study period of the past 30 years on average, while the rest of models could apply a short study period for a couple of years to provide ecosystem services representing the current conditions (ES: regulation & maintenance category). The model types were well combined among conventional statistical analysis or simulation algorithm based on forest inventory data (PSP and International Co-operative Program (ICP)) and recent remote sensing technologies. This integration seems to be the trend in providing ecosystem services. There was no major focus on specific defoliators, however, it was observed that coniferous trees are pines, spruces and firs while the majority of broadleaf trees belong to *Quercus* spp.

2.4 Discussion

2.4.1 Geographical distribution

Due to some differences among regions and countries in economic conditions, research funds and /or availability of professionals and experts (Morán-Ordóñez et al., 2018; Muller et al., 2018), the studies conducted on forest defoliations were concentrated in the developed countries in North America and Europe. For this reason, the higher number of studies in those developed countries does not necessarily indicate the higher number of existing defoliators or the larger area defoliated in their regions where studies are more extensively and frequently conducted. It may be due to the mere fact that some developing countries lack the research resources including knowledge, technology and financial support for detecting, measuring, mapping and monitoring forest defoliations as well as publishing research outcomes in English for international readers.

2.4.2 Spatial and temporal scales

A tradeoff between spatial resolution and extension is critical for deciding how much detail and how much space should be surveyed. In general, the larger geographical extent from national to regional and global scales requires low resolution satellite imagery (e.g. MODIS with time-series TIMESAT) while the use of sketch mapping and/or medium resolution satellite imagery (e.g. Landsat with time-series LandTrendr) is appropriate from local to subnational scales. In some other special cases requiring individual tree measurements, field data may be more appropriate even though the latest remote sensing is capable of capturing imagery at sub-metric high resolution, including spaceborne sensors and airborne technologies such as LiDAR, ALS and UAV. For measuring parameters observable only from the ground level in a single small study area, field surveys may be the fundamental source of data. It should be noted that repeating the same field survey method in different study areas by different surveyors may cause some biases derived from manual or visual measurements unless the parameter of interest can be measured by electronic devices such as lasers which are relatively consistent with measurements regardless of the surveyor. Nowadays, some tree parameters such as crown defoliation and height can be measured from airborne sensors where forest stands are not too dense to detect individual trees.

Temporal scale may refer to the period and frequency of detection for continuous monitoring. Most of detection methods reviewed were based on annual surveys to detect general changes from previous years while inter-annual surveys were effective for detecting any seasonal variation in plant phenology (i.e. annual phenological cycle). Some methods can track back over several years and decades as well as predict future values in upcoming years. The longest period observed in this literature review was 300 years, achieved by dendrochronological method using annual tree-ring analysis (Büntgen et al., 2009). Time-series analysis with satellite images such as Landsat and MODIS became available from year 1972 and 2000, respectively. On the other hand, the shortest period observed was single year as the initial year, found in 26 studies, to start up the methodology with or without the intention to continue monitoring from then.

2.4.3 Pest drivers and host trees

Native tree species may recover from defoliations in a relatively short time, however, negative consequences on growth and ecological functions of the forests often occur in plantations especially where certain species are introduced to outside of their natural range (Battisti et al., 2016).

Moreover, due to increasing droughts caused by climate change in the Mediterranean region, some insects benefit from stress-induced trees, depending on their feeding method (Koricheva et al., 2002; Huberty and Denno, 2004; Tiberi et al., 2016). While defoliators are negatively affected by water-stressed trees due to the increased allelochemical levels in leaf tissues (Inbar et al., 2001; Tiberi et al., 2016), bark or wood borers take advantage of the stressed trees for colonization (Tiberi et al., 2016). Increasing winter temperatures caused by global warming may also favor pest outbreaks as a result of reduced winter mortality of some insects (Tiberi et al., 2016). In addition, these climatic factors may increase the risk of wildfire, which would make stressed trees become even more susceptible to pest agents (Coelho and Campos, 2009; Tiberi et al., 2016).

2.4.4 Damage assessment methods and indicators

Integrated monitoring system

Since the absence of routine surveys may lead to temporal data gaps as well as spatial data gaps in the monitoring system, timing is critical for detecting certain damage, according to what time of the year and how long the damage is likely visible (Rullan-Silva et al., 2013; Hall et al., 2016). As a solution to reduce information gaps, remote sensing may complement field surveys towards an integrated, multi-scale, multi-source pest monitoring system (Hall et al., 2016).

Current remote sensing technologies enable to detect trends over long-term series of satellite imagery. Since the year 2008 initiated by the first open access to Landsat data, long-term continuous monitoring for land cover changes has been encouraged (Wulder et al., 2012; Hall et al., 2016). Consequently, pre-outbreak and post-outbreak images can be assessed for changes in tree damage and recovery using Landsat time-series analysis such as LandTrendr. Although assessment methods have been improving, assigning severity classes can be challenging with acceptable accuracy especially in mixed stands where the stand is composed of more than single species (Hall et al., 2016; Otsu et al., 2018).

Thus, remote sensing may play a complementary role in monitoring damage continuously and frequently to serve as a means to identify data gaps, address research questions of impacts on forest dynamics using damage data with high spatial resolutions, and develop predictive models to estimate damage trends (Hall et al., 2016). Traditionally, remote sensing has not played a significant role to detect early population endemics, however, the importance of the role will likely increase in the future especially in large remote areas at high altitudes and high latitudes where there is limited access to road networks (Hall et al., 2016).

Prediction and scenario modelling

The difficulty in predicting pest outbreaks involves the interpretation of ecological processes as well as biotic, abiotic and anthropogenic factors (Villemant and Andreï-

Ruiz, 1999; Tiberi et al., 2016). For this reason, establishing robust models for prediction of pest population dynamics remains challenging (Tiberi et al., 2016). Since there is great uncertainty about the frequency and severity of pest outbreaks due to global warming, the consequences of such climate change are also unknown (Flower and Gonzalez-Meler, 2015). However, some biological indicators may be useful to anticipate population outbreaks to the best knowledge in prediction models (Tiberi et al., 2016). Combined with climate factors, it is important to develop prediction models for assessing the forest response to climate changes (Duning, 1995; Tiberi et al., 2016). Specifically, sensitivity analysis testing the model robustness by increasing and decreasing predictive parameter values may reduce the uncertainty of response values (Otsu et al., 2019). Moreover, hierarchical processed-based biotic interactions should be taken into consideration for modelling physiological responses to pest outbreaks at tree and stand levels (Flower and Gonzalez-Meler, 2015; FAO, 2018).

Ecosystem services and future research

As forests offer a variety of ecosystem services such as timber, water purification and carbon sequestration (Thompson et al., 2011; Boyd et al., 2013; Ramsfield et al., 2016; Haines-Young and Potschin, 2018), it is important to mitigate economic and social impacts of damage caused by forest pests as well as impacts on biodiversity. By monitoring forest productivity as an indicator of tree growth, tools to quantify impacts of forest defoliation become useful for ecosystem services in pest and disease control (Thompson et al., 2011; Ramsfield et al., 2016). Ultimately, monitoring forest health may contribute to early detection of pest outbreaks and prevention of further damages in the following years to reduce the amount of loss in various ecosystem values. Such values should be well defined and standardized on a global scale for being able to compare assessments at the international level. This is why the CICES (Haines-Young and Potschin, 2018) was developed by the European Environmental Agency (EEA) with the aim of classifying what ecosystems as living processes do for human well-being.

2.5 Conclusions

Currently, biotic disturbances caused by defoliators are major causes of forest decline in many regions, even accelerated by climate change. We presented a systematic literature review on the studies over the past two decades associated with the world's forest defoliations, with the aim of filling the information gap among previous review articles that focused on forest disturbances, in general, limited by particular regions or detection techniques. We identified spatial and temporal distribution of defoliations, pest-host tree relationships, and specific detection methods for quantifying the defoliation degrees. Our findings highlighted that the effort on improving methods for pest detection and monitoring has been significantly increased over the past decade. Depending on the scales and types of defoliation in question, the latest modelling and remote sensing techniques, including an emerging UAV technology, are currently available to be combined with conventional ground surveys and statistical analyses.

The current limitations should be addressed with potential solutions as follows:

- Spatial data gaps on forest defoliations outside North America and Europe are evident, possibly due to scarce research funds and resources. Opportunities for increasing international projects focused on gap areas may be encouraged and collaborated by leading countries.

- Temporal data gaps in the past defoliations with the use of remote sensing images are inevitable prior to 1972. Towards the future, the timeline of available satellite images will increase with Landsat (posterior to 1972), MODIS (posterior to 2000), and Sentinel (posterior to 2015), which may be combined to enhance the temporal resolution as well.

- Identifying defoliation drivers combined with other biotic and/or abiotic factors and their relationships with specific host trees is complex. Monitoring changes in several potential factors based on climate, forest inventory, and remote sensing data may have the potential to distinguish the causes.

- Methods and indicators for detecting and quantifying defoliation damages are inconsistent. In addition to innovatively developed models, well-established existing methods may be tested with baseline (default) scenarios using forest inventory (e.g. PSP, ICP), dendrochronology (e.g. COFECHA), statistics (e.g. SAS, R), and/or time-series algorithm (e.g. TIMESAT, LandTrendr).

- Increasing uncertainty and variability in prediction models is significant, due to the current absence of robust models and the increased number of predictive variables interacted. Starting with the baseline scenario complemented with a sensitivity analysis may be encouraged by using existing (inter)nationally standardized data as inputs, if available, to generate comparable outputs such as the indicators defined by CICES.

As we conclude that optimal methods may be specific to each pest agent associated with host tree species, the advancement in pest detection and monitoring methods is promising for mitigating the future damage to high ecological, social and economic values of forests. For future research, we recommend that prediction models based on those monitoring methods should be well linked to ecosystem services related to pest and disease control in compliance with the IPCC scenarios.

Chapter 3

Article 1: Calibrating the severity of forest defoliation by pine processionary moth with Landsat and UAV imagery

Abstract
The pine processionary moth (*Thaumetopoea pityocampa* Dennis and Schiff.), one of the major defoliating insects in Mediterranean forests, has become an increasing threat to the forest health of the region over the past two decades. After a recent outbreak of *T. pityocampa* in Catalonia, Spain, we attempted to estimate the damage severity by capturing the maximum defoliation period over winter between pre-outbreak and post-outbreak images. The difference in vegetation index (dVI) derived from Landsat 8 was used as the change detection indicator and was further calibrated with Unmanned Aerial Vehicle (UAV) imagery. Regression models between predicted dVIs and observed defoliation degrees by UAV were compared among five selected dVIs for the coefficient of determination. Our results found the highest R-squared value (0.815) using Moisture Stress Index (MSI), with an overall accuracy of 72%, as a promising approach for estimating the severity of defoliation in affected areas where ground-truth data is limited. We concluded with the high potential of using UAVs as an alternative method to obtain ground-truth data for cost-effectively monitoring forest health. In future studies, combining UAV images with satellite data may be considered to validate model predictions of the forest condition for developing ecosystem service tools.

3.1 Introduction

Currently, pest insects are the principal biotic drivers causing disturbances threatening Mediterranean forests in combination with abiotic factors such as drought, fire and climate change (Rullan-Silva et al., 2013; Sangüesa-Barreda et al., 2014). The pine processionary moth (*Thaumetopoea pityocampa* Dennis and Schiff.), one of the major defoliating insects in Mediterranean pine forests, has been considered by the Intergovernmental Panel on Climate Change (IPCC) as an indicator of global warming (Rosenzweig et al., 2007) for being recorded in an expanded biogeographical range of host distribution from Southern Europe in the Mediterranean region

towards northern latitudes and higher elevations over the past twenty years (Battisti et al., 2005; Roques, 2015). Consequently, the defoliators may continue to increase with the future trend of climate change scenarios (Roques, 2015).

Outbreaks of *T. pityocampa* have been observed to be cycles of 6 years on average (Hódar et al., 2004; Sangüesa-Barreda et al., 2014), mainly in managed young stands (Robinet et al., 2007; Roques, 2015). In a normal year healthy forest stands recover from defoliation, however, periodic outbreaks attack large forests in which host trees may suffer up to 100% defoliation. Thus, severely affected stands may result in significant reductions of individual tree growth, stand productivity, and forest ecosystem health, from tree to stand and landscape levels (De Beurs and Townsend, 2008; Roques, 2015). Such growth reduction may accelerate the rate of tree mortality when the damage is accumulated due to other biotic factors as well as abiotic factors (Hódar et al., 2003). As a consequence, defoliation focused on host pine trees is more likely to change the structure and species composition in natural stands as well as lose economic values in planted stands (Hódar et al., 2003; Sangüesa-Barreda et al., 2014). Furthermore, forest ecosystems at the landscape level are major carbon sinks contributing to mitigate the impacts of climate change (Hyvonen et al., 2007; Luyssaert et al., 2010; Li et al., 2015). Therefore, to predict future scenarios on forest productivity and mortality in cases where the outbreaks may occur, reliable data from monitoring the pest distribution at regional and national scales are required (Li et al., 2015; Roques, 2015).

Despite the annual ground survey on forest health in the Mediterranean countries such as France, Portugal and Spain which are frequently affected by outbreaks of *T. pityocampa*, we currently lack accurate, fine-grained and timely information systems for monitoring the latest forest condition. Thus, an efficient tool to improve such regional or national monitoring systems spatially and temporally may be developed by adequately using the latest remote sensing technologies. In addition to conventional field surveys which are often time-consuming to cover large areas, satellite-based images such as MODIS and Landsat at medium spatial resolution (30–250 m) have been widely used for detecting defoliations in forest systems over the past two decades (Rullan-Silva et al., 2013). Currently, due to the free accessibility to medium-resolution (10–60 m) products from Landsat 8 (NASA, 2019) and Sentinel-2 (ESA, 2015), they are most commonly used for cost-effectively monitoring large areas. For sensors at high spatial resolution (<10 m), the private industry continued to launch satellites such as IKONOS, QuickBird, RapidEye and TerraSAR-X [1]. With further advancements in spaceborne technology, the sensor's spatial resolution nowadays can be as high as 0.3 m (WorldView-4), and continue to enhance temporal and spectral resolution as well. In Spain, using various sensors (Airborne Hyperspectral Scanner, Hyperion, ChrisProba, Quickbird, and Landsat), Cabello et al. (2011) have applied vegetation indices for mapping forest damage caused by T. pityocampa to estimate the Leaf Area Index in affected pine stands, followed by Sangüesa-Barreda et al. (2014) with the combined method of Landsat-derived vegetation indices and dendrochronology for assessing the tree growth reduction affected by outbreaks of T. pityocampa. Furthermore, the emergence of airborne laser scanning (ALS) characterized by point clouds complements the three-dimensional (3D) structure in addition to the spatial resolution higher than any spaceborne technology (Rullan-Silva et al., 2013; Roncat et al., 2014). Using ALS metrics, classification of defoliated Scots pines at the individual tree level was demonstrated by Kantola

et al. (2013).

Since the cost of above high-resolution products remains a limiting factor for small operational areas, the trend of monitoring forest health in recent studies has shifted to the alternative 3D technology based on cost-effective Unmanned Aerial Vehicle (UAV) at high temporal and spatial resolution over the past decade (Dash et al., 2017). While initial studies with UAVs were focused on crop management for agriculture applications, the latest UAV technology has proved to be effective for forestry applications (forest disturbances and diseases, forest cover mapping, tree species identification, and forest inventory measurements) as a sampling tool for acquiring ground-truth data (Torresan et al., 2017). To date only a few studies have examined on the classification accuracy of forest insect defoliations using UAV imagery. The classification methods include Random Forest (Dash et al., 2017), object-based image analysis (OBIA) (Lehmann et al., 2015; Brovkina et al., 2018), k-Nearest Neighbor (Näsi et al., 2015), and maximum likelihood (Cardil et al., 2017; Hentz and Strager, 2017). Moreover, no study has calibrated satellite-based vegetation indices as a predictive indicator of such defoliation with UAV-derived data as ground-truth while Pla et al. (2017) has recently made progress in calibrating some indices specific to fire damage using UAV imagery.

With the objective to quantify forest response to infestation, we developed remote sensing-derived indicators to measure the defoliation levels. In this study, we aim to evaluate the spatiotemporal degree of defoliation during a recent outbreak of *T. pityocampa* in Mediterranean pine forests by change detection analysis using a combination of satellite and UAV imagery. Our main objectives are: (1) examine regression models between vegetation indices (VI) derived from Landsat imagery and defoliation degrees interpreted by UAV imagery for calibration; (2) map defoliation classes based on the best-fit VI model to assess classification accuracy for validation.

3.2 Materials and methods

3.2.1 Study area

The study area is located near the city of Solsona, Catalonia, northeast of Spain (Figure 3.1a), encompassing 6809 hectares (Figure 3.1b) dominated by pine forests (elevation above sea level ranging from 600 m to 1100 m). Primary host species are *Pinus nigra* followed by *P. sylvestris*, which are the dominant tree species in mixed stands with *Quercus ilex* and *Q. humilis*. The climate is Mediterranean continental characterized by hot summer and cold winter. According to the local meteorological station, the mean annual temperature is 11.7 °C and the mean total annual precipitation is 864 mm. As larvae of *T. pityocampa* develop across winter, it has benefited from recent warmer fall and winter temperatures for overcoming the thermal thresholds and consequently increasing the rate of larval survival and growth as far as the host trees are present (Roques, 2015).

3.2.2 Field data

Ground and aerial sketch mapping data were first obtained from the regional forest health inventory during the years from 2010 to 2016. Since the project on evaluating the severity of infestations caused by *T. pityocampa* started, field surveys have been

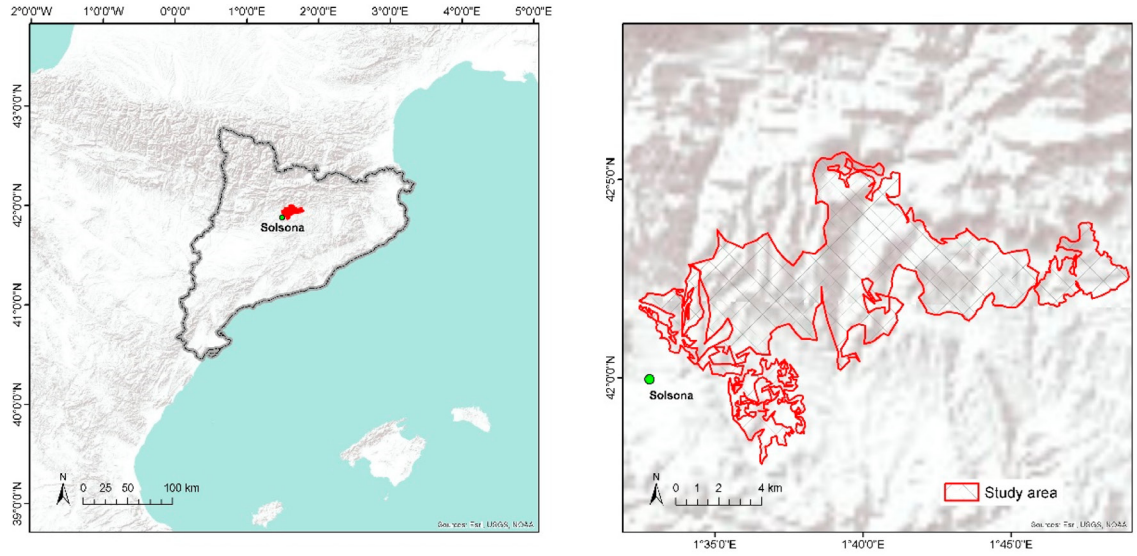

Figure 3.1: Study area showing: (a) Location of Solsona (41°59′40″ N, 1°31′04″ E), Catalonia (solid gray line), Spain; (b) one of the most severely affected areas mapped by rural agents (2016).

conducted by rural agents every winter when the symptoms are visually most evident from February to March after the larvae complete feeding on needles and go into the soil for pupation (Battisti et al., 2005). The survey form is standardized by the government (Generalitat de Catalunya) and filled out by rural agents. Affected stands are mapped as polygons, on average about 137 hectares per polygon ranging to the smallest of 0.03 hectare, with attributes such as observation date, forest type, aspect, tree species, and infestation severity. The severity scales are ranked from 1 to 4 at highest as follows: (1) several nests at the margins and some nests in the center of the forest stand; (2) partial defoliation at the margins on some trees and several nests in the center of the forest stand; (3) intense defoliation at the margins and partial defoliation in the forest stand; (4) very intense defoliation both at the margins and in the center of the forest stand. The total area infested by *T. pityocampa* was recorded at largest in 2016. Based on this inventory database with sketch map polygons, our study area was selected to be one of the most severely affected areas during winter 2015–2016 (Figure 3.1b).

3.2.3 Landsat images and vegetation indices

Pre-outbreak (20 September 2015) and post-outbreak (30 March 2016) images were obtained from Landsat 8 (path 198, row 31) with minimum clouds to capture the maximum defoliation period from fall to spring. Surface Reflectance (SR) products were downloaded from the GloVis (http://glovis.usgs.gov) USGS server. Furthermore, the Band Quality Assessment included in the SR product was applied to exclude pixels described as water, snow, cloud, and cloud shadow so that only pixels with values indicating clear terrain were extracted (Hantson and Chuvieco, 2011; Sangüesa-Barreda et al., 2014; Pla et al., 2017). Preprocessed images in the cartographic UTM projection were further extracted by forest cover classified as pine-dominated stands according to the Land Cover Map of Catalonia (MCSC) generated

in 2009. The best spectral regions for defoliation detection may correspond to reflectance bands from Landsat 8 such as near infrared (NIR = Band 5) and shortwave infrared (SWIR1 = Band 6 and SWIR2 = Band 7) which enable to capture a fast reduction of pine foliage and the consequent reduction in tree evapotranspiration (Rullan-Silva et al., 2013; Pla et al., 2017). In this study, we tested five VIs to predict the defoliation degree in pine forests as summarized in Table 3.1.

Table 3.1: Vegetation indices derived from Landsat 8 multispectral bands.

Index	Acronym	Formula	Reference
Middle Infrared Wavelengths	MID	Band 6 + Band 7	Lu et al. (2004)
Moisture Stress Index	MSI	$\frac{\text{Band 6}}{\text{Band 5}}$	Rock et al. (1986)
Normalized Difference Moisture Index	NDMI	$\frac{\text{Band 5} - \text{Band 6}}{\text{Band 5} + \text{Band 6}}$	Hunt Jr and Rock (1989)
Normalized Difference Vegetation Index	NDVI	$\frac{\text{Band 5} - \text{Band 4}}{\text{Band 5} + \text{Band 4}}$	Rouse et al. (1973)
Normalized Burn Ratio	NBR	$\frac{\text{Band 5} - \text{Band 7}}{\text{Band 5} + \text{Band 7}}$	García and Caselles (1991)

Comparing values of VI among multiple dates may function as a good indicator for change detection (Battisti et al., 2005; Cabello et al., 2011; Kantola et al., 2013; Rullan-Silva et al., 2013; Roncat et al., 2014). To distinguish annual defoliation during the outbreak from cumulative defoliation over several years, a pre-outbreak (20 September 2015) image was compared to additional images from Landsat 8 representing the month of September in the previous two years (2013 and 2014) to confirm that there was no abrupt change in the VI values used in our study area before outbreak. The difference in VI (dVI) was calculated by simply subtracting the value of each VI in year 2016 (post-outbreak) from year 2015 (pre-outbreak) to estimate annual defoliation:

$$VI(\text{pre-outbreak}) - VI(\text{post-outbreak}) = dVI \tag{3.1}$$

3.2.4 Visual interpretation with UAV Images

To assess the level of defoliation in selected locations, we used a camera (FC200, DJI, Shenzhen, China) mounted on a UAV (Phantom 2 vision+, DJI, Shenzhen, China). This camera can capture images, photos or videos, in the visible spectrum (RGB including blue, green and red bands) with a lens focal length of 5 mm and field of view of 120 degrees (DJI, 2015). The RGB imagery had a 14 megapixels-resolution and was collected from a flying altitude ranging at 50–100 m above the ground level, resulting in a ground sample distance (GSD) of 2.0–3.5 cm. Seven flight surveys were conducted between December 2015 and March 2016 covering approximately 193 hectares across the study area shown in Figure 3.2a, of which five were collected in photos (81 hectares) and two were recorded in videos (112 hectares) at speeds ranging from 4–8 m per second depending on light conditions.

The survey locations were selected to represent the stand types characterized by *P. nigra* and *P. sylvestris* and by various defoliation levels. Some surveys were recorded earlier than the post-outbreak image (30 March 2016) where high defoliation levels had been already observed at that time.

The total of 526 adjacent photos overlapped (forward 80%, side 60%) from the five flights with their geotagged locations were processed in the software PhotoScan Professional 1.4.0 (Agisoft LLC, St. Petersburg, Russia). In the image processing they were geometrically aligned to build a point cloud, 3D model, digital elevation model (DEM), and finally five orthomosaic images (Agisoft, 2018a). To collect more sample images, we included additional two videos flying at 4 m per second and recording 29 frames per second with the associated GPS files, which were imported into the software Video GeoTagger (Remote GeoSystems, Fort Collins, CO, USA) to tag geolocations. Extracting a frame per second resulted in the total of 339 frames in photo files. We repeated the same image processing used for the photos to generate two additional orthomosaic images derived from the video frames.

Using the ArcGIS version 10.5 software (ESRI, Redlands, CA, USA) each orthomosaic was georeferenced to the Landsat imagery in the UTM projection by performing a first order polynomial transformation with 4 control points, obtaining an accuracy of sub-meter root mean square error. The georeferenced orthomosaic images were further stratified to delineate non-forested or forested areas with the severity of defoliation in homogeneously affected stands by visual interpretation (Figure 3.2b).

As summarized in Table 3.2, the sampled grid cells of 30 m x 30 m on orthomosaic images, corresponding to the pixels captured by Landsat, were haphazardly selected by an analyst avoiding shadow pixels from each representative category. Upon delineating the surface area containing defoliated trees per grid cell, the defoliated portion of the total cell area (900 m^2) was calculated and expressed at 5% interval (Figure 3.2c). Finally, all selected grid cells were classified into four categories: nil (no change 0–5%); low (defoliation 10–30%); medium (defoliation 35–65%); and high (defoliation 70–100%), as a modified classification suggested by Hall et al. (2016).

Table 3.2: Selected UAV sample images for calibration in each category of defoliation severity.

Severity	Defoliation (%)	Number of Samples
Nil	0–5	10
Low	10–30	23
Medium	35–65	8
High	70–100	9

3.2.5 Regression analysis and threshold classification

We statistically analyzed relationships between two variables, predicted dVI (X) from Landsat imagery and observed defoliation % (Y) from UAV imagery. The relationships between X and Y were evaluated using the software R in various regression models including simple linear, logarithmic, exponential, polynomial, and logistic models. Provided that the range of defoliation % (Y) is limited as the response variable is bounded from 0 to 1 (Townsend et al., 2012; Rullán-Silva et al.,

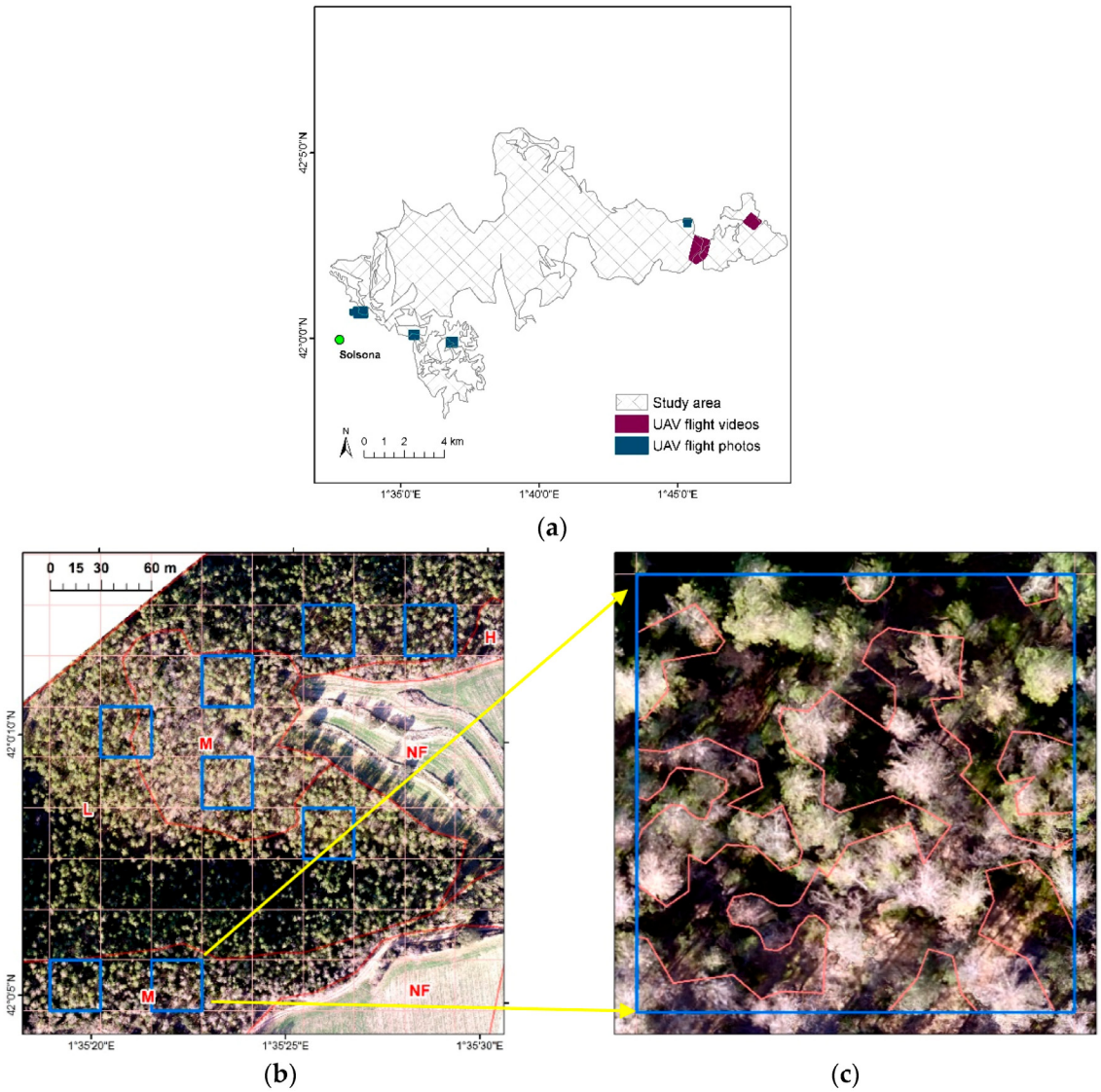

Figure 3.2: Observed defoliations based on UAV imagery showing: (a) the location of UAV sample images captured in photos and videos where sketch map polygons were identified as most severely affected areas in 2016; (b) an example of the orthomosaic stratified by land cover and defoliation degree (NF - not forested, L - low, M - medium, H - high) showing selected grid cells of 30 m x 30 m; (c) visual interpretation of defoliation in percentage per grid cell (50% in this sample).

2015; Zhu et al., 2018), logistic regression was employed to express proportion defoliated, following the equation:

$$Y = \frac{1}{1 + e^{-(a+bX)}} \tag{3.2}$$

where X represents the value of pixel in a selected dVI within the sample image, Y represents the percentage of defoliation interpreted within an individual UAV sample image, and a and b are the slope and intercept of the regression function. Based on fifty selected samples (sample size = 50) in the study area, regression models were fitted to evaluate the coefficient of determination, McFadden's R^2 (McFadden, 1973), which is most often reported in statistical software and recommended for measures

of fit for logistic regression (Allison, 2014). The dVI models were then compared to determine the best-fit indicator for estimating the severity of defoliation. With the known Y values of 10, 35 and 70 to separate the range of defoliation %, threshold limits in dVI (X) from the Equation 3.2 were recalculated as follows:

$$X = \frac{ln\left(\frac{Y}{1-Y}\right) - a}{b} \tag{3.3}$$

Finally, as defined in Table 3.2, the severity map of defoliation was generated by threshold classification (Miller and Thode, 2007; Parks et al., 2014; Pla et al., 2017).

3.2.6 Classification accuracy

To assess an overall accuracy of the threshold classification, we generated a confusion matrix of the four defoliation classes in the 50 selected grid cells, which were compared between the Landsat-based prediction and UAV-based interpretation. Validation of classes in the severity map was performed by assessing classification accuracy of dVIs referenced to UAV observations.

3.3 Results

In Figure 3.3 the resulting X and Y points were plotted and compared among selected VIs. Moreover, the coefficient of determination (R^2) by dVI is summarized in Table 3.3, which was statistically analyzed for logistic regression proposed by McFadden (1973). The goodness of fit was highest = 0.815 with dMSI while it was not improved by normalizing VIs such as dNDMI, dNDVI, and dNBR.

Using the equations in Table 3.3, the range of dVI values were determined as threshold limits in classification (Table 3.4). Applying values in dMSI to defoliation %, any value higher than -125 is classified as no defoliation (<10%): -125 to -295 (10–35%); -295 to -453 (35–70%); and lower than -453 (>70%). Based on the threshold limits, pixels assigned to four classes of defoliation were mapped to show the severity across the study area (Figure 3.4). The blank pixels in no color indicate either non-forested areas or stands dominated by other tree species, which were initially excluded from the analysis.

Table 3.3: Summary of logistic regression models.

Index	Formula	R^2 (McFadden's)
dMID	$Y = \frac{1}{1+e^{-(-3.1299111-0.0041928X)}}$	0.740
dMSI	$Y = \frac{1}{1+e^{-(-3.3570352-0.0092755X)}}$	0.815
dNDMI	$Y = \frac{1}{1+e^{-(-3.5552389+0.0014107X)}}$	0.749
dNDVI	$Y = \frac{1}{1+e^{-(-3.509468+0.001767X)}}$	0.787
dNBR	$Y = \frac{1}{1+e^{-(-3.6323329-0.0013874X)}}$	0.776

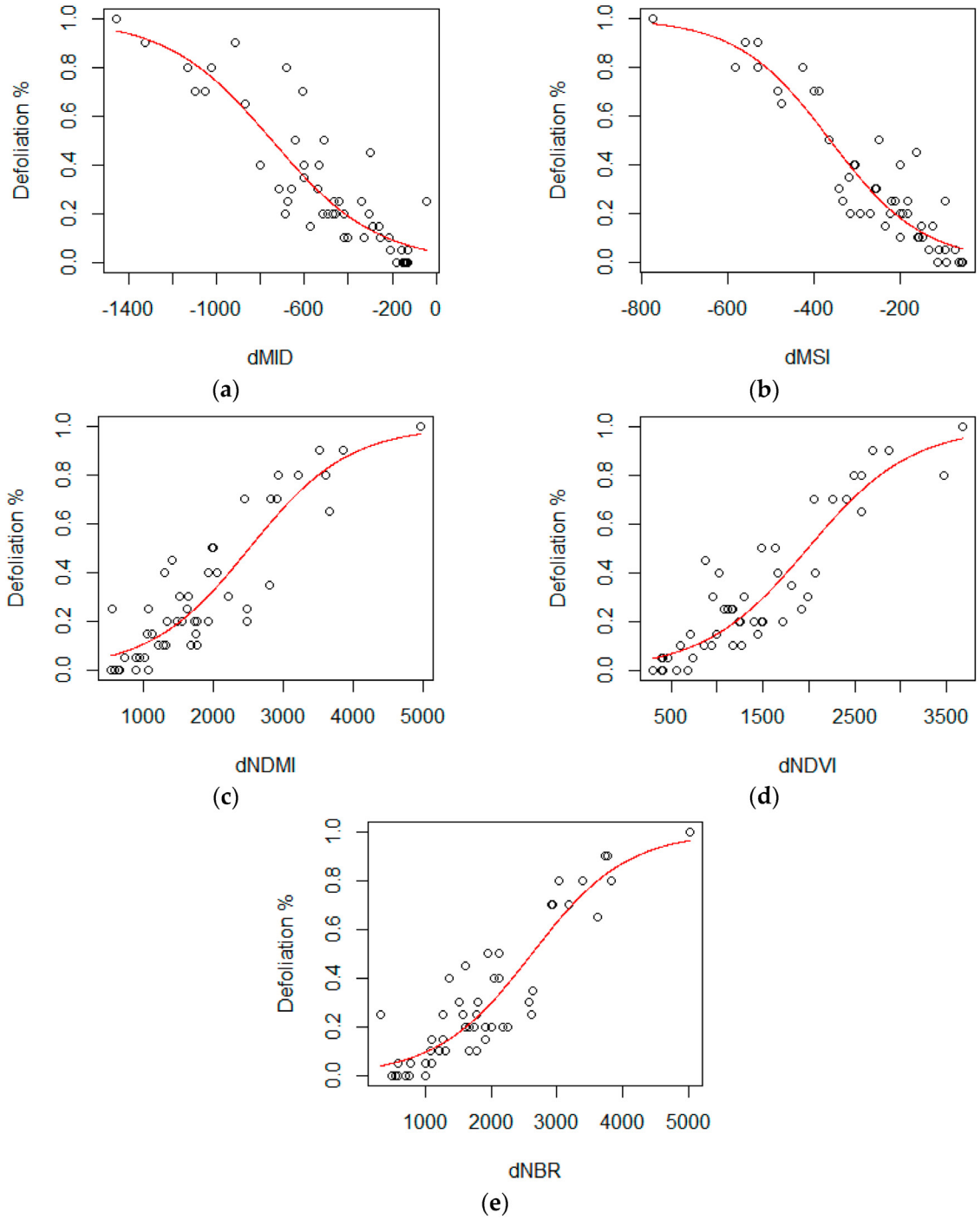

Figure 3.3: Scatterplots of defoliation (%) as response variable and dVI as predictor variable: (a) dMID; (b) dMSI; (c) dNDMI; (d) dNDVI; (e) dNBR.

The overall accuracy of the threshold classification was presented in Table 3.5 for the four defoliation classes (nil, low, medium, and high) in the 50 selected samples of dMSI referenced to UAV orthomosaic images. Greatest producer's accuracy representing a measure of omission error was 90% for the nil defoliation class, where nine out of the 10 cells observed as nil were correctly classified by predicted dMSI. On the other hand, the high defoliation class was mapped with greatest user's accuracy of 86% indicating commission error, which six out the seven cells predicted as

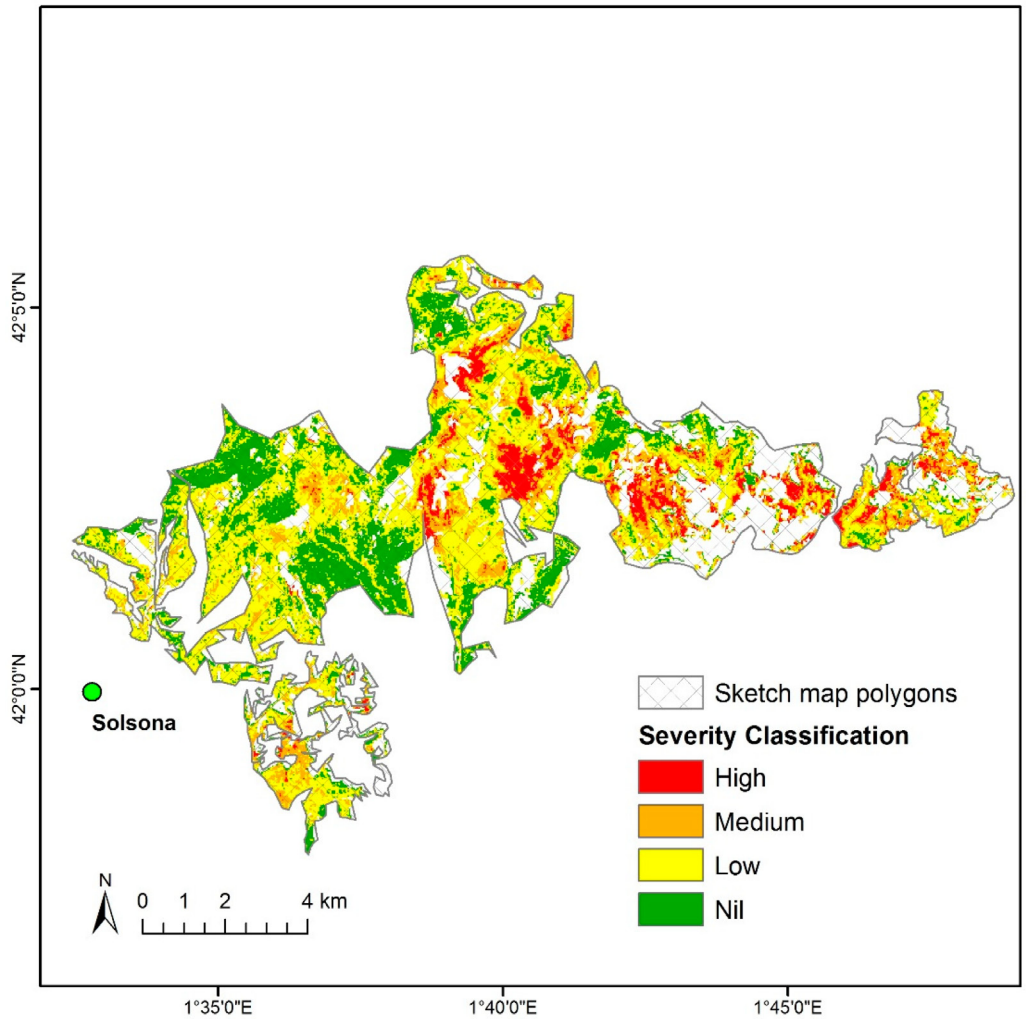

Figure 3.4: Severity map of defoliation classified by threshold limits of dMSI representing pine-dominant stands (excluding non-forested areas and stands dominated by other tree species).

Table 3.4: Threshold limits and the range of vegetation indices.

	Defoliation (%)		
Index	10	35	70
dMID	−222	−599	−949
dMSI	−125	−295	−453
dNDMI	963	2081	3121
dNDVI	743	1636	2466
dNBR	1034	2172	3229

high correctly represented the observed class. Overall, it should be noted that the number of cells classified as nil or medium defoliation was overestimated whereas the one classified as low or high defoliation was underestimated. Finally, the overall accuracy of the classification was 72% calculated by the ratio between the sum of the cells correctly classified from each class and 50 cells in total.

Table 3.5: Confusion matrix of a threshold classification using 50 pixel values of dMSI predicted from Landsat 8 in reference to four classes observed from UAV.

		Predicted (Landsat 8)					
	Class	Nil	Low	Medium	High	Total	Producer's Accuracy
Observed (UAV)	Nil	9	1	0	0	10	0.90
	Low	2	17	4	0	23	0.74
	Medium	0	3	4	1	8	0.50
	High	0	0	3	6	9	0.67
	Total	11	21	11	7	50	
	User's Accuracy	0.82	0.81	0.36	0.86		0.72

3.4 Discussion

Among five VIs tested in our study, the results with dMSI as the best predictor were consistent with recent studies on insect defoliations (Townsend et al., 2012; Sangüesa-Barreda et al., 2014; Rullán-Silva et al., 2015; Zhu et al., 2018). The SWIR band calculated in dMSI is known to be a good indicator for the plant moisture content in addition to the plant stress detected in the NIR band (Vogelmann et al., 2009; Rullan-Silva et al., 2013). It may be assumed that the MSI better indicated early symptoms of the host trees stressed by dehydration in our study. The first study examining MSI in relation to conifer damage was conducted by Vogelmann (1990), resulted with an R^2 of 0.830 in linear regression. Other studies with MSI have been conducted in pine forests by Sangüesa-Barreda et al. (2014) demonstrating the highest significance on ANOVA tests and most recently by Zhu et al. (2018) with an R^2 of 0.982 in logistic regression. The MSI was also effectively applied to defoliation in deciduous forests by Townsend et al. (2012) with an R^2 of 0.844 in logistic regression and Rullán-Silva et al. (2015) with an R^2 of 0.632 in sigmoidal mixed-effects models. For monitoring coniferous forests in general, the MSI has been found to be more effective than the NDVI which has been mainly applied to deciduous forests (Vogelmann, 1990; Vogelmann et al., 2009; Zhu et al., 2018). Nevertheless, several potentially robust VIs should be tested on each particular study area since tree-insect relationships vary from site to site (Rullan-Silva et al., 2013).

Our initial attempt was to use sketch map polygons from field data as training samples for supervised classification on the severity of defoliation. However, the significant discrepancy in spatial resolution between the field data provided by regional rural agents and Landsat data became evident. The sketch map polygons were delineated for classifying severity levels at a coarse scale in hectares including non-forested areas whereas the spatial resolution of Landsat imagery is as fine as 30 m per pixel, which resulted in a wide range of values among pixels within the same polygon. Yet, without any ground observation such as nests of *T. pityocampa*, it is often difficult to distinguish the cause of defoliation based on only spectral bands or even aerial surveys at low levels of defoliation (De Beurs and Townsend, 2008). Further integration by training the rural agents to apply UAV workflows to their annual health survey may fill this monitoring gap. As suggested in the most recent review on forest health monitoring by Hall et al. (2016), how spaceborne and airborne remote sensing may be integrated with aerial and field surveys into a

multi-scale, multi-source monitoring system should be explored.

Regarding stand dynamics and species compositions, we extracted pine-dominated stands from the Land Cover Map of Catalonia (MCSC) and assumed that sampled stands were dense enough to represent Landsat VIs based on the defoliation degree of dominant species in pine stands. Nonetheless, we acknowledge the possibility of misrepresenting the VIs in severely defoliated stands to some extent where understory species is non-host evergreen such as *Q. ilex* which is not affected by *T. pityocampa*. In such cases, healthy understory trees below defoliated pine trees may have reflected more greenness at the stand level. Moreover, it is also possible to overestimate the defoliation degree in stands mixed with non-host deciduous trees shedding their leaves in winter (Hall et al., 2016). This issue of overestimating or underestimating the impacts on host trees can be minimized by discrimination of deciduous species by detecting spectral variations due to vegetation phenology with Landsat time-series approach such as LandTrendr which can monitor cumulative defoliation as well as annual defoliation (Senf et al., 2017) while the satellite-based spatial resolution is not high enough to identify individual trees. Thus, for species identification at the tree level recent studies with UAV-derived multispectral bands and the associated indices (Torresan et al., 2017) may be further investigated to discriminate only those species of interest for calibration and validation of defoliation degrees.

Regression analysis may be improved by increasing the sample size in each severity category or the number of predictive parameters, or testing transformed dVIs (Miller and Thode, 2007; Parks et al., 2014; Pla et al., 2017). One simple way to increase the sample size can be achieved by reducing the cell size for sampling VIs from 30 m in Landsat 8 to 20 m in Sentinel-2 imagery. As multiple predictive parameters climate data (temperature and precipitation) or topographic features (elevation, slope and orientation) may be considered to improve the coefficient of determination in regression models. Moreover, we may introduce the number of nests formed by *T. pityocampa* as an additional predictive parameter to estimate the infestation severity as recent studies with the UAV technology have attempted to examine the severity of infestation at the individual branch level (Cardil et al., 2017; Hentz and Strager, 2017). However, the number of nests captured by UAV images from the air may be potentially underestimated if some nests on lower branches or in dense stands are not counted. Regarding observed parameters, our assessment on UAV-derived defoliation levels (%) was limited to manual photointerpretation, including shadows where some uncertainty remains. The automated removal of shadow pixels should be explored in future studies by testing various thresholds on spectral bands.

Threshold classification based on regression models in this study was one method to generate the defoliation severity map with the advantage of increasing or decreasing the number of classes by changing threshold limits of dVI (X) corresponding to the continuous defoliation degree (Y). Other classification methods using non-parametric algorithms may be taken into further consideration with a larger sample size to find the optimal method among unsupervised (ISODATA, K-means), supervised (maximum likelihood), and machine learning such as Random Forest, Decision Trees, k-Nearest Neighbor, and Support Vector Machine (Noi and Kappas, 2018). In general, those studies based on non-parametric models demonstrated that the classification accuracy significantly increased when the number of classes decreased (Näsi et al., 2015; Torresan et al., 2017).

Tradeoffs between spatial, temporal, and spectral resolution are critical to determine classification specific to case study. In our study sketch map polygons served as the primary information to filter affected areas most likely by *T. pityocampa* despite low spatial and temporal resolution. The defoliations over winter due to *T. pityocampa* can be discriminated by seasonal activity from other potential causes for defoliations during summer such as drought and summer-feeding insects (Zhu et al., 2018). Satellite-based Landsat imagery, at medium spatial and temporal resolution, enabled us to calculate various dVIs due to high spectral resolution. While Landsat has the advantage of allowing time-series analysis from the data archive to track back to 1972 (NASA, 2019), the use of Sentinel-2 has been recently increasing since its launch in 2015 due to the public access available at the higher temporal, spatial and spectral resolution (every 5 days at 10 m, 20 m, or 60 m for 13 bands) (ESA, 2015) than that of Landsat 8 (every 16 days at 15 m, 30 m, or 100 m for 11 bands). As shown in Figure 4, those dVIs at medium spatial resolution need to be calibrated with field observations to estimate the severity classification at a regional scale. Thus, UAV imagery observed at high spatial and temporal resolution may improve the efficiency of such calibration. Yet, current limitations of UAV technology include battery duration for 20–30 min, associated small area coverage for sample images per flight, and imagery acquisition permission due to privacy issues specific to some countries (Lehmann et al., 2015; Torresan et al., 2017). To cover a large area at landscape and regional scales, it would require multiple flights that may not be consistent with the time, sensor and weather conditions, therefore, it would not replace satellite-based imagery.

Nonetheless, the latest UAV can obtain dense point clouds and multispectral bands (sensors for red edge, NIR and SWIR outside the visible spectrum), which may be a promising technology with a high spatial and spectral resolution for small-scale forestry applications. Using the density of points at a tree level, as successfully demonstrated by Näsi et al. (2015), the structural change in individual trees may be detected and monitored for cumulative defoliation. While some studies (Garcia-Ruiz et al., 2013; Gini et al., 2014; Näsi et al., 2015; Michez et al., 2016) have used the UAV-derived NDVI as the most robust indicator for their analysis on insect defoliations, future studies shall compare it to the UAV-derived MSI which can be calculated from SWIR in the latest sensor technology. Where high spectral resolution is not required for small operational areas, compared to using both satellite and UAV imagery, preparing a UAV flight would greatly increase the time-efficiency and cost-effectiveness as well as flexibility in planning imagery acquisition (Lehmann et al., 2015; Näsi et al., 2015; Dash et al., 2017). In addition to such advantages as alternative methods for generating orthomosaic images and calculating VIs from multispectral bands, the use of UAVs enables to avoid clouds during flights, which often cannot be controlled by satellite orbit scheduling (Näsi et al., 2015; Dash et al., 2017). Thus, with relatively less efforts and lower costs, UAV imagery may increase the spatial quality to be equivalent to ground-truth data.

3.5 Conclusions

In this study the difference in vegetation index between pre-outbreak and post-outbreak images derived from Landsat imagery was calculated for estimating the severity of defoliation. Although satellite data was calibrated with the limited num-

ber of UAV images including photos and videos available from the study area, dMSI among five satellite-derived vegetation indices resulted in the best-fit logistic regression model with an acceptable overall accuracy of 72% for the severity classification. Therefore, the use of UAV images may hold great potential as an alternative cost-effective method to other conventional ground-truth data. In future studies, new additional UAV images should be incorporated to validate previously calibrated results in the same study area or adjacent areas affected by *T. pityocampa*. Upon validation the best-fit dVI model may become a robust tool to estimate the severity of defoliation for areas where ground-truth data is limited.

Chapter 4

Article 2: Quantifying pine processionary moth defoliation in a pine-oak mixed forest using unmanned aerial systems (UAS) and multispectral imagery

Abstract
Pine processionary moth (PPM) feeds on conifer foliage and periodically result in outbreaks leading to large scale defoliation, causing decreased tree growth, vitality and tree reproduction capacity. Multispectral high-resolution imagery acquired from a UAS platform was successfully used to assess pest tree damage at the tree level in a pine-oak mixed forest. We generated point clouds and multispectral orthomosaics from UAS through photogrammetric processes. These were used to automatically delineate individual tree crowns and calculate vegetation indices such as the normalized difference vegetation index (NDVI) and excess green index (ExG) to objectively quantify defoliation of trees previously identified. Overall, our research suggests that UAS imagery and its derived products enable robust estimation of tree crowns with acceptable accuracy and the assessment of tree defoliation by classifying trees along a gradient from completely defoliated to non-defoliated automatically with 81.8 percent overall accuracy. The promising results presented in this work should inspire further research and applications involving a combination of methods allowing the scaling up of the results on multispectral imagery by integrating satellite remote sensing information in the assessments over large spatial scales.

4.1 Introduction

The area covered by forest ecosystems in the Mediterranean has increased during the last century due to land abandonment and climate change impacts, which have led to significant changes in forest dynamics (Resco De Dios et al., 2007; Filho et al., 2017; Lasanta et al., 2017). These forest changes increase in the effects of pests on trees, partially due to more frequent large-scale outbreaks becoming an increasingly important disturbance in forest dynamics (Cayuela et al., 2011; Cardil et al., 2017). Amongst these pests we can highlight the increasing impact of the

pine processionary moth (*Thaumetopoea pityocampa* Dennis and Schiff.,Lepidoptera: Notodontidae; henceforth PPM), one of the main pests of *Pinus* sp., a native species of the Mediterranean region including North Africa, southern Europe and some areas of the Middle East (Hódar et al., 2004). Life cycle is characterized by a one-year development cycle for short-lived female moths which typically live for 1 or 2 days and longer-lived males (Battisti and Larsson, 2015). The cycle involves adult emergence in summer (June–September), larval feeding during fall and winter, and pupation in soil followed by a short or prolonged diapause up to several years under specific circumstances (Jactel et al., 2006; Cayuela et al., 2011; Tamburini et al., 2013; Battisti and Larsson, 2015). The area affected by PPM in Europe is expanding northwards to higher latitudes and upwards to higher altitudes from where it was absent, probably as a result of increasing winter temperatures (Hódar et al., 2004).

PPM caterpillars feed on conifer needles resulting in a general weakening of trees and eventually cause large scale defoliation at the stand and landscape levels. Intense defoliation negatively affects height and radial tree growth, increase the mortality rate of saplings and reduce the reproduction capacity of trees (Hódar et al., 2003; Kanat et al., 2005; Arnaldo et al., 2010). At the same time, PPM can trigger a decrease in tree resistance and resilience against other disturbances such as forest fires, drought conditions or other pests (Post, 2003; Moore and Allard, 2008; Cardil et al., 2017) that could influence and modify the tree species composition in mixed forests. PPM damages are associated with the spatial and temporal complexity of Mediterranean landscapes, as well as with its life cycle. Regarding the spatial complexity, trees in fragmented small stands suffer PPM damage with varying intensities. However, the current pattern of outbreaks at landscape level is still largely unknown (Cayuela et al., 2014). Regarding the temporal complexity, PPM defoliation is maximum at the beginning of spring. During the spring and summer, if weather conditions are not extremely stressful, the vegetation generally recovers its initial greenness. There is also lack of knowledge about the effects of forest diversity and mixed versus monospecific forests on overall pest tree damage (Guyot et al., 2016). Several studies showed that diverse forests are less prone to pest insects than monoculture forests (Jactel and Brockerhoff, 2007), which suggests associational resistance (Barbosa et al., 2009). However, recent studies also reported more damage in mixed forests suggesting associational susceptibility (Schuldt et al., 2010), or simply no effect of diversity (Haase et al., 2015). However, recovery time appears to depend on the site characteristics of each forest (Sangüesa-Barreda et al., 2014). Thus, quantifying defoliation processes at landscape level is key to improve the knowledge of PPM damage patterns and consequently to better guide control measures or improve ecological conditions to increase forest resistance and resilience to this kind of damages.

Historically, the degree of infestation and mortality by PPM in pine stands (Jactel et al., 2006; Battisti, 2008; Cayuela et al., 2014) has been visually assessed in the field (Hódar et al., 2003) by forestry technicians or through interpretation of aerial photographs (Rullan-Silva et al., 2013). However, field inventories are expensive and require a large amount of manpower and resources while aerial photographs taken in periods relevant to assess PPM impacts are not always readily available or may lack sufficient temporal details. In addition, visual interpretation can be subjective if not carefully validated and may not always provide the re-

quired quantitative information when assessing spatial variability in PPM impacts. More recently, multi-temporal satellite images and remote sensing products such as Landsat Thematic Mapper (TM), Moderate Resolution Imaging Spectroradiometer (MODIS), TerraSAR-X and light detection and ranging (LiDAR), have been extensively used in monitoring forest health attacks by pest insects (Wulder et al., 2006; Kantola et al., 2013; Ortiz et al., 2013; Rullan-Silva et al., 2013) and found to be useful for insect outbreak surveys at large scale (Näsi et al., 2015). Yet, even these medium-resolution remote sensing products have been unable to capture the spatial heterogeneity in agroforestry mosaics or complex defoliation patterns caused by PPM at local scale (Näsi et al., 2015) and, especially, in mixed forests at tree level.

Currently, unmanned aerial systems (UAS) platform have also become suitable tools to perform small-scale analyses as well as local-scale sampling, assessment and validation that can be complemented and integrated with aerial or satellite imagery for broader spatial scale analyses (Puliti et al., 2017; Dash et al., 2018). Most recent years have experienced an enormous increase in the use of UAS due to low infrastructure requirements, ease of deployment, acquisition and suitability for photogrammetric workflows (Whitehead and Hugenholtz, 2014; Puliti et al., 2015). The current availability of photogrammetric software allows for handling and processing of large spatial datasets. UAS have been applied in fine-scale studies to inventory forest resources (Puliti et al., 2015), map diseases (Dandois and Ellis, 2013), assess pest damages at tree level (Lehmann et al., 2015; Näsi et al., 2015; Cardil et al., 2017; Dash et al., 2017) and at the landscape level (Hung et al., 2014; Feng et al., 2015), quantify spatial gaps or estimate post-harvest soil displacement (Torresan et al., 2017). UAS platforms are establishing a niche in low cost image acquisition at local scales that make this technology an alternative cost-effective option in forestry applications. However, most common cameras employed in UAS surveys are digital RGB cameras (Zhang et al., 2016), or are adapting one of the visible bands for NIR imagery acquisition (Puliti et al., 2015). To date, only a few studies with multispectral cameras such as Tetracam ADC Lite, MicaSenseRedEdge (Tian et al., 2017) or SEQUOIA (Parrot SA, Paris, France) (Fernández-Guisuraga et al., 2018) have demonstrated improvements in the analysis of fine-scale forest dynamics.

In this study, we aimed at evaluating the potential use of multispectral high-resolution imagery acquired from a UAS platform and image processing techniques to quantitatively assess PPM impact on a pine-oak mixed forest. To achieve this objective, we used point clouds and multispectral orthomosaics from UAS generated through photogrammetric processes. Point clouds have proven useful to generate high resolution digital surface models (DSM) from which it is possible to automatically identify and delineate individual trees (Puliti et al., 2015, 2017; Mohan et al., 2017). We hypothesized that multispectral information will enable us to calculate vegetation indices such as NDVI to objectively quantify the degree of defoliation of the pines previously delineated from DSM (Deshayes et al., 2006; Townsend et al., 2012; Sangüesa-Barreda et al., 2014) after identifying tree species (Gini et al., 2014; Michez et al., 2016). Field data was used to validate our results and assess the level of detail and accuracy of our method to investigate the spatial dynamics of the pest. More precisely, the presented study attempts to develop a method using high resolution multispectral images collected with UAS to automatically quantify defoliation by PPM for individual trees and classify them as non-defoliated, partially defoliated

and completely defoliated in a pine-oak mixed forest.

4.2 Materials and methods

4.2.1 Study area

The study was conducted in Codo site (longitude = 1.544°; latitude = 42.127°; altitude = 1300m), a mixed forest area located near the city of Solsona (Lleida, Catalonia, NE Spain, Figure 4.1) dominated by holm oaks (*Quercus ilex* L.) and Scots pines (*Pinus sylvestris* L). The dimension of the study area was 350 x 350m (12.25 ha) representing a Mediterranean climate zone characterized by hot dry summers and mild wet winters.

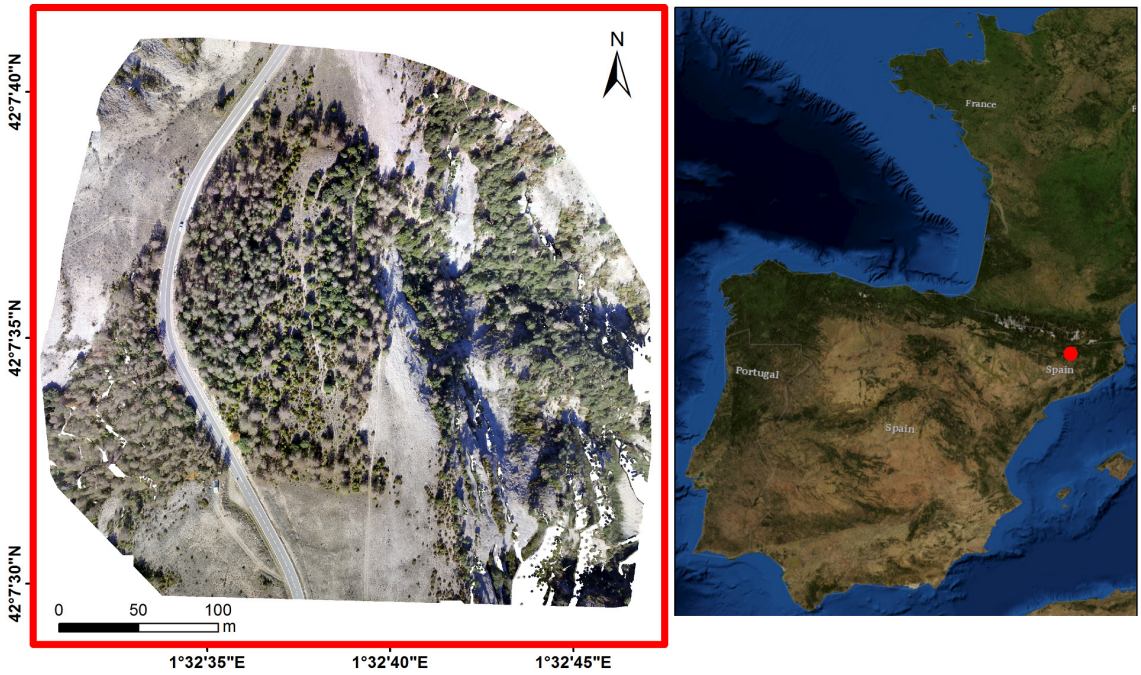

Figure 4.1: An RGB orthomosaic of the study are, Codo in Catalonia (Spain). Base map source: USGS National Map Viewer.

4.2.2 UAS-based image acquisition and data preprocessing

Multispectral high spatial resolution image data was collected using a quadcopter (UAS Phantom 3 from DJI) in two successive flights with one hour gap between both. This UAS is capable of autonomous, waypoint flight following a preplanned route. In the first flight, the UAS was equipped with the multispectral camera Parrot SEQUOIA and, in the second with RGB PC300S Phantom 3 camera, to create RGB orthomosaics. The Parrot SEQUOIA camera has four 1.2-megapixel monochrome sensors that collect global shutter imagery along four discrete spectral bands: green (center wavelength -CW- : 550 nm; bandwidth -BW- : 40 nm), red (CW: 660 nm; BW: 40 nm), red edge (CW: 735 nm; BW: 10 nm) and near infrared -NIR- (CW: 790 nm; BW: 40 nm). The horizontal (HFOV), vertical (VFOV) and diagonal (DFOV) fields of view of the multispectral camera are 70.6°, 52.6° and

89.6°, respectively, with a focal length of 4 mm. With a flight altitude of 120 m and an image overlap of 80%, a ground sample distance (GSD) of 15 cm was achieved. The camera was bundled with an irradiance sensor to record light conditions in the same spectral bands as the multispectral sensor. The total weight of the multispectral camera with the irradiance sensor is 107 g. This camera stored 16-bit RAW files (based on 10-bit data) during image shooting. The ISO value and exposure time were set to be automatic. Every image capture setting was saved in a text metadata file together with the irradiance sensor data. The text metadata files register information about ISO, aperture, shutter speed, sensor response and optical system and vignetting. The optical system and vignetting are registered by the irradiance sensor. Additionally, irradiance panels available by AIRINOV photos were taken at the beginning of the flight. An absolute reference for each spectral band was set through the calibration target, which allow getting absolute reflectance values. The aerial survey was carried out on November 26th, 2017 within one hour of the solar zenith in a clear sky and no winds. Finally, a total of 202 SEQUOIA photographs were collected to cover the study area of Codo.

Pix4Dmapper desktop photogrammetric software (https://pix4d.com/; accessed on 2 April 2018) following the "Ag Multispectral" template was used to generate point clouds, 3D reconstruction, radiometric calibrations and correction and finally the orthomosaics. This software integrates vision techniques with photogrammetry algorithms Puliti et al. (2015) to obtain high accuracy in aerial imagery processing. Pix4Dmapper Pro computes key points on the single images and uses them to find matches between images. From these initial matches, the software runs several automatic aerial triangulation (AAT), bundle block adjustments (BBA) and camera self-calibration steps iteratively until optimal reconstruction is achieved (Fernández-Guisuraga et al., 2018). Then, a densified point cloud is generated to obtain a highly detailed digital surface model (DSM) that will be used to generate the final reflectance orthomosaics maps for every plot. The reflectance maps were achieved applying radiometric calibrations and corrections. First, the images of the irradiance panels taken at the beginning of the flight allow the radiometric calibration. Second, we also applied a "Camera and Sun irradiance" radiometric correction to correct for factors that distort the true reflectance pixel values and achieving a radiometric trustful measure of the terrain reflectance taking into account the information registered in the text metadata files (EXIF and XMP tags) for every single photogram. Pix4Dmapper applies this calibration and correction process to every single photogram just before achieve the final reflectance orthomosaic for every spectral band. Once the radiometric corrections were done for every photogram, the final orthomosaic was generated through automated workflows and SFM (structure from motion) methods (Lucieer et al., 2014) with image identification and feature matching. After the initial alignment through bundle adjustment, the resultant sparse cloud was assessed for projection errors, followed by reconstruction of dense point clouds using the cartographic UTM projection system. With original photos projected onto the 3D models, blending the overlap areas produced the reflectance orthomosaic for each spectral band.

The UAS-derived 3D point cloud was used to compute a digital terrain model (DTM) and a canopy height model (CHM) based on the approach developed by Mohan et al. (2017) (Figure 4.2). First, one m DTM was created using the GridSurfaceCreate function in FUSION/LDV 3.42 (Kraus and Pfeifer, 1998) after classifying

ground points using a progressive Triangulated Irregular Network (TIN) densification algorithm implemented in lasground (settings: step is 10 m, bulge is 0.5 m, spike is 1 m, offset is 0.05 m), LAStools (Isenburg, 2015). Secondly, the UAS-derived 3D point cloud was normalized to height above ground by subtraction of the DTM elevation from the Z coordinate of each point projected on the ground using the ClipData tool. Lastly, the CanopyModel function, also in FUSION/LDV, was used to compute the CHM at 0.5 m spatial resolution for the study site.

4.2.3 Field validation data

A randomly selected sample of 110 trees from the Codo forest was acquired through a visual assessment at tree level (Figure 4.3). The sample consisted of 25 holm oak (they were excluded from the analysis to assess percentage of defoliation at tree level because they were not defoliated), 13 non-defoliated pines, 29 partially defoliated pines and 43 completely defoliated pines depending on the level of defoliation. Pines were classified as non-defoliated, partially defoliated and completely defoliated trees when having defoliation <15%, between 15% and 85%, and >85%, respectively.

4.2.4 Data analysis

Individual tree identification and delineation (ITDe)

The rLiDAR package (Silva et al., 2017) in R (R Core Team, 2016) was used in this study for individual tree delineation and defoliation assessment on the UAS-derived CHM. First, the FindTreesCHM function from this package, based on a local maximum algorithm, was applied for automatic detection of tree tops on the UAS-derived CHM using fixed tree and smoothed window sizes of 3 x 3 pixels. Secondly, the ForestCAS function from the same package, based on the Voronoi tessellation (Aurenhammer, 1991), was applied for individual tree delineation (ITDe) on the UAS-derived (Figure 4.1) based on Silva et al. (2017). Independently, the 110 randomly selected trees in the field were manually onscreen-digitized on the orthomosaic image in order to assess the accuracy of the automatic ITDe and compare the results obtained with this method in terms of PPM defoliation. We analyzed spatial discrepancies in each tree between ITDe and manual tree crown delineation (MCDe) by using the Sørensen's coefficient (SC) (Legendre and Legendre, 1998) calculated as follows:

$$SC = \frac{2A}{2A + B + C} \tag{4.1}$$

where A is the area coded as "tree crown" for both ITDe and MCDe, B is the area coded as "tree crown" in the ITDe and "no crown" in the MCDe and, C is the area coded as "tree crown" in the MCDe and "no crown" in the ITDe. SC coefficient values range between 0 and 1, with values close to 1 indicating very high spatial agreement between the variables.

Tree species identification and defoliation assessment based on NIR and RGB imagery

In addition to visible bands in RGB images, the near-infrared (NIR) reflectance of the multispectral camera was use for tree species identification and defoliation

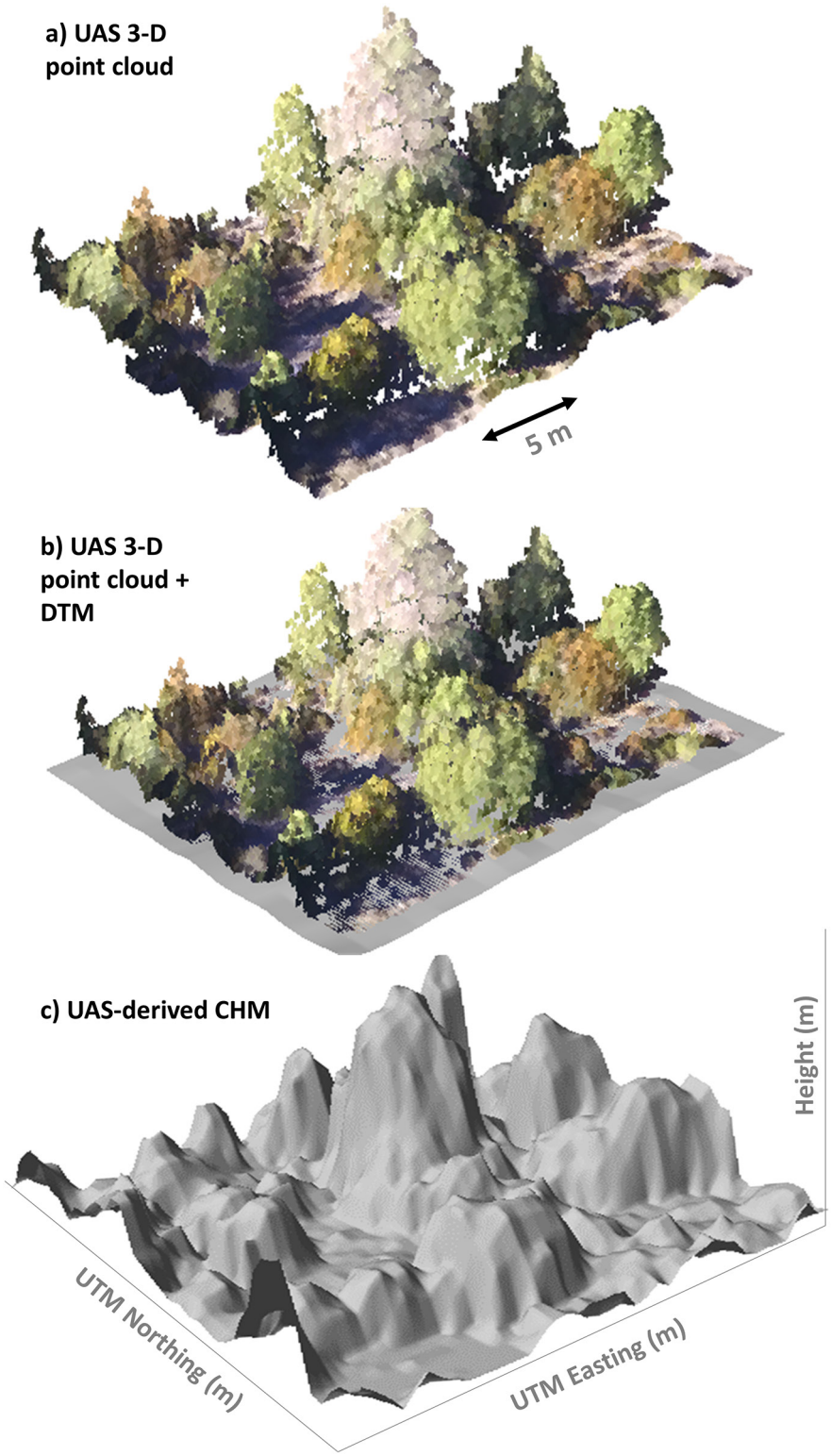

Figure 4.2: A canopy height model (CHM) derived from UAS-derived 3D point cloud and a digital terrain model (DTM). (a) UAS-derived 3D point cloud. (b) Digital terrain model. (c) Canopy height model.

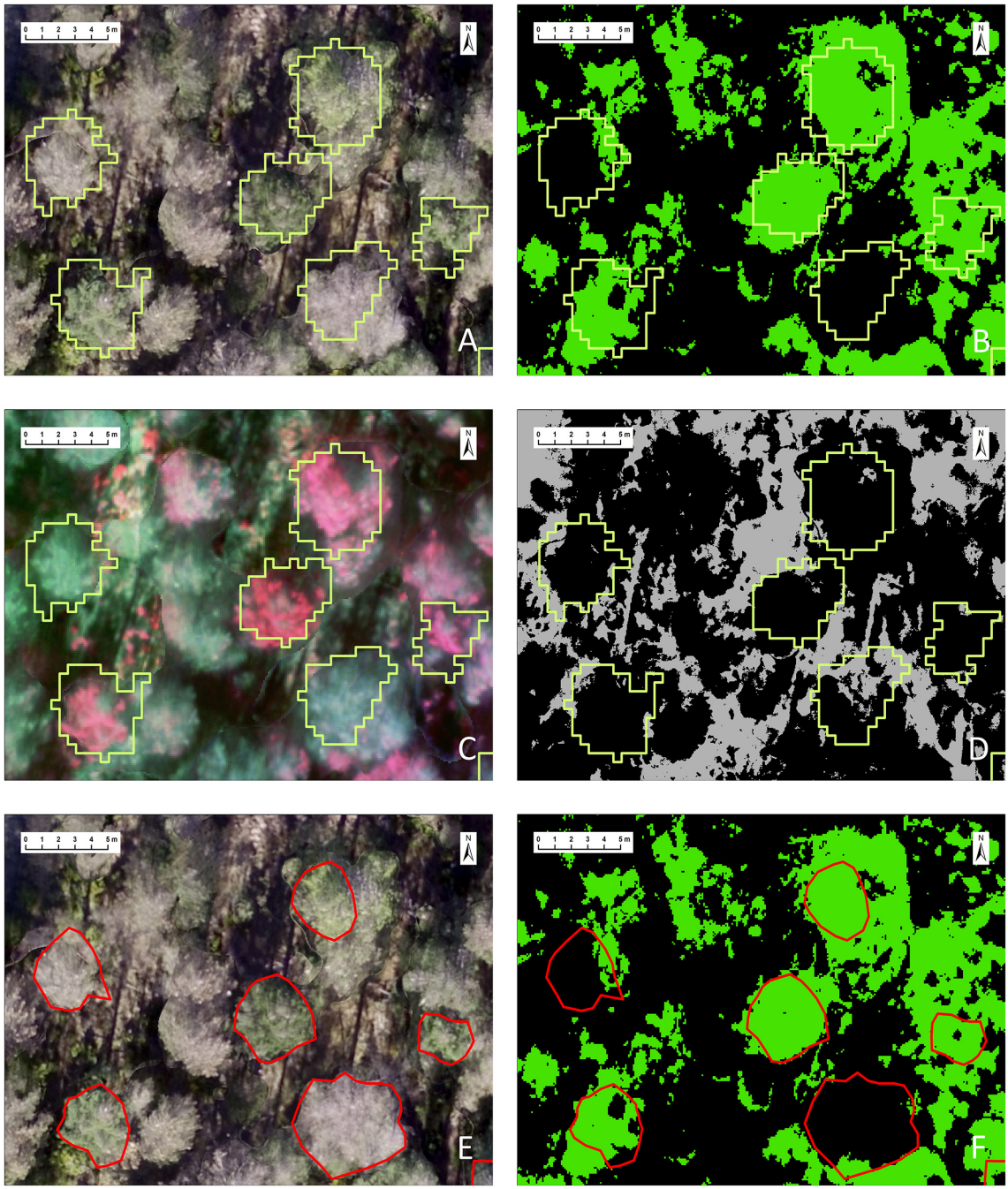

Figure 4.3: Object-based image analysis. (a) RGB orthomosaic image with crown surfaces delineated by ITDe. (b) Image classification with NDVI for non-defoliated (in green) surfaces and defoliated / non-vegetation background (in black) with ITDe. (c) Colour-infrared composite using green, red and nir reflectance bands with crown surfaces delineated by ITDe. (d) Unsupervised classification with ExG for isolating shaded pixels (in grey). (e) Manual digitization of tree crowns (MCDe) for validating the results by ITDe. (f) Image classification with NDVI for non-defoliated (in green) surfaces and defoliated / non-vegetation background (in black) with MCDe.

detection as a stress indicator, which may measure plant health more precisely than visibly evident greenness (Wang et al., 2010; Townsend et al., 2012; Rullan-Silva et al., 2013). Thus, we considered normalized difference vegetation index (NDVI), a ratio between the red (R) and NIR values, as potentially the most robust and widely tested indicator in order to predict the tree species and defoliation degree (Rullan-Silva et al., 2013).

$$NDVI = \frac{NIR - R}{NIR + R} \tag{4.2}$$

In order to separate the vegetation from the background to assess PPM defoliation, excess green index (ExG) was calculated in this study. Previous studies successfully applied this index together with NDVI to image classification in their object-based image analysis (OBIA) (Torres-Sánchez et al., 2015; Lottes et al., 2017).

$$ExG = 2\left[\frac{G}{R+G+B}\right] - \frac{R}{R+G+B} - \frac{B}{R+G+B} \tag{4.3}$$

After automatically identifying and delineating tree crowns of the 110 selected trees, we identified tree species by using the mean NDVI of pixel values for each of the delineated crown. The default threshold value to classify the selected trees as holm oak (NDVI >0.42) or pine (NDVI <0.42) was selected by sensitivity analysis on the NDVI range in comparison with field data (increasing by 0.01) considering the mean NDVI of pixel values per each delineated crown.

Image classification with NDVI was first processed for separating defoliated crown surfaces from non-defoliated ones by threshold analysis. The default threshold value was selected by automated unsupervised classification and compared to sensitivity analysis on the NDVI range (increasing by 0.01) against the orthomosaic images. Then threshold classification was applied at the pixel level: defoliated in black (NDVI <0.27) or non-defoliated in green (NDVI >0.27) as illustrated in Figure 4.3b.

It was noted that some shaded pixels in the RGB orthomosaic image, corresponding to dark grey-black areas by heavy shadowing in Figure 4.3a, were not visually distinguishable between defoliated and non-defoliated crown surfaces. Therefore, we decided to exclude those from thresholding with NDVI for the purpose of effectively validating classification accuracy. Since NDVI in general can detect non-defoliated leaves in shaded pixels (Lottes et al., 2017), it was not successful to achieve the threshold value of NDVI for isolating shaded pixels exclusively. However, calculating such specific vegetation index as ExG enabled automated isolation of shaded pixels by unsupervised classification, where ExG is lower than -0.06 (Figure 4.3d). Finally, we applied another class 'shaded' to automatically mask all shaded pixels, regardless of the NDVI value, so that those pixels were excluded from the crown surface area for further analysis.

To evaluate the accuracy of threshold classification (defoliated, non-defoliated, shaded), we show a confusion matrix by assessing 100 pixels that were randomly selected and visually interpreted against the orthomosaic image. The overall classification accuracy between classified imagery and reference imagery was calculate as:

$$\text{Accuracy } (\%) = \frac{\text{number of pixels correctly classified}}{\text{total number of pixels referenced}} \tag{4.4}$$

We systematically quantified the percentage of defoliation by PPM in each pine by using both the automatic ITDe and the MCDe (Figure 4.3b and 4.3f). For evaluating the overall defoliation degree at tree level, pixels classified as defoliated were grouped by tree ID and calculated as follows:

$$\text{Defoliation per tree (\%)} = \frac{\text{number of defoliated pixels}}{\text{sum of defoliated and non-defoliated pixels}} \tag{4.5}$$

We statistically analyzed relationships between the predicted defoliation degree with NDVI (X) and the observed defoliation % on the orthomosaic image (Y). The relationship is expressed in linear regression:

$$Yi = aXi + b \tag{4.6}$$

where Yi represents the percentage of defoliation per tree interpreted on the orthomosaic image, Xi represents the portion of pixels classified as defoliated with NDVI per tree, and a and b are the slope and intercept of the regression line. Based on the same 110 selected sample trees from the study area used to MCDe, linear regression models were fitted to evaluate both the slope of the regression line and coefficient of determination (R^2).

Accuracy of defoliated tree identification and validation of percent defoliation

To assess image classification accuracy in our PPM defoliation estimates at tree level and to distinguish between non-defoliated, partially defoliated and completely defoliated trees, we computed a confusion matrix of the 110 selected trees that were field identified and compared them with the obtained image classifications. Validation of the defoliation classification was performed by comparing field measured defoliation against the classification derived defoliation at tree level using both ITDe (Figure 4.3a and 4.3b) and MCDe (Figure 4.3e and 4.3f).

4.3 Results

4.3.1 Accuracy of the individual tree detection and species identification

The algorithm on the UAS-derived CHM effectively detected individual trees. The algorithm correctly identified all the 110 trees randomly selected through the field survey (Figure 4.4a). The accuracy of the automatic ITDe was also analyzed in comparison to the MCDe on the orthomosaic. The overall spatial agreement of crown area for the 110 selected trees was high with a mean SC of 0.75 and a standard deviation of 0.11.

The NDVI-based tree species identification after identifying and delineating tree crowns was effective. We found significant differences in the mean NDVI of pines and holm oaks (p-value <0.001; Figure 4.5a) and among non-defoliated, partially defoliated and completely defoliated pines and holm oaks at the same statistical significance (Figure 4.5b). All pines were correctly classified by the method. However, 5 of 25 holm oaks were wrongly identified, being classified as healthy pines (Tables

4.1 and 4.2). Therefore, the overall rate of success to identify the tree species was 95.5%.

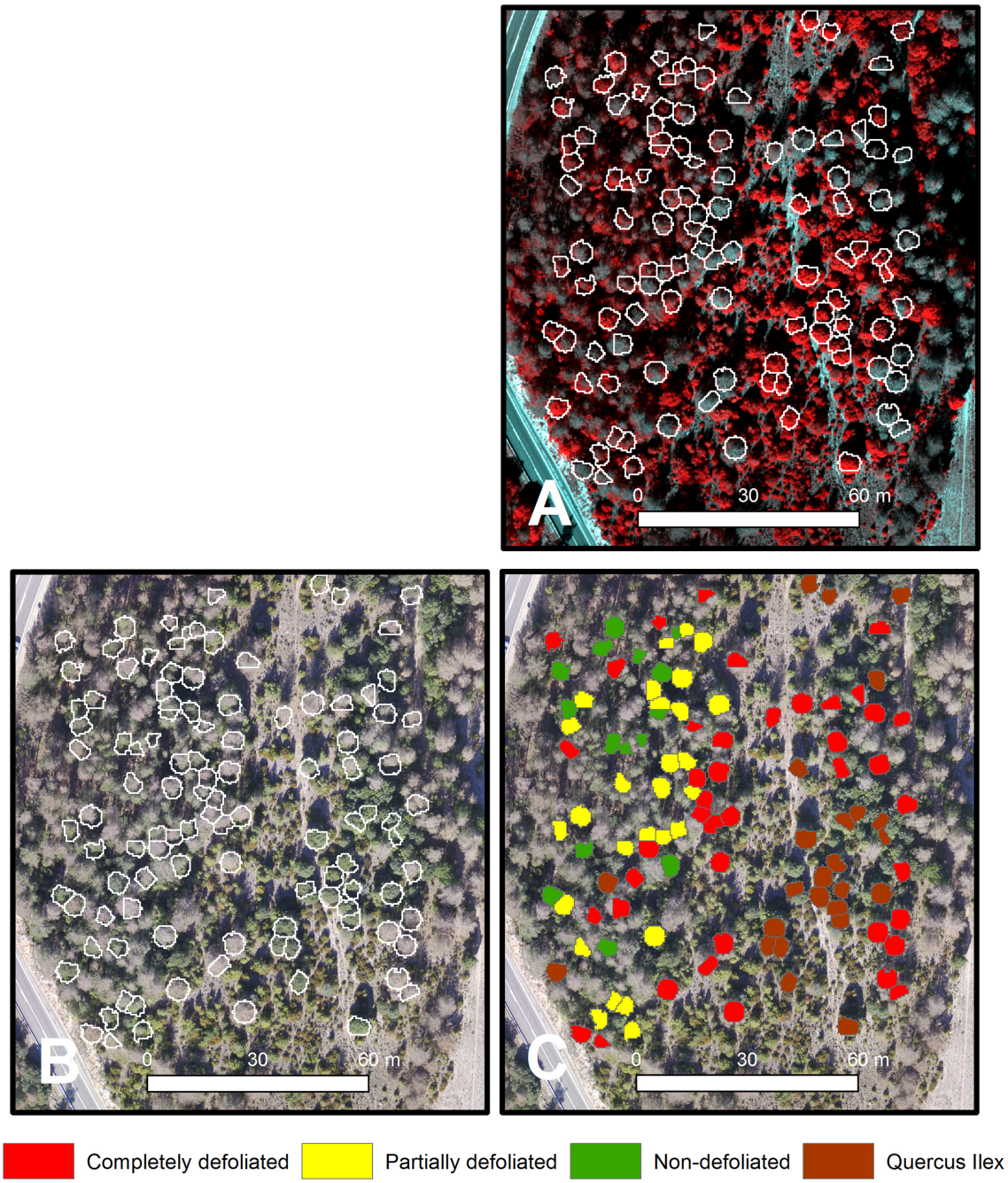

Figure 4.4: Tree species identification and pine processionary moth defoliation in pines in the Codo forest site. (a) Individual automatic tree delineation on the colour-infrared composite orthomosaic using green, red and NIR reflectance bands. (b) Individual automatic tree delineation on the RGB orthomosaic. (c) Automatic tree classification in the field as holm oak or non-defoliated, partially defoliated and completely defoliated pine through multispectral high-resolution imagery.

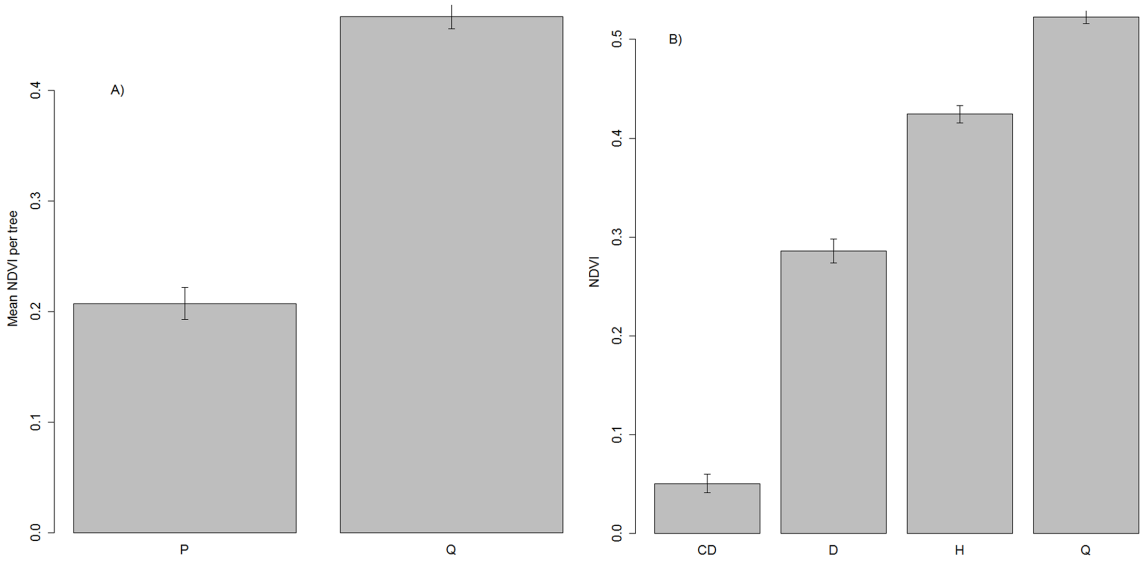

Figure 4.5: Mean NDVI at the tree level. (a) Mean NDVI values and standard error for pines (P) and holm oaks (Q). (b) completely defoliated (CD), partially defoliated (D) and non-defoliated pines (H) and holm oaks (Q) of the 110 randomly selected trees.

Table 4.1: Confusion matrix for non-defoliated, partially defoliated and completely defoliated trees measured in the field or classified by using the multispectral imagery with the automatic ITDe.

		Multispectral imagery with automatic ITDe					
	Class	Completely defoliated	Partially defoliated	Non-defoliated	Holm oak	Total	Accuracy (%)
Field	Completely defoliated	32	11	0	0	43	74
	Partially defoliated	0	28	1	0	29	97
	Non-defoliated	0	4	9	0	13	69
	Holm oak	0	2	3	20	25	80
	Total	32	45	13	20	110	
	Accuracy (%)	100	62	69	100		81

4.3.2 PPM defoliation at pixel level

We assessed the classification accuracy of the three defoliation classes (defoliated, non-defoliated, and shaded) by randomly selecting 100 pixels and validating with the reference of the orthomosaic image. The results were presented in a confusion matrix (Table 4.3). Out of the selected 100 pixels, 41 pixels were classified as defoliated with the NDVI threshold (NDVI = 0.27) while 34 were correctly classified as defoliated. Among 43 pixels classified as non-defoliated, 37 of them were correct (86%). Class 'shaded' found 10 out of 16 pixels correctly classified (62.5%). It should be noted that the number of pixels classified as defoliated was underestimated (omission errors) whereas the one classified as non-defoliated was overestimated (commission errors).

Table 4.2: Confusion matrix for non-defoliated, partially defoliated and completely defoliated trees measured in the field or classified by using the multispectral imagery with the manual onscreen-digitized tree segmentation (MCDe).

		Multispectral imagery with automatic ITDe					
	Class	Completely defoliated	Partially defoliated	Non-defoliated	Holm oak	Total	Accuracy (%)
Field	Completely defoliated	40	3	0	0	43	93
	Partially defoliated	2	24	3	0	29	83
	Non-defoliated	0	1	12	0	13	92
	Holm oak	0	1	4	20	25	80
	Total	42	29	19	20	110	
	Accuracy (%)	95	83	63	100		87

Table 4.3: Confusion matrix for classification assessment at the pixel level. The classified image was based on vegetation indices while RGB orthomosaic was used as the reference image.

		Classified image					
	Class	Defoliated	Non-defoliated	Shaded	Total	Accuracy (%)	Kappa
Reference image	Defoliated	34	4	6	44	77	
	Non-defoliated	3	2	10	16	63	
	Shaded	4	2	10	16	63	
	Total	41	43	16	100		
	Accuracy (%)	83	86	63		81	
	Kappa						69

The overall accuracy of classification was calculated as follows:

$$\text{Overall accuracy (\%)} = \frac{(34 + 37 + 10) \text{ pixels correctly classified}}{100 \text{ pixels in total}} = 81\% \qquad (4.7)$$

Finally, the kappa coefficient indicates a level of agreement of 69%.

4.3.3 PPM defoliation at tree level

The results of our method using UAS multispectral imagery and ITDe to classify trees as non-defoliated, partially defoliated and completely defoliated pines and holm oaks was related to the data of 110 randomly selected trees though the field survey in a confusion matrix to calculate accuracy (Table 4.1 and Figure 4.4). The overall accuracy of the classification was 81.8% (94.1% when combining partially defoliated and completely defoliated trees in the same category without considering holm oaks).

The method correctly distinguished all pines while 5 of the 25 holm oaks were wrongly classified as pines (Tables 4.1 and 4.2). All completely defoliated trees identified by this method were correctly classified. Among the 13 non-defoliated pines, 9 trees were correctly classified while 4 were wrongly classified as partially defoliated and none was classified as completely defoliated (Table 4.1). Although the classification accuracy for completely defoliated trees was 74% (Table 4.1), 11 completely defoliated trees in the field were classified as partially defoliated. The average percentage of defoliation of those trees was 74.8% and none of them was classified as non-defoliated.

The overall accuracy of classification with MCDe increased up to 87.2% of the 110 selected trees (95.2% when considering only non-defoliated and partially defoliated pines). Table 4.2 shows the accuracy for classifying the trees as non-defoliated, partially defoliated and completely defoliated pines or holm oaks by using the multispectral imagery with MCDe, which was overall higher than that with ITDe.

A linear regression model indicated the significant relationship between the percentage of defoliation measured through UAS multispectral images with ITDe or MCDe in pines and percentage of defoliation measured in the field (Figure 4.6). Our results showed that the relationship between the field measured defoliation and through UAS multispectral images with ITDe or MCDe was highly significant (p-value<0.001), and that the model's predictive accuracy was very high in both cases ($R^2 = 0.91$ for ITDe and $R^2 = 0.93$ for MCDe).

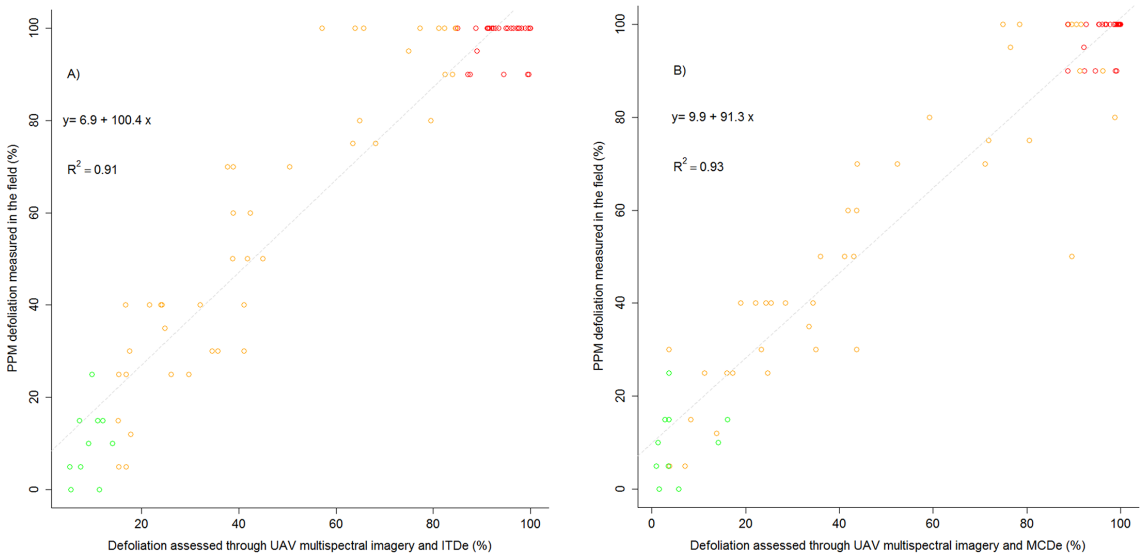

Figure 4.6: Linear regression model between PPM defoliation measured in the field and through UAS multispectral images in Codo forest site with ITDe (a) and MCDe (b). Green: non-defoliated trees; orange: partially defoliated; red: completely defoliated.

4.4 Discussion

Under a global change context with more frequent extreme climatic events (Jactel et al., 2006; Cardil et al., 2014, 2015; Robinet et al., 2014) PPM outbreaks are expected to become more frequent on Mediterranean coniferous and mixed forests.

In this context, effective monitoring techniques are urgently required over a large spatial scales. The use of UAS-based image acquisition technology is emerging research in assessment of forest pests such as the PPM over representative spatial and temporal scales. Furthermore, the acquisition of data through UAS may also be useful to complement, or even substitute field assessments with large scale quantitative evaluations when detailed results are required. Several authors have suggested low-cost image acquisition with UAS platforms as an alternative option to assess the percentage of defoliated trees and the level of defoliation in each tree quantitatively, and obtain promising validation results with field measurements (Näsi et al., 2015; Cardil et al., 2017). In this study, we have used RGB and NIR imagery to account for tree species and degree of defoliation in mix pine-oak stands. We identified pine and holm oak and classified pines as non-defoliated, partially defoliated and completely defoliated, after being identified and delineated by a local maximum algorithm on a CHM, as well as assessing the percentage of defoliation of each tree.

Our results showed that the use of UAS multispectral images through NDVI after automatically delineating tree crowns can be very useful for identifying tree species in mixed forests in order to assess PPM impacts on forests. The rate of success identifying the two tree species was very high on the 110 selected trees although further research would be needed to have a more robust methodology to be applied in other locations. In this sense, the combination of various metrics using the multispectral images, as well Green Normalized Difference Vegetation Index (GNDVI), Normalized Green-Red Vegetation Index (GRVI), Normalized Green-Blue Index (GBNDVI) or Normalized NIR-Blue Index (BNDVI), could improve the results (Lisein et al., 2015; Michez et al., 2016). Also, other recent studies used a larger sample size for species identification (Gini et al., 2014; Lisein et al., 2015; Michez et al., 2016), determining when is the best time window to achieve an optimal species discrimination, an approach that could be useful given the PPM life cycle.

Field validation showed that defoliation assessment through UAS multispectral images with ITDe was accurate. The statistical models showed a significant correlation between the defoliation degree measured in the field and UAS technology at tree level and, therefore, our methodology may be used by forest managers to quantitatively assess the level of defoliation of individual trees. Moreover, this approach enabled us to classify pines among non-defoliated, partially defoliated and completely defoliated automatically after tree species identification with a classification accuracy of 81.8% with ITDe and even higher with MCDe (87.2%). This result was slightly more accurate than that obtained in the previous study (Cardil et al., 2017) using RGB imagery in pure pine forest, in which the overall accuracy of the methodology to classify trees as partially defoliated or non-defoliated with MCDe was 79%. Our methodology using NDVI and removing shaded pixels detected by the ExG increased the classification accuracy between non-defoliated and partially defoliated trees up to 95.2% with MCDe. Therefore, in addition to RGB imagery, the use of multispectral imagery and vegetation indices such as NDVI may have improved assessment of PPM defoliation (Näsi et al., 2015). Although NDVI is the most widely used and tested index for monitoring of forest insect defoliation (Rullan-Silva et al., 2013), further research would be needed to evaluate whether other indices among the spectral band scan improve the accuracy of PPM defoliation assessments. Furthermore, improvements in algorithms to identify and delineate individual trees may enhance the accuracy of the defoliation estimations

at tree level as our results with MCDe demonstrated. In the Codo case study, the algorithm based on the UAS derived CHM was able to successfully identify all the selected trees. Previously, other studies with different tree species, canopy cover and tree heights have found the accuracy higher than 85% in detecting individual trees, suggesting that the tree identification accuracy was high in general (Kattenborn et al., 2014; Sperlich et al., 2014; Mohan et al., 2017). Yet, there is no standardized accuracy assessment procedure for ITDe, therefore, it is extremely difficult to compare ITDe algorithms unless multiple approaches are tested on a single study area using the same datasets and metrics (Zhen et al., 2016). Nonetheless, it seems evident that improvements in ITDe will enhance the estimation accuracy of PPM defoliation (Jaafar et al., 2018). Our approach provides accurate PPM impact assessments with an efficient data processing to delineate individual trees in terms of time and staff, allowing the quantitative estimation of defoliation at tree-level scale in larger scales than MCDe. As expected, the accuracy levels of this methodology to analyze PPM defoliation at high resolution were higher than other previous studies using other techniques and methods with airborne laser scanning or satellite data such as Landsat or MODIS at medium resolution (Dennison et al., 2009; Eklundh et al., 2009; Solberg, 2010; Townsend et al., 2012; Cardil et al., 2017) and can be used in mixed forest to assess PPM defoliation at tree level.

At the pixel level, the overall classification accuracy among partially defoliated, non-defoliated and shaded was 81% in the high resolution NIR imagery, which was as high as that at the tree level with ITDe. The use of NDVI in general has the advantage of detecting non-defoliated pixels that cannot be visibly detected by RGB imagery due to shade as has been demonstrated in agricultural areas (Lottes et al., 2017), but we think that it is still necessary to achieve some improvements in the multispectral sensors and/or in radiometric calibrations for forest areas as Codo. This type of invisibility in the orthomosaic image may make it difficult to validate the classification accuracy of predicted non-defoliated pixels based on NDVI. Another limitation was the one hour difference between the flights with the RGB camera and the multispectral camera. This temporal difference may have contributed to slight increases in the uncertainty in shaded pixels. In the future study the simultaneous flight with both RGB and multispectral cameras, as the UAS technology advances, may improve our methodology and the results.

The use of UAS technology offers several advantages when applied to the defoliation assessment caused by insect pests in spite of the fact that substantial investment in equipment, infrastructure and training of people is necessary. The key highlights of those advantages include (1) data acquisition is usually more efficient in terms of time, quality and manpower, (2) the technology has a great capacity to monitor and assess areas with difficult access (3) researchers can easily derive quantitative methods to estimate defoliation at tree level and (4) this information can be analyzed at forest stand scale which is the work scale of forest managers and eventually be repeated in time thus providing the potential for the development of long term forest health monitoring programs. Finally, (5) UAS high-resolution data can be a great source of information to calibrate medium resolution remote sensing information derived from satellites to map information in coarser scales (Fraser et al., 2017; Pla et al., 2017). Nevertheless, it should be noted that several methodological constraints need to be considered when planning for the large area deployment of UAS technologies in the estimation of defoliation levels such as the regulations to

use UAS in urban areas and areas located near airfields.

4.5 Conclusions

In this study, we investigated the use of multispectral high-resolution imagery acquired from a UAS platform and image processing techniques to quantitatively assess PPM impact on a pine-oak mixed forest at tree level. Overall, this research suggested that UAS imagery and its derived products, such as canopy height model and normalized difference vegetation index, enabled us to estimate tree species, count individual trees with acceptable accuracy and assess defoliation using canopy cover at tree level by classifying pines non-defoliated, partially defoliated and completely defoliated automatically with high accuracy. Moreover, the accuracy of our proposed methodology at tree level was higher than previous studies. This proposed framework highlights the future potential of UAS, multispectral imagery and structure-from motion algorithms for individual tree detection, PPM quantification, qualification and monitoring. Thus, we believe that the promising results presented here in should inspire further research and applications to the forest health assessments.

Chapter 5

Article 3: Estimating the threshold of detection on tree crown defoliation using vegetation indices from UAS multispectral imagery

Abstract
Periodical outbreaks of *Thaumetopoea pityocampa* feeding on pine needles may pose a threat to Mediterranean coniferous forests by causing severe tree defoliation, growth reduction, and eventually mortality. To cost–effectively monitor the temporal and spatial damages in pine–oak mixed stands using unmanned aerial systems (UASs) for multispectral imagery, we aimed at developing a simple thresholding classification tool for forest practitioners as an alternative method to complex classifiers such as Random Forest. The UAS flights were performed during winter 2017–2018 over four study areas in Catalonia, northeastern Spain. To detect defoliation and further distinguish pine species, we conducted nested histogram thresholding analyses with four UAS-derived vegetation indices (VIs) and evaluated classification accuracy. The normalized difference vegetation index (NDVI) and NDVI red edge performed the best for detecting defoliation with an overall accuracy of 95% in the total study area. For discriminating pine species, accuracy results of 93–96% were only achievable with green NDVI in the partial study area, where the Random Forest classification combined for defoliation and tree species resulted in 91–93%. Finally, we achieved to estimate the average thresholds of VIs for detecting defoliation over the total area, which may be applicable across similar Mediterranean pine stands for monitoring regional forest health on a large scale.

5.1 Introduction

Climate change is predicted to continue increasing global temperatures over this century (Collins et al., 2013), which may lead to an alteration of forest disturbances including pest insects that are strongly dependent on climatic variables (Netherer and Schopf, 2010; Robinet and Roques, 2010; Battisti and Larsson, 2015; Battisti et al., 2016). Such a combination of biotic and abiotic disturbance factors may accel-

erate forest damage as defoliation, growth reduction and tree mortality in relation to global changes (Roques, 2015). In Mediterranean forests dominated by *Pinus* spp., outbreaks of the pine processionary moth (*Thaumetopoea pityocampa* Dennis and Schiff.) have become more frequent over the past two decades and have extended their spatial distribution due to warmer winters favoring the survival of the pest (Battisti et al., 2005; Robinet et al., 2007; Roques, 2015; Battisti et al., 2016). Traditionally, annual forest health surveys by practitioners have been and still remain the fundamental means for monitoring forest conditions at local and national administrative levels. However, due to the recent pest expansion and associated threats to the forest health (FAO, 2018), a more frequent interannual monitoring system at a finer spatial scale is currently required to meet the demand for keeping forest information up to date.

Consequently, the use of airborne-based UAS technology with enhanced spatial and temporal resolutions has significantly increased over the past decade for detecting and monitoring forest defoliation on host trees (Lehmann et al., 2015; Näsi et al., 2015; Cardil et al., 2017, 2019; Dash et al., 2017; Hentz and Strager, 2017; Brovkina et al., 2018). While spaceborne satellites have been more commonly used for defoliation detection and time-series monitoring over large areas, their images can be either free to the public at medium spatial resolutions (30–250 m) provided by Landsat and MODIS or costly at high spatial resolutions (0.3–10 m) available from WorldView-4, IKONOS, QuickBird, RapidEye, and TerraSAR-X (Rullan-Silva et al., 2013). Since medium-high spatial resolution images from Sentinel-2 (10–20 m) became freely downloadable in 2015 (ESA, 2015), cost–effective monitoring of large areas is increasing. With such further advancements in spaceborne technology, sensors' spatial resolution continues to enhance temporal and spectral resolutions (Manfreda et al., 2018). Furthermore, airborne laser scanning (ALS) featuring point clouds complements the three-dimensional (3D) structure besides capturing two-dimensional (2D) imagery at higher spatial resolutions than any spaceborne technology (Rullan-Silva et al., 2013; Roncat et al., 2014). Using such ALS metrics, an innovative study by Kantola et al. (2013) demonstrated the classification of defoliated *Pinus sylvestris* at the individual tree level.

Since the cost of these satellite and ALS high-resolution products remains a limiting factor for the purpose of targeting small operational areas, the use of cost-effective unmanned aerial systems (UASs) as an alternative 3D technology at a high spatial resolution has increased in recent studies for monitoring forest health over the past decade (Pajares, 2015; Manfreda et al., 2018). While initial studies with UASs were focused on crop management for agriculture applications, the latest UAS technology has proved to be effective for forestry applications as a sampling tool to acquire ground-truth data (Dash et al., 2017; Torresan et al., 2017). To date, only a few studies have examined the classification accuracy of forest defoliation by insects using UAS imagery applied to methods such as Random Forest (Dash et al., 2017), object-based image analysis (OBIA) (Lehmann et al., 2015; Brovkina et al., 2018), k-nearest neighbor (Näsi et al., 2015), maximum likelihood (Cardil et al., 2017; Hentz and Strager, 2017), and unsupervised classification (Cardil et al., 2019), which demonstrated that the UAS technology enabled to examine their defoliation detection method at individual tree level with a high overall accuracy. An object-based classification approach with the Random Forest classifier was used by Dash et al. (2017) to predict discoloration classes of *Pinus radiata* in New Zealand, based

on spectral indices such as normalized difference vegetation index (NDVI) and red edge NDVI with the kappa coefficient of 0.694. Lehmann et al. (2015) used a blue NDVI to distinguish infested *Quercus robur* in Germany by OBIA classification with overall accuracies of 82-85%. Another OBIA technique was applied by Michez et al. (2016) to assess defoliation and discoloration of *Alnus glutinosa* in Belgium using vegetation indices (VIs) derived from red, green, blue (RGB) and near-infrared (NIR) bands, with an overall accuracy of 90.6%. In Finland, with a combination of NDVI, NIR, red edge and RGB bands, Näsi et al. (2015) detected infested *Picea abies* by object-based k-nearest neighbor classification with an overall accuracy of 75%. Using a pixel-based approach, in Scotland, Smigaj et al. (2015) extracted canopy temperatures of *Pinus sylvestris* with a combination of thermal infrared (TIR) and NIR bands derived from UASs to evaluate the correlation with the tree infection level estimated from the ground, resulting in a moderate linear regression ($R = 0.527$). In the United States, Hentz and Strager (2017) combined RGB bands and elevation values to classify damage on deciduous trees using a pixel-based maximum likelihood classification (MLC) technique, with the kappa coefficient of 0.86. Cardil et al. (2017) also used the MLC based on RGB bands to distinguish infested or healthy trees of *Pinus* spp. in Spain with an overall accuracy of 79%, which was improved to 81% by adding an NIR band to classify three categories of defoliation and using unsupervised classification with NDVI (Cardil et al., 2019).

The traditional image classification by histogram thresholding analyses has been mainly used for detecting shadow areas in satellite-based high spatial resolution images (Otsu, 1979; Dare, 2005; Chen et al., 2007; Adeline et al., 2013; Jan-Chang C, 2016) as it is considered to be the simplest to compute and minimize intraclass variance when a clear separation is observed in a bimodal distribution (Adeline et al., 2013; Tang and Shao, 2015; Aasen et al., 2018). However, no study has applied such a simple classification method, combined with very high spatial resolution UAS imagery, to forestry applications. This is due to the recent trend in research of UAS technology combined with object-based classification methods such as OBIA and Random Forest which have demonstrated excellent performance for analyzing complex high spatial resolution data including multispectral, geospatial, and textural properties (Blaschke, 2010; Weih and Riggan, 2010; Duro et al., 2012; Qian et al., 2015; Hossain and Chen, 2019). Although these object-based image classification techniques are generally considered to be more robust and accurate (Blaschke, 2010; Weih and Riggan, 2010; Duro et al., 2012; Qian et al., 2015; Hossain and Chen, 2019), it may require extra knowledge and training with software applications to perform such complex analysis correctly. Based on the same study area analyzed by Cardil et al. (2019) with UAS multispectral imagery for quantifying defoliation degrees due to *T. pityocampa* in Catalonia where regional forest health surveys are officially conducted on an annual basis, we seek for further improvements to their approach using simple and robust methods applied to similar pine-dominated stands, for forest practitioners to obtain timely information and monitor forest defoliation at the operational level. In this context, the main objectives of this study are: (1) to explore simple histogram thresholding classification tools for forest practitioners to detect defoliation of host pine trees affected by *T. pityocampa* using UAS-derived NIR imagery and (2) to estimate the threshold values of various VIs averaged over our study areas for detecting defoliation and distinguishing pine species at the pixel level to examine the robustness in extended study areas. Achieving our objectives

may provide forest practitioners with the classification options of adopting the histogram thresholding method and directly applying the estimated average threshold values according to selected VIs.

5.2 Materials and methods

5.2.1 Study area

The study was conducted in four pine-dominant stands, including Codo, Hostal, Bosquet, and Olius in the region of Solsona, Catalonia, Spain (Figure 5.1a), covering 64 hectares in total where the recent expansion of *T. pityocampa* has been recorded in the regional forest health inventory (Generalitat de Catalunya). They represent a Mediterranean continental climate with hot dry summers and mild wet winters at elevations ranging from 600 m to 1300 m. According to the Land Cover Map of Catalonia (MCSC) for 2009, forest stands were typically dominated by *Pinus nigra* and *P. sylvestris*, which are often mixed with evergreen oak species such as *Quercus ilex*.

5.2.2 UAS image acquisition and processing

In this study, a quadcopter (Phantom 3, DJI) was used as an UAS platform, equipped with a high spatial resolution multispectral camera (SEQUOIA, Parrot) carrying a payload of 72 g, to capture both visible RGB and invisible NIR images simultaneously. The RGB camera has a resolution of 16 megapixel with a lens focal length of 5 mm and fields of view (FOV) with horizontal (HFOV): 63.9°, vertical (VFOV): 50.1°, and diagonal (DFOV): 73.5°. In addition, another 1.2 megapixel sensor, with a lens focal length of 4 mm, and fields of view with HFOV: 61.9°, VFOV: 48.5°, and DFOV: 73.7°, captures four spectral bands in green (530–570 nm wavelength), red (640–680 nm wavelength), red edge (730–740 nm wavelength), and near infrared (770–810 nm wavelength). Both RGB and NIR images were collected simultaneously from a flying altitude at 76–95 m above the ground level with 80% forward and side overlap at speeds ranging from 4–8 per second, achieving a ground sample distance of 2.0 cm with the RGB camera and 7.4 cm with the NIR camera, on average. Four flights were conducted in winter 2017–2018 on clear sunny days around noon to minimize the effects of clouds and shadows, covering the total area of 64 hectares. The flight features with the RGB and NIR cameras were summarized in Table 5.1.

A total of 1042 adjacent photos, overlapped from the flights with their geotagged locations, were processed separately for those captured with the RGB and NIR cameras in the software, PhotoScan Professional 1.4.0 (Agisoft LLC, St. Petersburg, Russia). In image processing, the photos were geometrically aligned to build a point cloud, 3D model, digital elevation model (DEM), and digital surface model (DSM). For generating orthomosaic images, those composed of multispectral bands were radiometrically corrected to calibrate the reflectance values corresponding to each band, by using reflectance panels which were captured before each flight specific to the lighting conditions of the date, time, and location of the flight (Agisoft, 2018b; Pla et al., 2019). The use of a reflectance panel captured as an image of calibrating a white balance card enabled the PhotoScan to recognize the images'

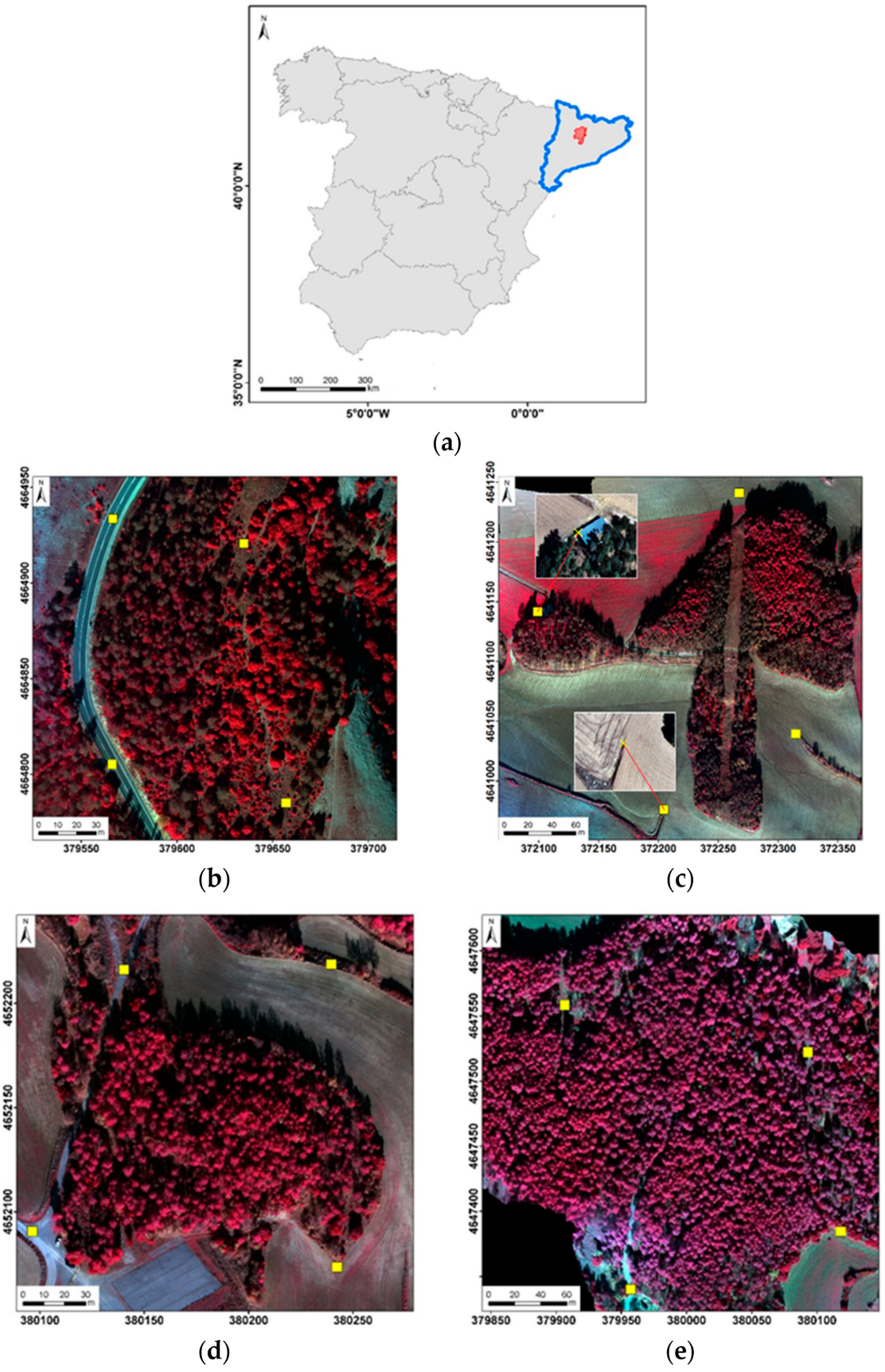

Figure 5.1: Location map of study areas in the region of (a) Solsona (41°59′40″ N, 1°31′04″ E) in red line and Catalonia in blue line, projected in the UTM Zone 31 North showing: (b) Codo; (c) Hostal; (d) Bosquet; and (e) Olius, with calibration ground control points in yellow georeferenced to orthophotos.

Table 5.1: RGB and NIR imagery features for orthomosaic generation in the Agisoft PhotoScan.

Site	**Codo**	**Hostal**	**Bosquet**	**Olius**
Camera	RGB/NIR	RGB/NIR	RGB/NIR	RGB/NIR
Date (dd/mm/yy)	26/11/2017	19/01/2018	23/01/2018	30/01/2018
Time (duration)	12:43–12:50	12:05–12:14	12:16–12:22	11:55–12:03
Elevation (m)	1300	820	620	720
Flight height (m)	95	78	76	85
Area (ha)	14.1	16.2	7.4	26.3
Number of images	210	333	155	344
Data size (GB)	0.93 / 0.49	1.65 / 0.78	0.39 / 0.36	1.05 / 0.80
Processing time (h)	4.8 / 3.3	7.6 / 5.0	3.9 / 2.4	5.7 / 3.8
Software platform	(Microsoft	Windows	7	64 bits)
Ground resolution (cm/pix)	2.32 / 8.64	1.90 / 6.82	1.80 / 6.58	2.12 / 7.49
RMS reprojection error (pix)	2.45 / 0.66	2.51 / 0.70	2.34 / 0.64	2.19 / 0.62

reflectance according to known values of all spectral bands written on the panel for radiometric calibration (Agisoft, 2018b). Using the ArcGIS version 10.5 software (ESRI, Redlands, CA, USA), each orthomosaic was georeferenced to the 1:2500 orthophotos (ICGC, 2018) in the cartographic UTM projection by performing a first order polynomial transformation with four ground control points (GCPs) of clearly visible features such as roads, structures, and field edges across each study area (Figure 5.1b-e), obtaining an accuracy of sub-meter root mean square error (RMS). As alternative ground validation data, we used the UAS orthomosaic images and DSM captured at a very higher spatial resolution (2.0 cm) with the RGB camera.

5.2.3 Vegetation indices

Given the four bands in NIR imagery obtained from UAS flights, we calculated vegetation indices (VIs) which may extract the relevant information on different vegetation features for further analysis. The chlorophyll absorption is very high in the visible spectrum, where the reflectance is the highest for green wavelengths (Rullan-Silva et al., 2013). In shifting from the range of visible wavelengths to invisible towards the NIR, the reflectance starts to increase for red edge wavelengths as the chlorophyll absorption ceases (Rullan-Silva et al., 2013). For automated classification and repeated application, four normalized VIs based on various combinations

of spectral bands were selected as comparable thresholding values among the four different study areas (Table 5.2). NDVI has been most commonly used for detecting land cover change and mapping forest defoliation due to its sensitivity to low chlorophyll concentrations (Gitelson et al., 1996; Rullan-Silva et al., 2013). On the contrary, green NDVI (GNDVI) is sensitive to high chlorophyll concentrations and accurate for assessing chlorophyll content at the tree crown level (Gitelson et al., 1996). By exploring various combinations of available spectral bands, we additionally examined the sensitivity of other indices such as green-red NDVI (GRNDVI) and NDVI red edge (NDVIRE) to find the most sensitive VI to classify forest defoliation and tree species.

Table 5.2: Vegetation indices derived from UAS multispectral bands.

Index	Acronym	Formula	Reference
Normalized Difference Vegetation Index	NDVI	$\frac{\text{NIR - Red}}{\text{NIR + Red}}$	Rouse et al. (1973)
Green Normalized Difference Vegetation Index	GNDVI	$\frac{\text{NIR - Green}}{\text{NIR + Green}}$	Gitelson et al. (1996)
Green–Red Normalized Difference Vegetation Index	GRNDVI	$\frac{\text{NIR - (Green + Red)}}{\text{NIR + (Green + Red}}$	Wang et al. (2007)
Normalized Difference Vegetation Index Red Edge	NDVIRE	$\frac{\text{RE - Red}}{\text{RE + Red}}$	Chevrel et al. (2002)

5.2.4 Pixel-based thresholding analysis

In this study, histogram thresholding analyses, known as the classical approach to classification (Otsu, 1979; Adeline et al., 2013; Shahtahmassebi et al., 2013), were explored in a nested method for excluding shadow from sun pixels, detecting defoliation from foliated green pixels, and discriminating pine from evergreen oak. Using the ArcGIS version 10.5 software, available spectral bands and VIs from the UAS-derived NIR imagery were analyzed in a histogram distribution by the first valley detection thresholding with local minima. Figure 5.2 simplifies a workflow of the nested histogram thresholding analyses per study area, from the initial shadow removal with the NIR band to the final separation of pixels by defoliation and tree species for monitoring, so that this method can be repeated to conduct a time series image analysis.

Shadow removal

Although all flights were conducted around noon when the sun angle is considered to be minimum to generate shadows in images, there are often some limitations to achieving shadow-free images. Among several shadow detection algorithms suggested and compared by Adeline et al. (2013), a histogram thresholding analysis performed well as the most robust method and demonstrated good results with an NIR band alone. Generally, the location of shadows in the histogram should be separated at the first valley of multimodal distribution with two or more peaks (Chen et al., 2007; Adeline et al., 2013; Lehmann et al., 2015). We then applied

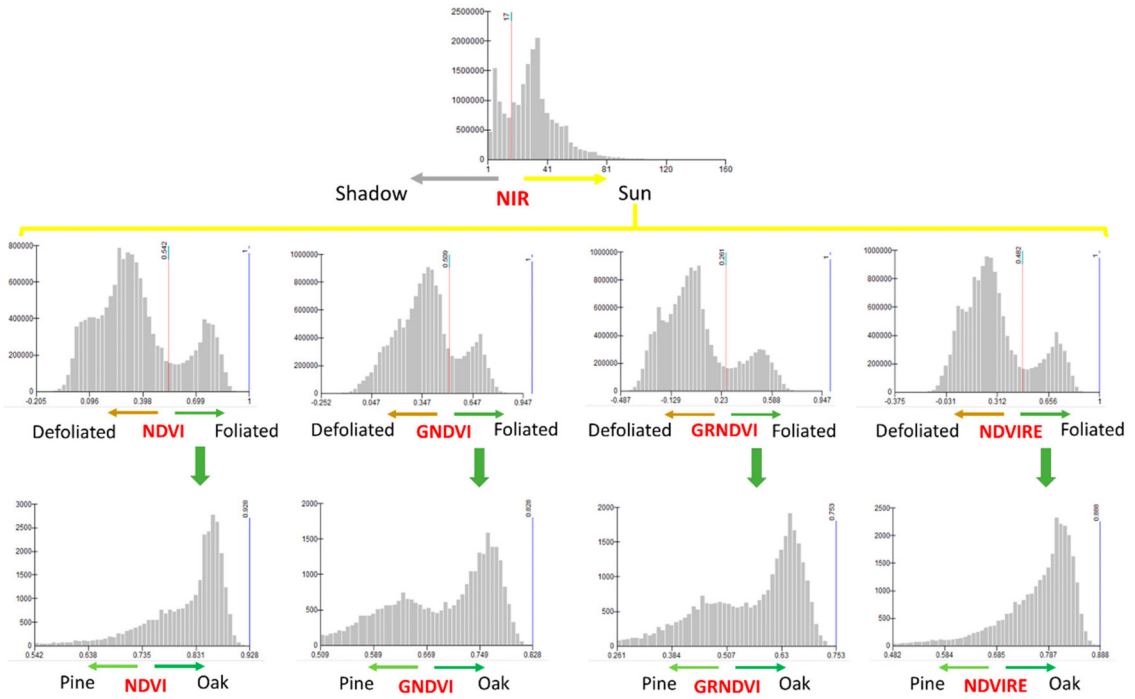

Figure 5.2: Overall workflow of classification methods per study area by nested histogram thresholding analyses, indicating pixel intensity on the x-axis and frequency on the y-axis, with four VIs derived from NIR imagery for monitoring defoliated and foliated pine trees.

the method, first valley detection thresholding, using the UAS-derived NIR band to exclude shadow pixels from further analysis to reduce uncertainty.

Defoliation detection

Following shadow removal, shadow-free pixels in each study area were extracted by a mask of pine-dominated forest polygons mapped on the MCSC. The same histogram thresholding approach was applied to separate the masked pixels representing green tree crown from non-green in each study area with four VIs (Table 5.2). In this analysis, green pixels with leaves were defined as foliated class, while non-green pixels without leaves belonged to the defoliated class. While the previous study in the Codo area (Cardil et al., 2019) applied pixel-based unsupervised classification with NDVI to calculate the percentage of defoliation per tree crown area identified by individual tree delineation algorithm, in this study we simply focused on determining the threshold values of four VIs and their variations among four study areas as well as evaluating the performance of each VI.

Foliated species discrimination

To distinguish shadow-free foliated trees of pine species from evergreen oak, we first visually interpreted RGB images. Once 10 pines and 10 evergreen oaks in each of two study areas (Codo and Olius) were manually selected in RGB orthomosaic images (Figure 5.3a) and delineated to extract sample pixels based on NIR imagery representing each species (Figure 5.3b), histogram thresholding analyses were applied to those selected pixels showing the spectral profiles in Figure 5.3c. Relatively,

the color intensity and texture of pine species are softer than evergreen oak species (Riemann Hershey and Befort, 1995). Moreover, broadleaf vegetation reflects notably higher values of NIR than needle-leaf vegetation (Aronoff, 2005) as observed in our study area with spectral profiles of the two species for the wavelength range of 770–810 nm (Figure 5.3c). However, the previous study in the Codo area (Cardil et al., 2019) suggested that NIR alone or standard NDVI (Rouse et al., 1973) may not be sufficient to distinguish two species by thresholding analysis. Thus, for further exploring species discrimination, we applied the histogram thresholding method with the three additional VIs (Table 5.2) to pixels extracted by sample crown polygons. There were only a few evergreen oak samples observed in the other two study areas (Hostal and Bosquet), which were not included in this analysis.

5.2.5 Object-based Random Forest

In contrast to determining threshold values for pixel-based classification, we used another method, object-based Random Forest, with the advantage of analyzing combined data of multiple spectral bands, spatial parameters, and textural properties. As shown in Figure 5.4a, color infrared (CIR) images composed of NIR, red, and green bands were first computed for automatically aggregating adjacent pixels that are similar in spectral properties as image segments (Figure 5.4b) in the ArcGIS version 10.5 software. To supervise Random Forest classification, sample data were then trained as segments of shadow, defoliation, and tree species such as pine and evergreen oak, which were comparable to the thresholding analysis in Codo and Olius study areas. CIR images may contain more effective parameters as predictive indices characterized by relative color, color intensity, and texture (Riemann Hershey and Befort, 1995).

5.2.6 Validation and accuracy assessment

Ground validation data were obtained by photointerpretation of the RGB orthomosaic images (Figure 5.5a) and DSM (Figure 5.5b), at a very high spatial resolution (2.0 cm), which was higher than the resolution of NIR imagery (7.2 cm) based on the separate multispectral camera from the same UAS flight. The DSM profile, in particular, enabled to generate a 3D stand structure and distinguish soils from defoliated tree branches, which might have been misinterpreted due to the similar colors in the RGB orthomosaic images. We then observed plots of the RGB images classified as: (1) shadow or sun pixels, (2) defoliated or foliated for the sun pixels, and (3) pine or evergreen oak species for the foliated pixels. Such validation by photointerpretation has been increasingly used as an alternative to conventional ground truth data in recent studies with promising results (Hentz and Strager, 2017; Mohan et al., 2017; Pla et al., 2017; Otsu et al., 2018; Cardil et al., 2019).

In each study area 100 pixels were randomly selected to assess the accuracy of final classification results by histogram thresholding analyses and Random Forest, separately, with predicted indices derived from the NIR imagery, in reference to ground observations based on the RGB orthomosaic images. A confusion matrix was then generated to compare producer's and user's accuracy indicating omission and commission errors, respectively, as well as overall accuracy. To explore the uncertainty in the best performed results over the total study area, the overall

accuracies were further investigated in a sensitivity analysis, testing the robustness of the estimated thresholds by increasing and decreasing values.

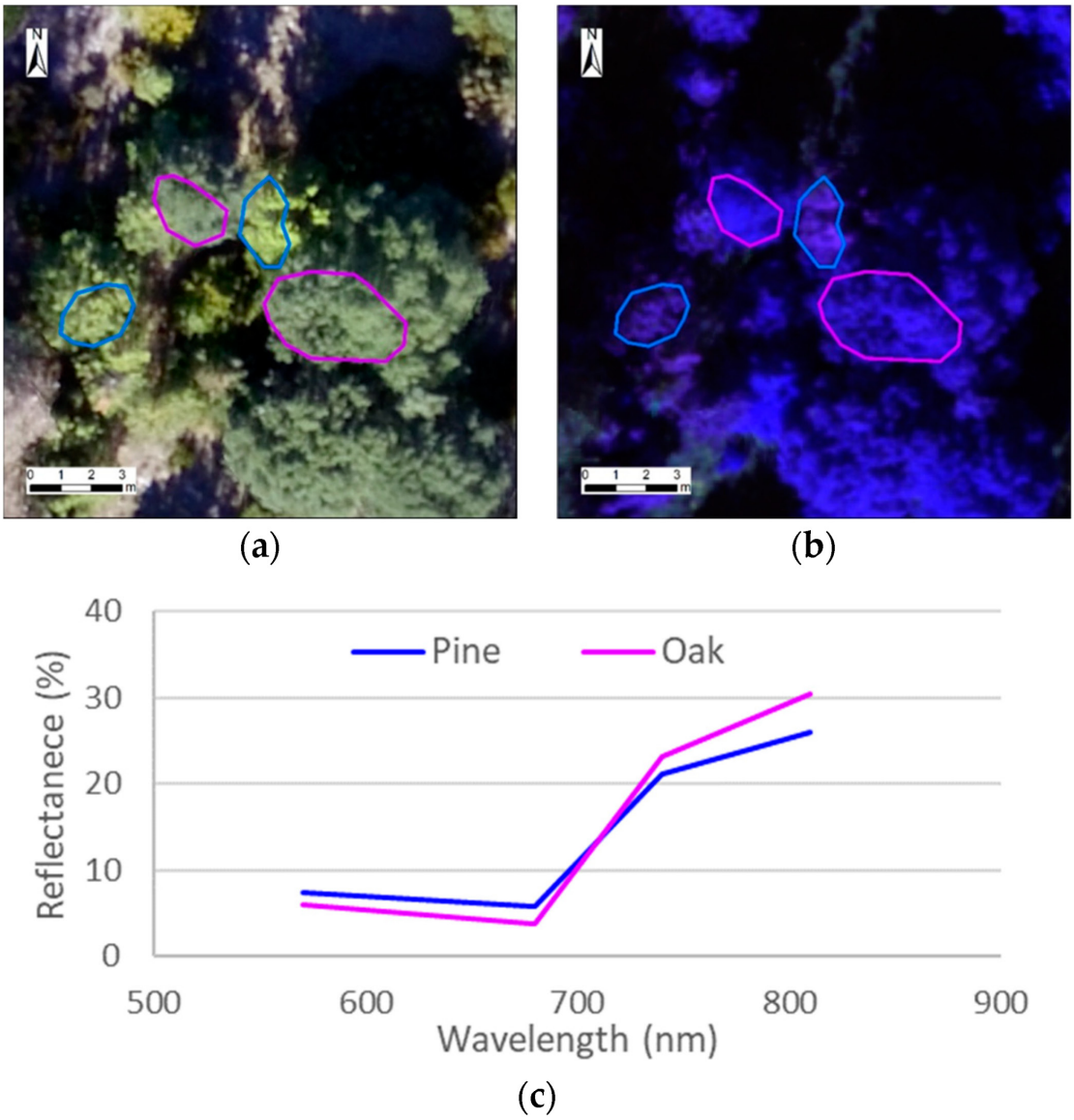

Figure 5.3: Examples of tree characteristics by foliated evergreen oak in purple line and foliated pine in blue line observed in: (a) an RGB image; (b) a NIR image; and (c) spectral profiles of the two tree species in Codo study area.

5.3 Results

5.3.1 Pixel-based thresholding analysis

Shadow removal

A multimodal histogram distribution of NIR values was shown by study area in Figure 5.6, with the first valley determined as the thresholding value to exclude shadow pixels indicating the lowest class of reflectance in the NIR band. As shown

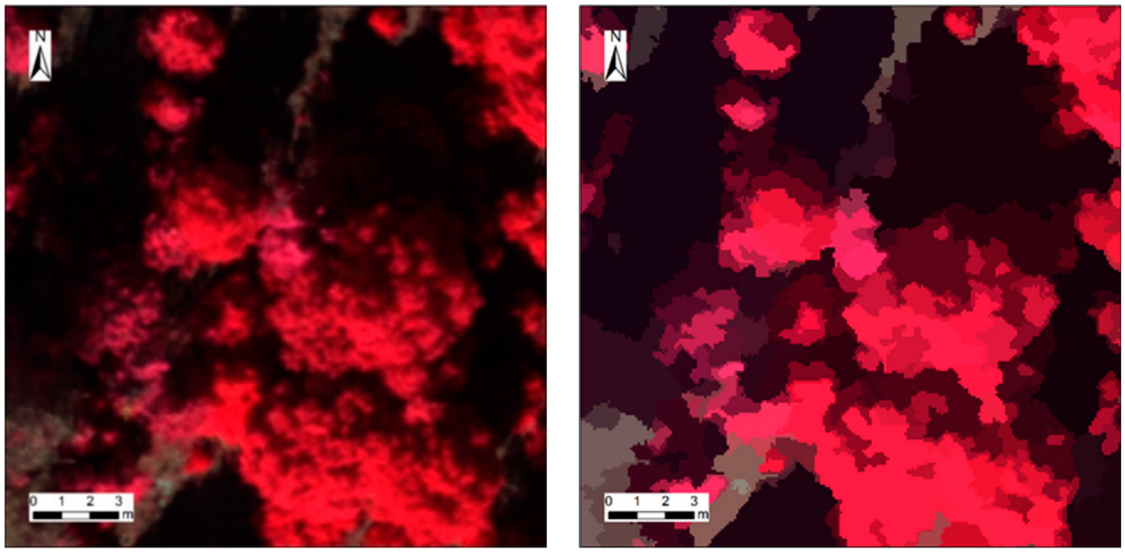

(**a**) (**b**)

Figure 5.4: Comparison of: (a) CIR image and (b) segmentation of the CIR-derived pixels that are similar in spectral properties as image objects.

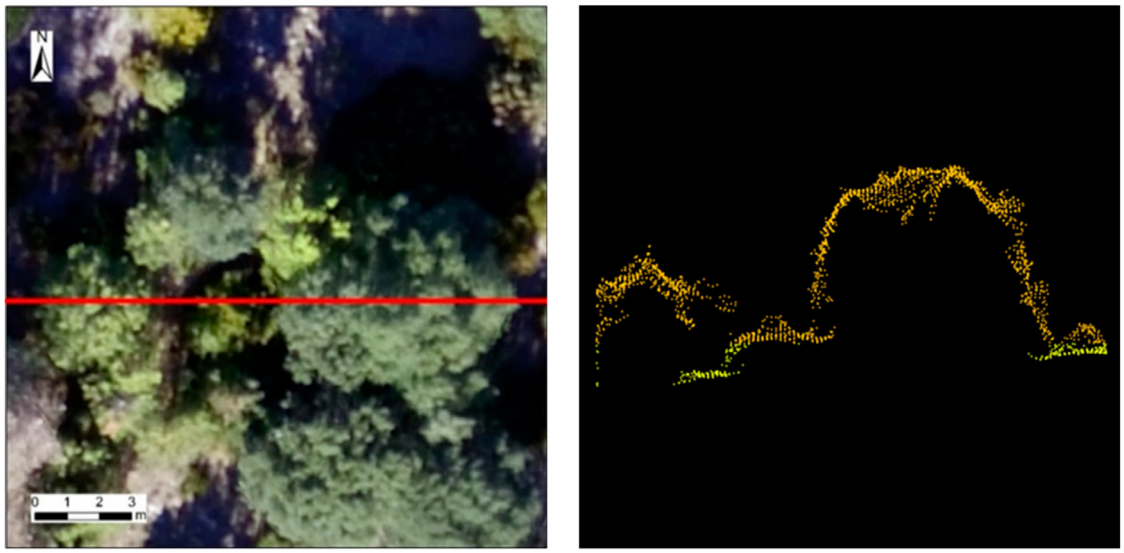

(**a**) (**b**)

Figure 5.5: Comparison of: (a) RGB image with a line of sight in red line and (b) corresponding point cloud profile of RGB-derived DSM.

in Figure 5.6a for the Codo area, those pixels with the value smaller than 17 were classified as shadow areas, counting for 29% of the total number of pixels, thus excluded to reduce uncertainly. Likewise, shadow areas resulted in 14% for Hostal (Figure 5.6b), 17% for Bosquet (Figure 5.6c) and 35% for Olius (Figure 5.6d) study areas, respectively. We found a variation in those threshold values among four study area compared in Table 5.3, ranging from 17-28.

Table 5.3: Summary of threshold values determined by multimodal histogram distributions with various indices for classifying shadow, defoliated, and tree species.

Classification	Index	Codo	Hostal	Bosquet	Olius	Total Average
Shadow	NIR	17	23	27	28	24
Defoliated	NDVI	0.584	0.529	0.481	0.490	0.52
	GNDVI	0.561	-	-	0.393	-
	GRNDVI	0.295	0.254	0.171	0.175	0.22
	NDVIRE	0.515	0.475	0.416	0.431	0.46
Species	NDVI	-	-	-	-	-
	GNDVI	0.681	-	-	0.631	-
	GRNDVI	0.539	-	-	-	-
	NDVIRE	-	-	-	-	-

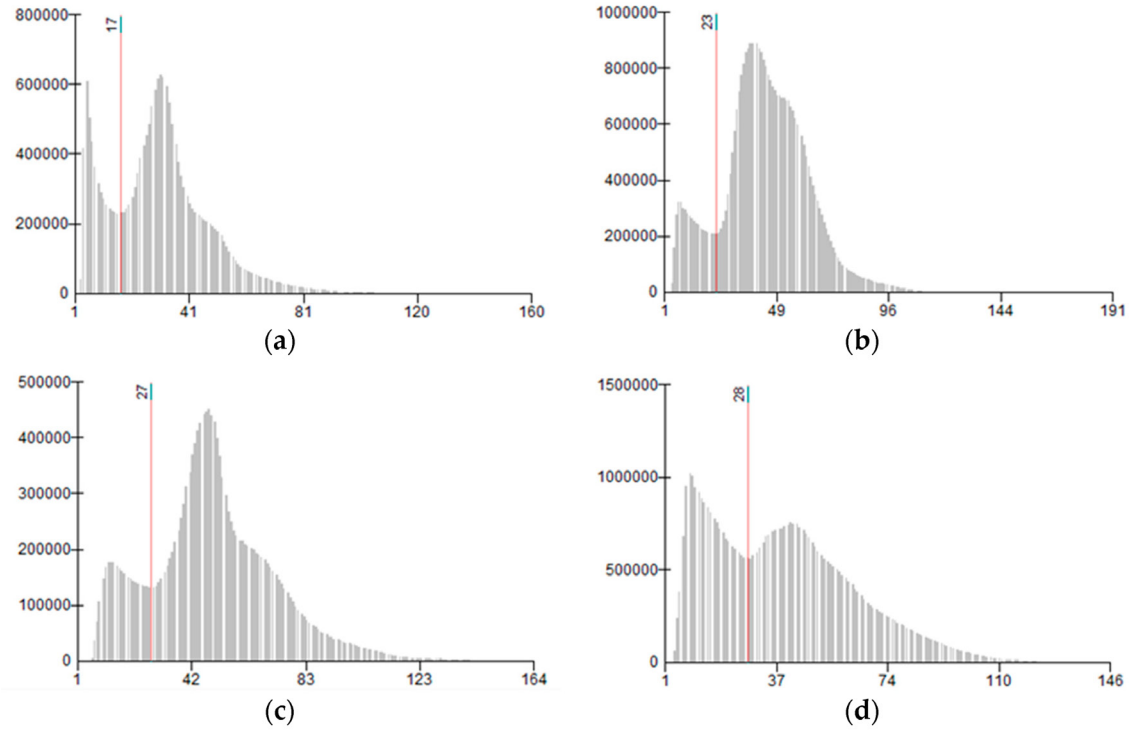

Figure 5.6: The valley detection thresholding to separate shadow class toward the lowest NIR values in a multimodal distribution, with pixel intensity on the x-axis and frequency on the y-axis, in the four study areas: (a) Codo; (b) Hostal; (c) Bosquet; and (d) Olius.

Defoliation detection

Each histogram distribution of pixel values calculated for NDVI, GNDVI, GRNDVI, and NDVIRE was presented in Figure 5.7 for the Codo study area. The final valley of multimodal distribution determined the threshold value to separate the highest class of reflection in each index classified as foliated to mask green tree crown pixels. All threshold values determined by the same method in the other three study areas (Appendix: Figures 5.11, 5.12 and 5.13) are summarized in Table 5.3, with a various range of NDVI (0.481–0.584), GNDVI (0.393–0.561), GRNDVI (0.171–0.295), and

NDVIRE (0.416–0.515) including the average values. We found some exceptions for those unimodal distributions with no valley detected with GNDVI in Hostal (Appendix: Figure 5.11b) and Bosquet (Appendix: Figure 5.12b).

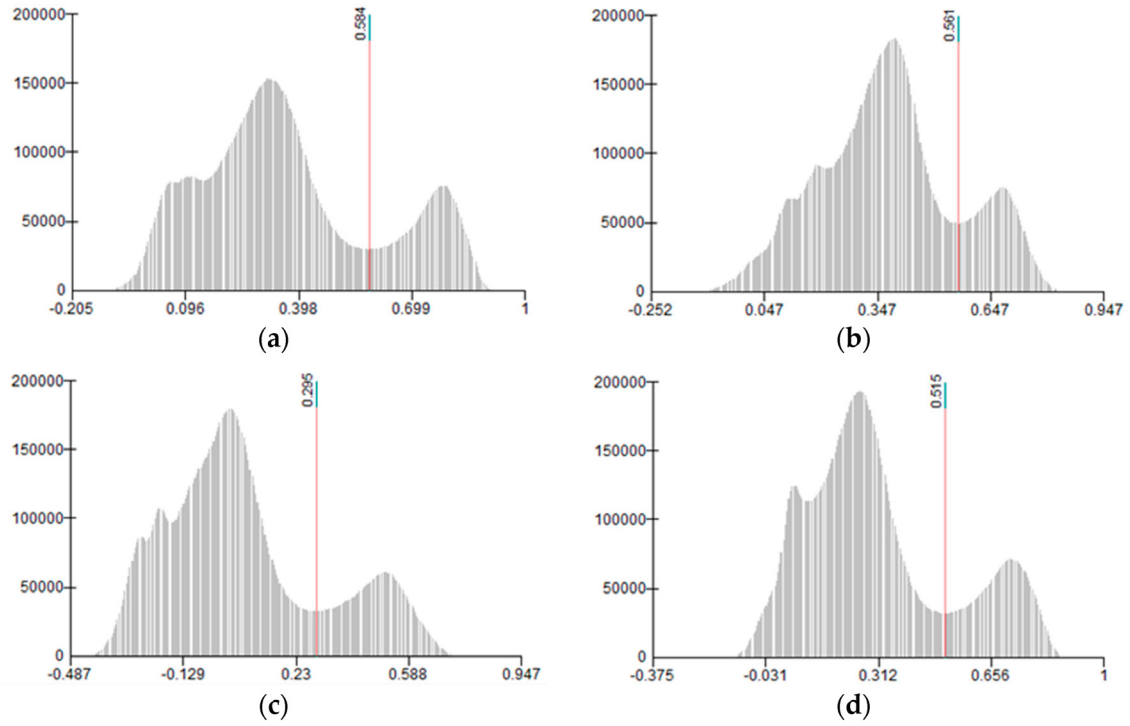

Figure 5.7: The valley detection thresholding to separate foliated class towards the highest VI values in a multimodal distribution, with pixel intensity on the x-axis and frequency on the y-axis, for detecting defoliation in the Codo study area with: (a) NDVI; (b) GNDVI; (c) GRNDVI; and (d) NDVIRE.

Foliated species discrimination

For discriminating species between pine and evergreen oak in Codo and Olius study areas, shadow-free foliated pixels were classified as shown in Figure 5.8. Among the four VIs analyzed, GNDVI and GRNDVI resulted in a bimodal distribution in Codo (Figures 5.8b,5.8c), revealing two distinguishable species classes between pine and evergreen oak, while the rest of our results with NDVI (Figure 5.8a) and NDVIRE (Figure 5.8d) did not achieve this distinction. The first valley of bimodal distribution, indicating the lower class of reflectance in each index, was classified as pine to mask host tree species. In Olius, on the other hand, only the histogram with GNDVI showed a bimodal distribution (Appendix: Figure 5.14b). However, we found that the threshold value of GNDVI for separating pine from evergreen oak in Codo (0.681) was notably close to the one (0.631) in Olius, as summarized in Table 5.3.

The above results of histogram thresholding analysis are illustrated in Figure 5.9, starting with a CIR image (Figure 5.9a) overlaid with NIR highlighting shadow pixels in gray (Figure 5.9b). Following shadow removal, the CIR image was overlaid with GNDVI highlighting shadow-free defoliated pixels in meshed yellow and foliated

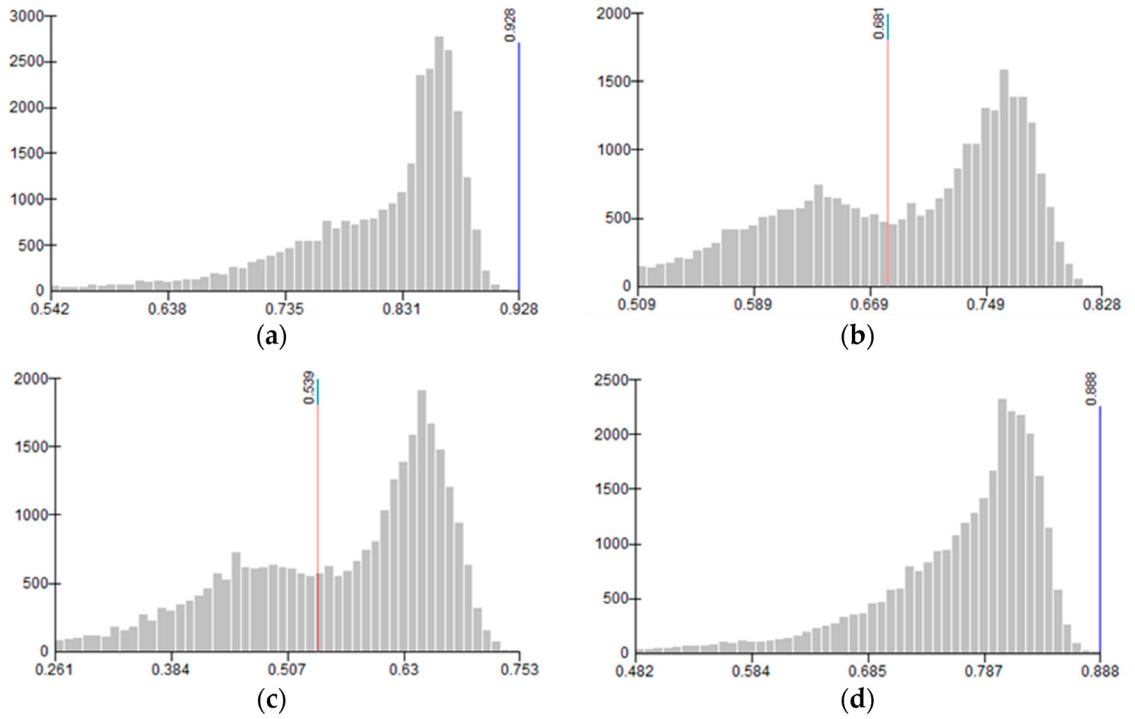

Figure 5.8: The valley detection thresholding to discriminate pine toward lower VI values from evergreen oak, with pixel intensity on the x-axis and frequency on the y-axis, in the Codo study area with: (a) NDVI; (b) GNDVI; (c) GRNDVI; and (d) NDVIRE.

pixels in green (Figure 5.9c), which were further classified and highlighted as pine in blue and evergreen oak in purple (Figure 5.9d).

5.3.2 Object-based Random Forest

As shown in Figure 5.9e, image segmentation enabled the aggregation of adjacent pixels with similar spectral properties in CIR imagery (Figure 5.9a). Following training sample segments with supervised Random Forest classification, the resultant segments were classified into shadow, defoliated, pine, and evergreen oak (Figure 5.9f) in comparison to the results of thresholding classification (Figure 5.9d).

5.3.3 Validation and accuracy assessment

Classes defined by histogram thresholding analyses (Tables 5.4, 5.5, 5.6 and 5.7) and Random Forest (Tables 5.8 and 5.9) were validated by a confusion matrix evaluating shadow, defoliation, and species with referenced RGB images and DSM as ground observations. The confusion matrix for classifying shadow and sun is detailed in Table 5.4 based on totaling 400 randomly selected pixels, showing that the higher producer's accuracy was 96% for the sun class where 212 out of the 220 pixels observed as sun were correctly classified by predicted NIR, while the shadow class showed a higher user's accuracy of 95% where 167 out of the 175 pixels predicted as shadow correctly represented the observed class. To analyze any variation among all study areas, overall accuracies were calculated by each area to compare the

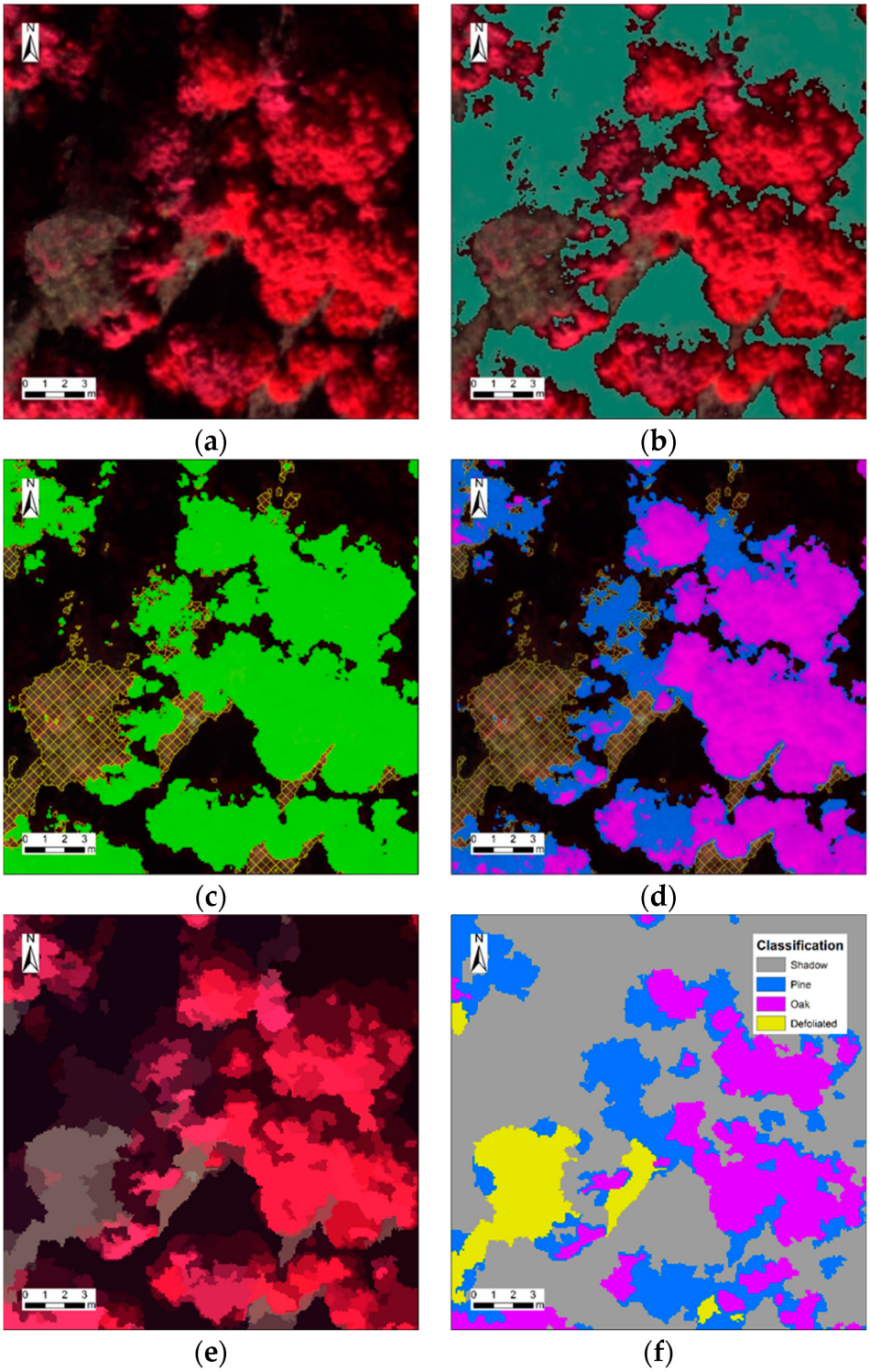

Figure 5.9: Process of histogram thresholding analysis in Codo: (a) CIR image; (b) CIR image with NIR highlighting shadow pixels in gray; (c) CIR image with GNDVI highlighting foliated pixels in green and defoliated in meshed yellow; and (d) CIR image with GNDVI highlighting foliated pines in blue, foliated evergreen oaks in purple, and defoliated in meshed yellow. The process of Random Forest classification in Codo: (e) CIR-derived segmentation as image objects and (f) supervised Random Forest classifying shadow in gray, defoliated in yellow, pine in blue, and evergreen oak in purple.

performance to the one totaled in Table 5.5, resulting in a total overall accuracy of 95% without any significant discrepancy by study area.

Table 5.4: Confusion matrix of NIR for shadow removal in the four study areas with the total of 400 randomly selected pixels, referenced to RGB images as ground observations.

		Predicted			
	Class	Shadow	Sun	Total	Producer's Accuracy
Observed	Shadow	167	13	180	93%
	Sun	8	212	220	96%
	Total	175	225	400	-
	User's Accuracy	95%	94%	-	95%

Table 5.5: Summary of overall accuracies from the confusion matrix of NIR in the four study areas for shadow removal, with each 100 randomly selected pixels referenced to ground observations.

Index	Codo	Hostal	Bosquet	Olius	Total
NIR	96%	93%	96%	94%	95%

Table 5.6: Summary of overall accuracies from the confusion matrix of four VIs in the four study areas for defoliation detection, with each 100 randomly selected pixels referenced to ground observations.

Index	Codo	Hostal	Bosquet	Olius	Total
NDVI	93%	91%	97%	98%	95%
GNDVI	91%	-	-	86%	-
GRNDVI	93%	84%	95%	97%	92%
NDVIRE	94%	90%	97%	97%	95%

Table 5.7: Summary of overall accuracies from the confusion matrix of GNDVI in the Codo and Olius study areas for species discrimination, with each 100 randomly selected pixels referenced to ground observations.

Index	Codo	Hostal	Bosquet	Olius	Total
GNDVI	96%	-	-	93%	-

For classifying defoliated and foliated pixels, overall accuracies were assessed in the same manner and compared among the four predicted VIs in the four study areas (Table 5.6). When the total overall accuracy based on totaling 400 randomly selected pixels was calculated per study area, NDVI and NDVIRE equally performed the best with a total overall accuracy of 95%, followed by GRNDVI with 92%, while it was not evaluable with GNDVI due to undetermined threshold values in Hostal and Bosquet. Since we were also able to estimate the average thresholds of best performed NDVI and NDVIRE over the total study area, the accuracy assessment was complemented with a sensitivity analysis, shifting the average threshold values

by 0.02–0.1. As shown in Figure 5.10a,b, the optimal threshold values (0.50 for NDVI and 0.44 for NDVIRE), where the difference in overall accuracies is the smallest across the four study areas, were highlighted resulting in slightly lower values than the estimated average.

For evaluating the accuracy of species discrimination, we conducted a third confusion matrix in the same manner by assessing overall accuracies with GNDVI in each of two study areas, Codo and Olius, as shown in Table 5.7. With an overall accuracy of 96%, GNDVI performed better in Codo study area than in Olius (93%). After visual inspection, we found that most errors derived from those randomly selected pixels that occurred to be near the boundary area between two classes.

Finally, Tables 5.8 and 5.9 by study area show the integrated confusion matrix of object-based Random Forest, which enabled to segment CIR images composed of three spectral bands and distinguish four classes of shadow, defoliated, pine, and evergreen oak at the same time with overall accuracies of 93% in Codo and 91% in Olius, as high as those results combined from Tables 5.5, 5.6 and 5.7.

Table 5.8: Summary of overall accuracies from the confusion matrix of Random Forest classification in Codo study area for shadow, defoliated, and species, with 100 randomly selected pixels referenced to ground observations.

		Predicted					
	Class	Shadow	Defoliated	Pine	Oak	Total	Producer's Accuracy
	Shadow	22	1	3	0	26	85%
	Defoliated	0	31	0	0	31	100%
	Pine	0	1	21	2	24	88%
Observed	Oak	0	0	0	19	19	100%
	Total	22	33	24	21	100	-
	User's Accuracy	100%	94%	88%	90%	-	93%

Table 5.9: Summary of overall accuracies from the confusion matrix of Random Forest classification in Olius study area for shadow, defoliated, and species, with 100 randomly selected pixels referenced to ground observations.

		Predicted					
	Class	Shadow	Defoliated	Pine	Oak	Total	Producer's Accuracy
	Shadow	22	1	1	0	24	92%
	Defoliated	0	26	0	0	26	100%
	Pine	0	2	26	0	28	93%
Observed	Oak	4	0	1	17	22	77%
	Total	26	29	28	17	100	-
	User's Accuracy	85%	90%	93%	100%	-	91%

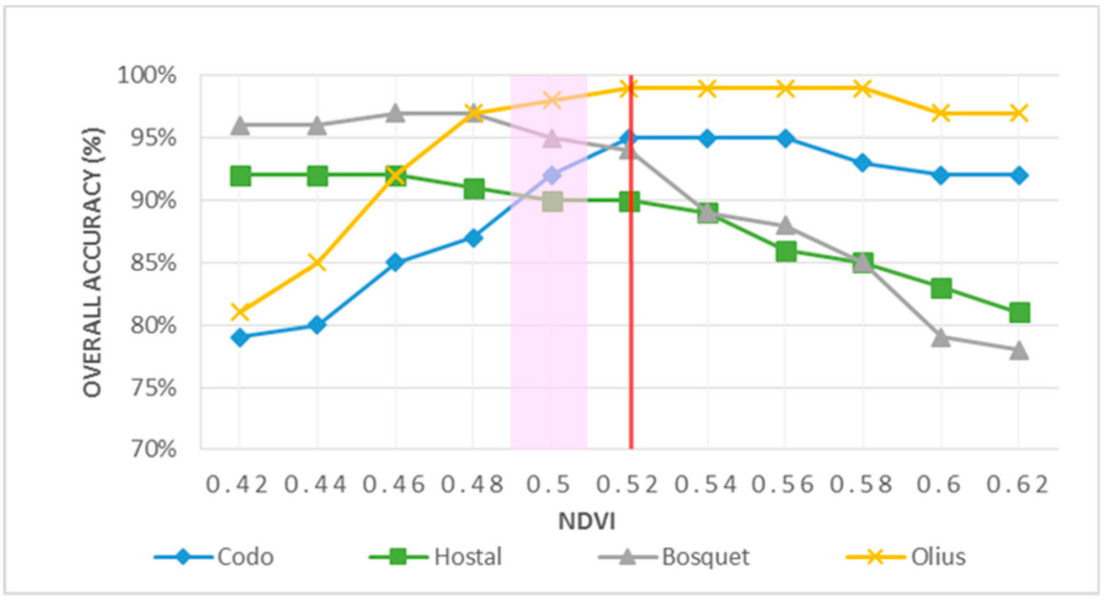

(a)

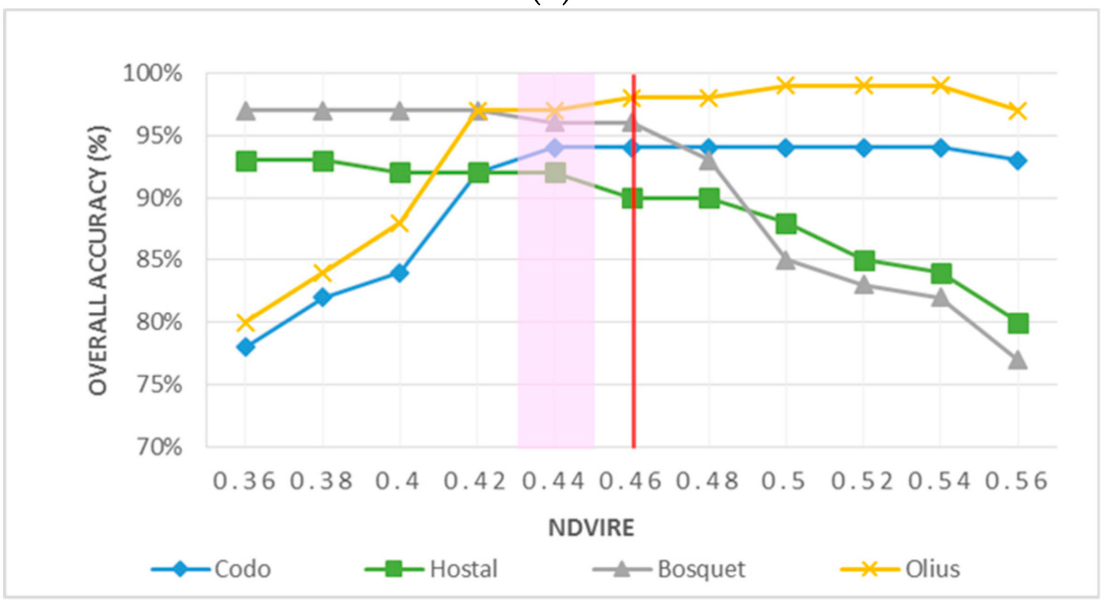

(b)

Figure 5.10: Sensitivity analysis testing the robustness of best performed VIs: (a) NDVI and (b) NDVIRE for defoliation detection in the four study areas. The optimal thresholds were highlighted in pink resulting in slightly lower values than the estimated average drawn in red line.

5.4 Discussion

Our methodology explored the capabilities of UAS-derived high spatial resolution NIR imagery for monitoring forest defoliation caused by *T. pityocampa* in small pine-dominated stands mixed with evergreen oak. Using a simple histogram thresholding analysis as a classification technique, the overall results showed that specific spectral bands or NIR-derived VIs perform better than the others for discriminating shadow, defoliation, and foliated tree species, which was determined by accuracy assessment in a confusion matrix. In contrast to this simple classification approach, we also used a more complex and robust object-based image classification technique with Random Forest, resulting in overall excellent performance as expected from the literature reviews (Blaschke, 2010; Weih and Riggan, 2010; Duro et al., 2012; Qian et al., 2015; Hossain and Chen, 2019).

5.4.1 Shadow removal

Shadow detection using a histogram thresholding analysis with an NIR band has been explored in several studies on forest areas following urban and agricultural areas (Shahtahmassebi et al., 2011; Adeline et al., 2013; Shahtahmassebi et al., 2013; Aasen et al., 2018). One of the disadvantages of this technique is that it can often be dicult to distinguish shadow areas and other dark surfaces such as water bodies (Shahtahmassebi et al., 2013); however, this limitation did not apply to our small study areas where no water features such as river, lake, or ocean were found. Miura and Midorikawa (Miura and Midorikawa, 2013) classified shadow areas by a histogram thresholding analysis using the NIR band from IKONOS data in order to eliminate shadow pixels that were difficult to accurately detect slope failure based on the difference in NDVI between the pre- and post-earthquake images. Lu (2007) also separated vegetation from shadows with the thresholds based on the IKONOS NDVI or NIR images, although it was difficult to extract cloud shadows from tree shadows. Martinuzzi et al. (2007) developed a method for detecting shadow areas in the NIR band from Landsat data to mask cloud shadows, including topographic shadows which were not successfully discriminated from each other. This type of limitation to separating topographic shadows from cloud shadows is not an issue in the UAS imagery as flights can be conducted under clouds.

Although in our study shadow areas were eliminated with high overall accuracies, those may be corrected by supervised classification training samples for different shadowed land cover types, instead of excluding them from further analysis. Other types of shadow corrections include deshadowing by scaling shadow pixels with combined spectral criteria of NIR and shortwave infrared bands derived from satellite images (Richter and Müller, 2005), which are more sensitive to shadow effects than visible bands, while a combination of RGB and NIR bands captured by airborne cameras was explored for diffusing shadow effects and validated by field measurements with a good agreement (Schläpfer et al., 2012). Thus, shadow correction methods should be explored for our further studies by developing a tool to combine spectral criteria from available bands and/or conducting extra flights within the following days or weeks over the same area of interest around the same time of the day to be comparable among them.

5.4.2 Defoliation detection

Focusing on forestry applications over the past decade, NDVI derived from UAS has been increasingly used for detecting defoliation at high spatial resolutions and assessing damage severity by classification techniques (Lehmann et al., 2015; Näsi et al., 2015; Smigaj et al., 2015; Michez et al., 2016; Cardil et al., 2017; Hentz and Strager, 2017; Torresan et al., 2017; Cardil et al., 2019). A continuous improvement in overall accuracy was demonstrated in our study by using histogram thresholding classification with the four VIs. NDVI and NDVIRE performed the best with an overall accuracy of 95%, followed by GRNDVI with 92% while GNDVI was excluded due to poor performance in determining the threshold values, which may be explained by the difference in reflectance between two bands selected for calculating each index. We could explain that the reflectance is generally higher in the green band due to chlorophyll absorption in blue and red bands (Aronoff, 2005; Rullan-Silva et al., 2013). Another explanation could be that unhealthy leaves show a notably higher reflectance than healthy leaves in the range of RGB visible light due to a decrease in chlorophyll content, while healthy leaves show significantly increased and exceeding reflectance in both the red edge and NIR bands (Xiao and McPherson, 2005; Masaitis et al., 2013; Hentz and Strager, 2017). Therefore, a larger difference in reflectance between the two bands used in any formula (Table 5.2) leads to higher index values and indicates healthier leaves. At least for the forest types analyzed in our study, there was no significant difference between NDVI and NDVIRE. In other words, the red edge band was not particularly more sensitive to defoliation than the NIR band.

Opportunities for future improvements include defoliation detection at the pixel level in integration with the UAS-derived canopy height model (CHM) at the 3D tree level to automatically delineate individual tree crowns and extract only pixels detected by the height of interest (Cardil et al., 2017, 2019; Mohan et al., 2017). For monitoring the forest inventory as a function of ecosystem services, it will be necessary to estimate the overall defoliation degree per individual tree which can be calculated by the ratio between pixels grouped as defoliated and foliated per tree (Cardil et al., 2019). For further 3D tree research, detecting the structural change of defoliated trees may be explored as an additional parameter by quantifying a dense point cloud (Harwin and Lucieer, 2012; Dandois and Ellis, 2013; Mathews and Jensen, 2013; Wallace et al., 2016; Hentz and Strager, 2017), which may contain information on cumulative defoliation in time series imagery, where the density of points on defoliating trees may start to decrease over time (Wallace et al., 2016).

5.4.3 Foliated species discrimination

As the UAS technology advances, studies on species discrimination for forestry applications (Gini et al., 2014; Lisein et al., 2015; Michez et al., 2016; Baena et al., 2017) have increased using various classification methods. Most recently, Cardil et al. (2019) applied thresholding classification with NDVI to distinguish among *Pinus* spp. with three levels of defoliation and from *Quercus ilex* in Codo, Spain, with an overall accuracy of 81%. The classification accuracy was re–evaluated in two of our study areas where we distinguished foliated *Pinus* spp. from *Q. ilex* by histogram thresholding classification with GNDVI with an increased overall accuracy of 93–96%. We again demonstrated that this comparison among various VIs led

to improve the classification results on species discrimination with GNDVI showing a bimodal histogram distribution in both the two study areas. This may suggest that the relation between green and NIR bands is the key measure to distinguish broad leaves from needle leaves among healthy trees, while GNDVI showed poor performance in defoliation detection. Several studies have suggested that the use of green bands in NDVI is more sensitive to chlorophyll which is well correlated to leaf area index (Yoder and Waring, 1994; Gitelson et al., 1996; Wang et al., 2007) as well as that broad leaves show a much higher reflection in the NIR range than needle leaves (Aronoff, 2005; Baldridge et al., 2009; Motohka et al., 2010). To examine the robustness of GNDVI for species discrimination, the similar threshold values determined in Codo and Olius should be reapplied to additional pine–oak mixed stands in new study areas.

It should be noted that UAS imagery has the advantage of separating pine trees from other species in mixed stands at tree level, enabling the exclusion of non-pine pixels for further analysis, while this may not be capable with Sentinel-2 (ESA, 2015) or Landsat 8 (NASA, 2019) data at medium spatial resolutions (10–30 m), which are too coarse to assess an individual tree crown area. Although the enhancement at spatial and temporal resolution is one of the significant advantages for using UAS imagery, the spectral resolution by Parrot SEQUOIA is limited to capturing RGB, red edge, and NIR bands, with wider bandwidths in the wavelength in comparison to other airborne sensors and satellites which are required to detect more features with narrower and/or specific bandwidths. Nonetheless, the Parrot SEQUOIA has been widely used for a relatively good economic performance tradeoff in operational forestry and agriculture applications, with the additional advantage of applying such high-resolution data to calibrate medium-resolution satellite data (Fraser et al., 2017; Pla et al., 2017, 2019; Otsu et al., 2018).

5.4.4 Classification techniques

General findings in the above-mentioned studies suggest that the overall accuracy for shadow removal, defoliation detection, and species discrimination should increase as the number of classes decreases, regardless of the technique used for classification. As observed in our study, a series of pixel-based thresholding analyses generated slightly higher overall accuracies in each confusion matrix for predicting two classes than object-based Random Forest for predicting four classes in one combined confusion matrix. One of the limitations of histogram thresholding analyses is that spatially isolated and fragmented pixels (Figure 5.9b-d) were as small as a ground resolution of approximately 7 cm to identify the class and assess the accuracy against the referenced orthomosaic image, unless pixels with similar digital number (DN) values were aggregated. To restrict pixels at a very high spatial resolution from being dispersed, object-based classification techniques enable to merge them with adjacent segments according to certain minimum segment size or shape (Blaschke, 2010). Despite these limitations, our study highlighted the simplicity of the histogram thresholding method to suggest combining the best indices for a series of classifications to extract the relevant information on different vegetation features.

5.4.5 Future research directions

Among four study areas defined as pine–dominated by land cover map, we noted that all threshold values of VIs in Codo study area for detecting defoliation were relatively higher than those in the other three study areas (Table 5.3). This may be explained by the seasonal difference in reflectance since the UAS imagery in Codo was captured in the end of November 2017, which was almost two months before the rest of the UAS flights were conducted in January 2018. It should also be noted that in Hostal study area the valley detection thresholding to separate foliated class in the multimodal distribution with GRNDVI (Appendix: Figure 5.11c) was not as clear as those with NDVI (Appendix: Figure 5.11a) or NDVIRE (Appendix: Figure 5.11d), which is one of the disadvantages of histogram thresholding analyses (Adeline et al., 2013; Aasen et al., 2018). Consequently, due to this ambiguous discrimination between defoliated and foliated classes, the classification accuracy with GRNDVI in Hostal turned out to be 84%, notably the lowest among the four study areas and VIs tested. As a solution to mitigate any potential errors, multiple flights over the same study area should be repeated at different dates to determine whether each threshold value is specific to a study area and/or season for accuracy improvement and monitoring purposes. Provided that the variation in the threshold limits among our study areas may have been affected by different flight dates, weather conditions, stand structures, and species composition which are not distinguishable by land cover map, the estimated average limits in Table 5.3 are not yet well established to be directly applied to new study areas on a large scale. Whether the similarity in the range of threshold limits can be achieved in similar forest types should be explored by applying the average or optimal threshold values (Figure 5.10a,b) to additional study areas.

Nevertheless, the enhanced UAS technology enabled us to achieve flights with both RGB and NIR multispectral cameras simultaneously in one platform. In contrast to conducting separate flights with each type of camera individually, our approach should have contributed to the consistency of reflectance between RGB and NIR images recorded at the same time of the day without any temporal delay, which was evidently visible in shadow areas (Cardil et al., 2019). Ultimately, such continuous advances in technology may improve our methodology and hence the classification results as well.

5.5 Conclusions

Using various VIs derived from very high spatial resolution UAS multispectral imagery, our study demonstrated quantitative assessments with high overall accuracies in small operational areas in Catalonia for detecting insect defoliation and potential host tree species in pine-dominated stands mixed with evergreen oak. With the aim of seeking a simple and robust monitoring tool for forest practitioners, we explored nested histogram thresholding analyses that achieved the highest overall accuracy of 95% with NDVI as well as NDVIRE for defoliation detection in the total study area, while accuracy results for foliated tree species discrimination were only achievable with GNDVI in two of the four study areas. In addition, the estimated average thresholds of NDVI and NDVIRE to detect defoliation were highlighted for evaluating accuracy and uncertainty in sensitivity analyses. Provided that the robustness

of selected VIs is sound, applying the average thresholds may become a promising simple tool to monitor forest defoliation and an alternative classification method to complex object-based Random Forest. In future studies, the robustness of the best performed indices for differentiating specific vegetation features should be explored in new study areas and repeated at multiple dates to contribute to regional forest health monitoring at the operational level.

5.6 Appendix

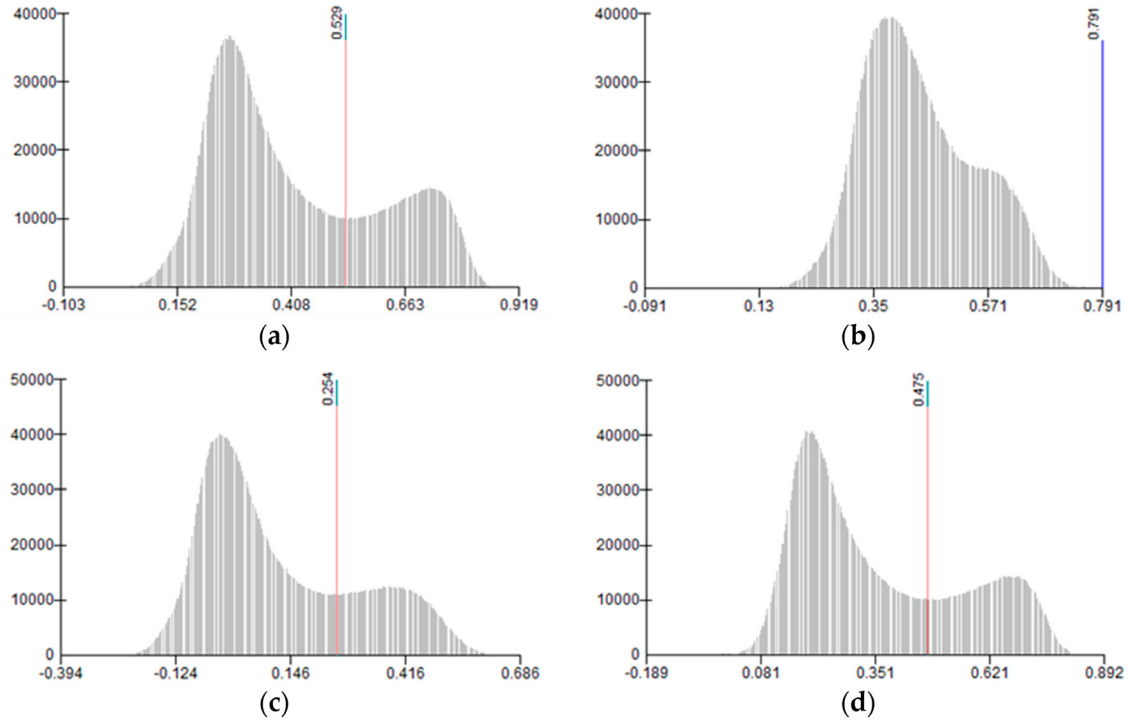

Figure 5.11: The valley detection thresholding to separate foliated class towards the highest VI values in a multimodal distribution, with pixel intensity on the x-axis and frequency on the y-axis, in the Hostal study area with: (a) NDVI; (b) GNDVI; (c) GRNDVI; and (d) NDVIRE.

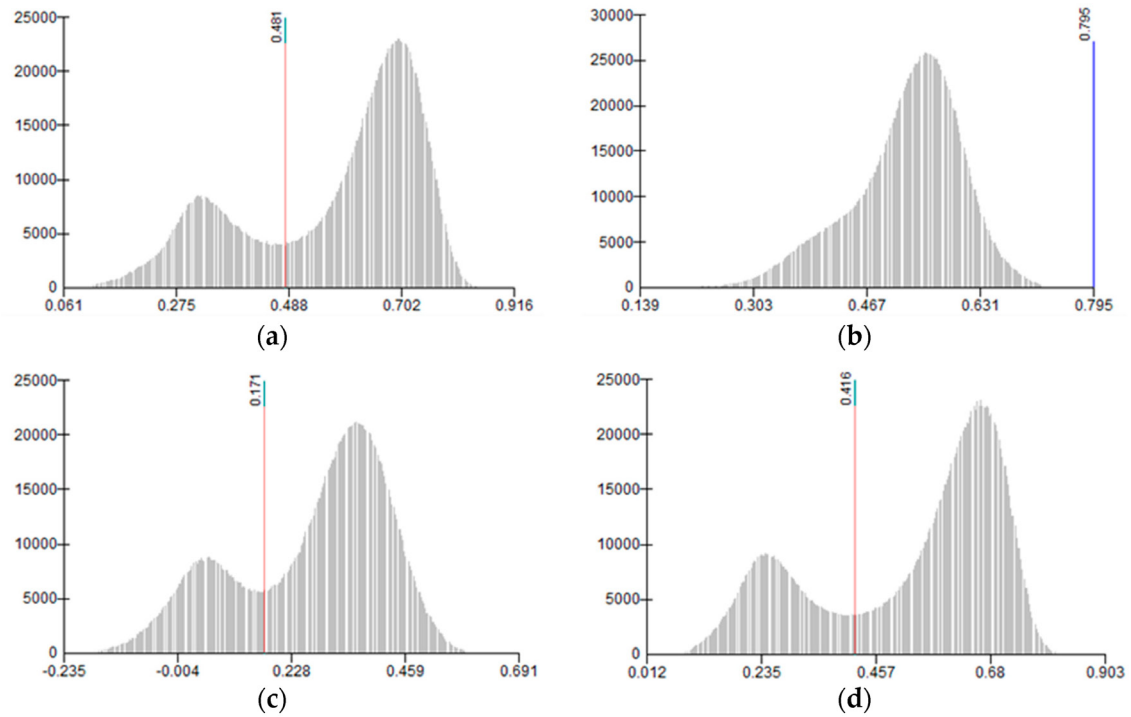

Figure 5.12: The valley detection thresholding to separate foliated class towards the highest VI values in a multimodal distribution, with pixel intensity on the x-axis and frequency on the y-axis, in the Bosquet study area with: (a) NDVI; (b) GNDVI; (c) GRNDVI; and (d) NDVIRE.

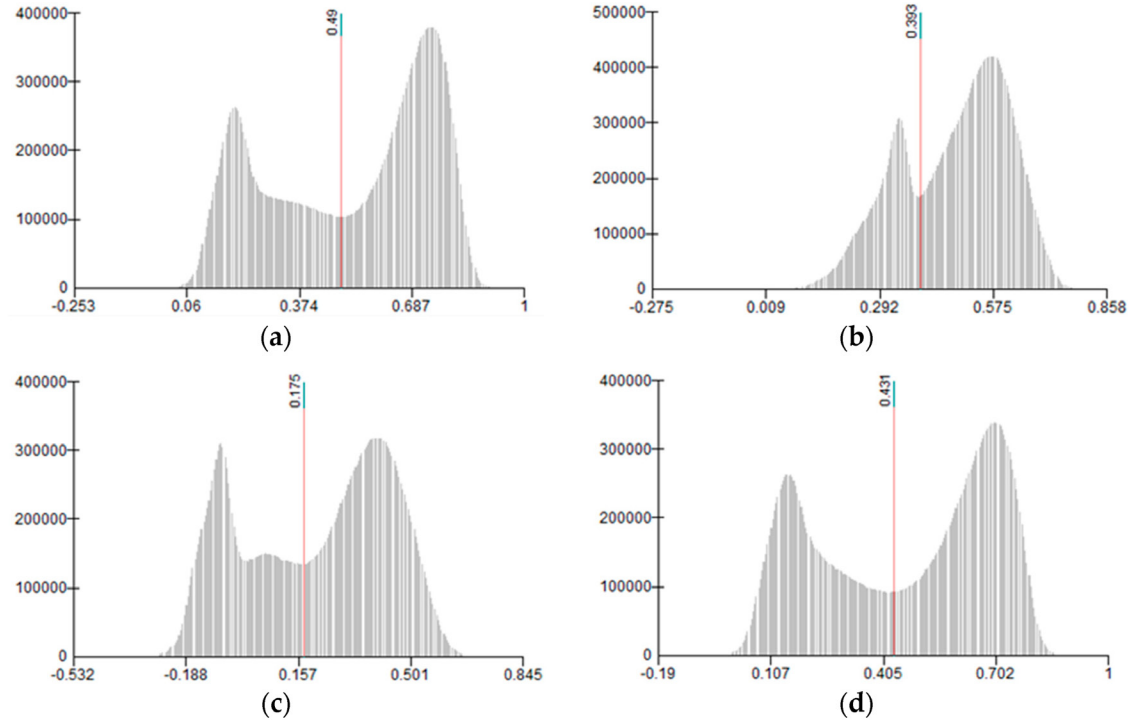

Figure 5.13: The valley detection thresholding to separate foliated class towards the highest VI values in a multimodal distribution, with pixel intensity on the x-axis and frequency on the y-axis, in the Olius study area with: (a) NDVI; (b) GNDVI; (c) GRNDVI; and (d) NDVIRE.

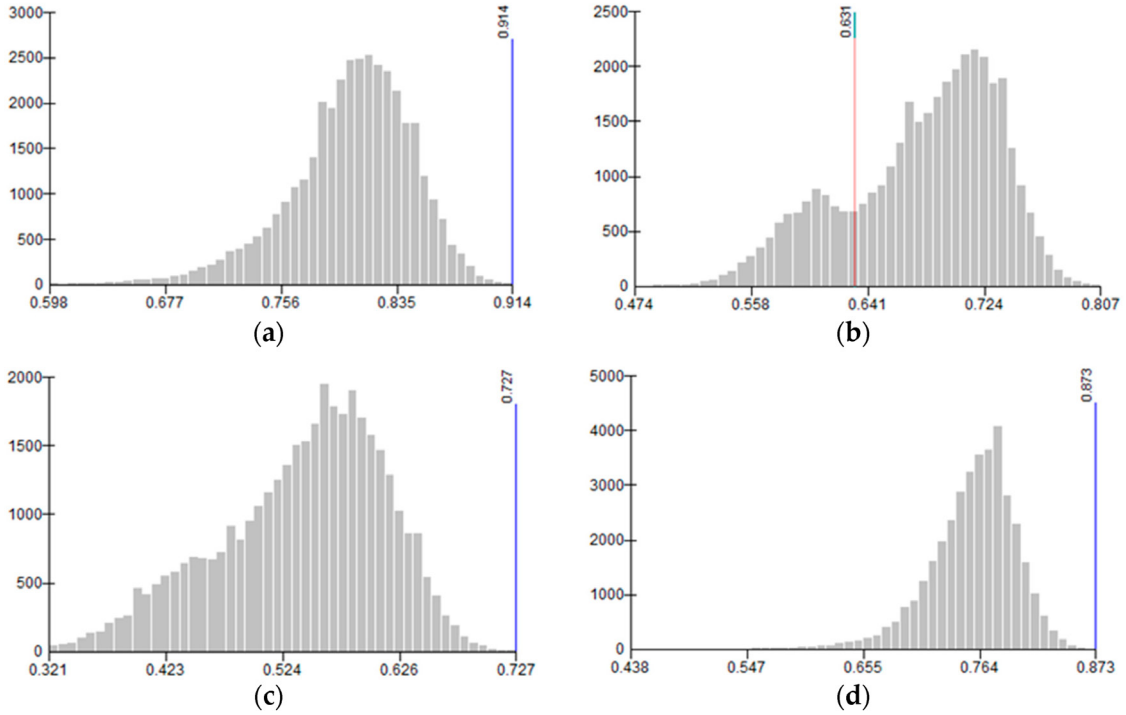

Figure 5.14: The valley detection thresholding to discriminate pine class towards lower VI values from evergreen oak class, with pixel intensity on the x-axis and frequency on the y-axis, in the Olius study area with: (a) NDVI; (b) GNDVI; (c) GRNDVI; and (d) NDVIRE.

General discussion and conclusions

The impact of insect defoliation on forest dynamics is complex in the current global change context. We need to consider that this impact cannot always be measured for one single disturbance driver but is often the result of combined causes in which insects interact with other biotic and/or abiotic factors (Rullan-Silva et al., 2013; Sangüesa-Barreda et al., 2014; Roques, 2015). Moreover, some indicators to be measured are not always quantitative but can often be qualitative, descriptive or categorical. Due to an increasing concern with climate change and extreme disturbance events (Jactel et al., 2006; Cardil et al., 2014, 2015; Robinet et al., 2014), continuous monitoring forest health with time-series analysis using a combination of remote sensing technologies including UAV is critical to detect any change in the current state and mitigate potential damages intensified due to the delayed detection.

With this research interest, I started my thesis with a systematic literature review (**Chapter 2**) on tree defoliation caused by insects throughout the world at any spatial scale, assessing the past and current impact of defoliation on forest ecosystem dynamics during the period of 1996-2016. Although the review was systematically conducted without limiting to any geographic extension, the spatial distribution of insect defoliations was reported and published in some regions concentrating in Europe and North America. This spatial data gap may be explained by the regional differences in economic, political and educational conditions between developed and developing countries (Morán-Ordóñez et al., 2018; Muller et al., 2018). Thus, it is critical to consider the high uncertainty in the rest of the world's forests, which may remain unreported or unobserved even if they have been defoliated. That said, nowadays earth observations from satellite images can easily capture burned and disturbed forests, which are being monitored through Global Wildfire Information System collaborated by GEO, NASA and Copernicus. Although the majority of developing countries may not afford to conduct annual or routine forest surveys, opportunities for increasing international projects on monitoring gap areas may be encouraged and collaborated by the world's leading space agencies such as NASA and ESA.

Despite the effort of advanced monitoring systems, it is predicted that the future impact of insect defoliations on forest dynamics may increase the intensity and extension. The intensity may be accelerated by a combination of complex and interacting disturbance factors such as climate change (e.g. IPCC scenarios with increased temperatures and extreme climate events). The extension of defoliated forests also may increase once we begin to account for previously unreported or unobserved forests that have been already affected. Moreover, the currently expanding biogeographical range of host tree distribution towards higher latitudes and higher elevations (Battisti et al., 2005; Roques, 2015) may favor pest invasion and survival

due to the future trend of climate change scenarios.

Based on the review in **Chapter 2**, temporal data gaps using remote sensing images became evident in the defoliation estimates prior to 1972. Future solutions include that the timeline of available satellite images will increase with Landsat (posterior to 1972, at 30m every 8 days), MODIS (posterior to 2000, at 200m every 16-day), and Sentinel (posterior to 2015, at 10-20m every 5 days), which may be combined to enhance the temporal resolution as well. Temporal data gaps often exist in the current defoliations since the satellite images are provided at a regular interval (every 5-8-16 days), however, calibrating UAV-based observations with the satellite-based VIs may fill those monitoring gaps (**Chapter 3**). Integration with UAV flights by training forest practitioners to complement their annual health survey may also contribute to increasing the survey frequency. Moreover, the potential of including citizen science to local mapping applications should be considered for increasing the frequency and extension of monitoring forests with additional UAV images uploaded by citizens although such voluntary participation by citizens may not guarantee effective monitoring systems since temporal resolutions are not fixed but rather random.

Evaluation on research approaches

For effective detection and monitoring, I argue that the methods should be selected according to the spatial and temporal scales, forest types and structures, classification techniques, and pest-host tree relationships. One of the technological limitations observed was inconsistency among multiple spatial scales and heterogeneous data sources, mainly between spaceborne Landsat or Sentinel and airborne UAV (**Chapter 3**). As the spectral resolution of spaceborne sensors is still much higher than airborne, the use of satellite imagery has the advantage of more options and combinations among a large number of spectral bands (e.g. Near Infrared (IR), Shortwave IR, Middle IR, Thermal IR) for selecting VIs and detecting more features with narrower and/or specific bandwidths. Such medium-resolution satellite images may be sufficient for standard monitoring as a coarse filter to observe the trend in the forest state and detect any significant change (Rullan-Silva et al., 2013; Näsi et al., 2015).

On the other hand, once research requires an additional analysis with high spatial and/or temporal resolution images, options of using airborne sensors such as LiDAR, ALS and UAV can provide fine-scale information as well as 3D structure data (Kantola et al., 2013; Rullan-Silva et al., 2013; Roncat et al., 2014). In particular, the spatial and temporal resolutions of UAV imagery are generally much higher and more flexible than spaceborne imagery. However, current limitations of UAV technology with quadcopters include battery duration for up to 30 minutes, resulting in small area coverage per flight, while the latest model with fixed-wing UAV is advancing to fly longer and farther than quadcopters (Lehmann et al., 2015; Torresan et al., 2017). To cover a large area at landscape and regional scales, it would require multiple flights that may not be consistent with the time, sensor and weather conditions, therefore, it would not replace satellite-based imagery. Nonetheless, where high spectral resolution is not required for small operational areas, instead of using satellite-based imagery, UAV flights would greatly increase the time-efficiency and cost-effectiveness as well as flexibility in planning imagery acquisition (Lehmann et al., 2015; Dash et al., 2017; Brovkina et al., 2018).

An additional inconsistency was observed among different dates, times and sites in processed images (**Chapter 3, 4 and 5**) despite the effort of applying atmospheric and/or radiometric corrections. This may be explained by some differences in reflectance due to the season of the year and/or the time of the day as well as the site topography. One of the advantages for using UAVs enables to conduct flights under clouds (**Chapter 3, 4 and 5**), which often cannot be controlled by satellite orbit scheduling and also can be difficult to extract cloud shadows from tree and topographic shadows. Another advantage is that the latest UAVs enable to capture RGB and NIR imagery simultaneously with both cameras on the same flight (**Chapter 5**), which can mitigate potential differences and errors in capturing images due to the delay at the time of the day and ultimately reduce the uncertainty in shadow areas shifting over time. In contrast to conducting separate flights with each type of camera individually, this approach shall contribute to the consistency of reflectance between RGB and NIR images recorded at the same time of the day without any temporal delay (Cardil et al., 2019), which was evidently visible in shadow areas as observed in **Chapter 5**.

As forest types and structures are mainly determined by species age and composition, the difficulty in analyzing mixed forest stands remains where the phenology of each tree species is different (**Chapter 3**). The issue of overestimating or underestimating damage degrees on host trees can be minimized by discrimination of non-host species through detecting spectral variations due to vegetation phenology with Landsat time-series approach such as LandTrendr, which can monitor cumulative defoliation as well as annual defoliation (Senf et al., 2017) although the Landsat spatial resolution is not high enough to identify individual trees. Nonetheless, integration of modelling species phenology and stand complexity and diversity in response to insect disturbances may be modelled by monitoring indicative parameters such as LAI and biomass production as a function of effects of defoliation severity at the stand level (Flower and Gonzalez-Meler, 2015). In addition, some VIs are more suitable for predicting the health of trees, depending on whether the species is coniferous or deciduous (higher GNDVI than coniferous **Chapter 5**). Recent studies used a larger sample size for species identification (Gini et al., 2014; Lisein et al., 2015; Michez et al., 2016), determining when is the best time window to achieve an optimal species discrimination, provided information of the pest life cycle. Therefore, the development of time-series analysis models with airborne imagery (e.g. LiDAR, ALS, and UAV) may be encouraged following the examples of TIMESAT with MODIS and LandTrendr with Landsat imagery. At the tree level, especially in mixed stands with the composition of multiple species, a point cloud density may be more suitable for monitoring individual trees over time (Harwin and Lucieer, 2012; Dandois and Ellis, 2013; Mathews and Jensen, 2013; Näsi et al., 2015; Wallace et al., 2016; Hentz and Strager, 2017). For further 3D tree research, the structural change in individual trees may be detected and monitored for cumulative defoliation in time series imagery where the density of points on defoliating trees may start to decrease over time (Wallace et al., 2016).

Beside the above technological variation, inconsistency in classification among forest practitioners including surveyors, interpreters and observers should be accounted for potential human errors (**Chapter 2 and 3**) due to manual and/or subjective data entry, which can be minimized by standardized measurements and automated image processing techniques (**Chapter 4 and 5**). Especially, improve-

ments in algorithms to identify and delineate individual trees (i.e. ITDe in **Chapter 4**) may enhance the accuracy of the defoliation estimations at tree level. Yet, there is no standardized accuracy assessment procedure for ITDe, therefore, it is still difficult to compare ITDe algorithms unless multiple approaches are tested on a single study area using the same datasets and metrics (Zhen et al., 2016; Cardil et al., 2019).

Solutions to methodological limitations

For establishing robust classification techniques, it still requires increasing the number of sample study areas captured by UAVs for standardizing the threshold values of detecting defoliation with robust VIs. Thus, average and/or optimal threshold values (**Chapter 5**) should be tested on a large number of pine dominated stands in the Mediterranean region. One of the limitations in pixel-based thresholding analysis should be noted that spatially fragmented pixels can be too small to identify the class and assess the accuracy against the referenced orthomosaic image (**Chapter 3 and 5**), unless pixels with similar digital number (DN) values were aggregated. To restrict pixels at a very high spatial resolution from being dispersed, object-based classification techniques with Random Forest (**Chapter 5**) enable to merge them with adjacent segments according to certain minimum segment size or shape (Blaschke, 2010). Another disadvantage in histogram thresholding analysis (**Chapter 5**) is the ambiguity for discriminating classes when the multimodal distribution is unclear, which may result in lowering the classification accuracy.

Despite the need to establish robust models for pest population dynamics, difficulty in predicting pest outbreaks involves the interpretation of ecological processes as well as hierarchical process-level understanding of biological interactions (Anderegg et al., 2015; Flower and Gonzalez-Meler, 2015). Increasing uncertainty and variability in prediction models is significant, due to the absence of robust indices and the increased number of predictive variables interacted (**Chapter 2**). Sensitivity analysis for testing the model robustness by increasing and decreasing predictive values, including the frequency and severity of outbreaks as well as extreme climate events, may reduce the uncertainty of response values (**Chapter 5**). Starting with the baseline scenario complemented with a sensitivity analysis may be encouraged by using nationally or internationally standardized data scales as inputs, if available, to generate comparable outputs such as the indicators defined by CICES (**Chapter 2**). In addition to innovatively developed models, well-established existing methods may be tested as the baseline scenarios using forest inventory data, dendrochronological analysis, statistical analysis, geospatial analysis, classification and/or time-series algorithm, as summarized in **Chapter 2**.

Currently, monitoring the expanding biogeographical range of host tree distribution towards higher latitudes and higher elevations plays an important role in detecting any pest invasion due to the future trend of climate change scenarios (Battisti et al., 2005; Roques, 2015). However, the costs are also high with remote sensing (Hall et al., 2016), or worse, it may not be easily accessible to those large remote areas using only UAVs due to the limited access to road networks and the short flight duration. Moreover, there are ongoing controversial discussions regarding the use of UAV orthomosaic images as ground-truth data without field measurements although this trend is increasing in recent scientific articles (Hentz and Strager, 2017; Mohan et al., 2017; Pla et al., 2017; Otsu et al., 2018; Cardil et al., 2019). Thus,

data validation between canopy-level observations and ground-level measurements may also be encouraged.

Future research directions

Overall findings highlighted that the effort on improving methods for pest detection and monitoring has been significantly increased over the past decade. Depending on the spatial and temporal scales and types of defoliation in question, the latest modelling and remote sensing techniques, including an emerging UAV technology, are currently available to be combined with conventional ground surveys and statistical analyses. Further exploration should address how such spaceborne and airborne remote sensing images may be integrated with aerial and field surveys into a multi-scale, multi-source monitoring system for the forest health (Hall et al., 2016). Since it is challenging to distinguish a single defoliation driver combined with other biotic and/or abiotic factors and also identify their relationships with specific host trees, continuous monitoring changes in several potential factors based on climate, forest inventory, and remote sensing data may be able to separate the causes. In particular, UAV high-resolution data can be a great source of information to calibrate medium resolution remote sensing information derived from satellites to map information in coarser scales (Fraser et al., 2017; Pla et al., 2017). Thus, calibration of stand-level satellite data (e.g. Landsat-derived NDVI) with tree-level UAV-derived NDVI will enable to enhance efficiency and potential accuracy of mapping information.

Future researches should consider the integration of process-based prediction models at various temporal scales as well as spatial scales (Anderegg et al., 2015; FAO, 2018), at the tree, stand and landscape levels, which can be transparent to other users by incorporating their output indicators as provisioning and regulating ecosystem services. Furthermore, those quantitative indicators (e.g. wood production, carbon and nutrient cycling) to measure changes in ecosystem services, considered as a function of stand resilience and response to forest disturbances, are therefore encouraged to follow international standards such as CICES so that the discrepancy due to incomparable and/or inconsistent measuring schemes can be avoided. I conclude that optimal detection and monitoring methods are often specific to each pest agent associated with host tree species. Therefore, the advancement in prediction models linked to ecosystem services in pest and disease control would be promising for mitigating the future damage to our forests under climate change from short-term to long-term trends.

Conclusions

- Chapter 2
  - The systematic literature review quantifying the past and present impact of major defoliators on forest dynamics revealed some study trends during the period of 1996-2016 throughout the world's forests. The impact assessment parameters such as pest drivers, tree effects, spatial and temporal distributions, detection methods, and ecosystem service types were identified then summarized in a database. It is highlighted that according to defoliation types and scales, the latest modelling and remote sensing techniques, including an emerging UAV technology, have been

increasingly combined with conventional ground surveys and statistical analyses.

  - As optimal methods for detection and monitoring may be specific to each pest agent associated with host tree species, recent technology advancements are promising for mitigating the future damage to high ecological, social and economic values of forests. For future research, predictive models based on those monitoring methods may be linked to ecosystem services in pest and disease control in compliance with the IPCC scenarios.

- Chapter 3

  - A recent outbreak of the pine processionary moth in Mediterranean forests has been an increasing threat to extensive pine dominated stands in Catalonia, Spain. For estimating the damage severity, the difference in vegetation index (dVI) between pre-outbreak and post-outbreak images derived from Landsat imagery was calculated as the change detection indicator. Although satellite data was calibrated with the limited number of UAV images, dVI using Moisture Stress Index (MSI) resulted in the best-fit logistic regression model with an acceptable overall accuracy of 72% for the severity classification.

  - As an alternative cost-effective method to other conventional ground-truth data, the use of UAV imagery may hold great potential for estimating the severity of defoliation in affected areas where ground-truth data is limited. Combining UAV images with satellite data may be considered to validate model predictions of the forest condition for developing ecosystem service tools.

- Chapter 4

  - Multispectral high-resolution UAV imagery was used to quantitatively assess defoliation caused by the pine processionary moth at the tree level within a pine-oak mixed forest in Catalonia. Multispectral orthomosaics and canopy height model (CHM) generated from the UAV imagery enabled to automate individual tree delineation (ITDe) for counting tree crowns and calculate NDVI for assessing defoliation degrees of canopy cover as well as estimating tree species.

  - Classifying pines that are non-defoliated, partially defoliated and completely defoliated resulted in an overall accuracy of 81% with the automated ITDe. The automated methodology highlighted the future potential of UAV multispectral imagery and structure-from-motion algorithms for individual tree detection, quantifying and monitoring defoliation.

- Chapter 5
  - To cost–effectively monitor temporal and spatial damages by the pine processionary moth in pine–oak mixed stands using UAV multispectral imagery, a simple thresholding classification tool for forest practitioners was explored as an alternative method to complex classifiers such as Random Forest (RF). With the aim of seeking a simple yet robust monitoring tool, nested histogram thresholding analyses with four UAV-derived NDVIs were conducted over small operational areas in Catalonia to detect defoliation and further distinguish pine species.
  - Standard NDVI and NDVIRE performed the best in thresholding classification for detecting defoliation with an overall accuracy of 95%. For discriminating pine species, accuracy results of 93–96% were only achievable with GNDVI in the partial study area, where the RF classification combined for defoliation and tree species resulted in 91–93%. In addition, the estimated average thresholds of NDVI and NDVIRE over the total area to detect defoliation were highlighted for evaluating accuracy and uncertainty in sensitivity analyses, which may be applicable across similar Mediterranean pine stands.

Bibliography

Aasen, H., E. Honkavaara, A. Lucieer, and P. J. Zarco-Tejada
2018. Quantitative remote sensing at ultra-high resolution with UAV spectroscopy: A review of sensor technology, measurement procedures, and data correctionworkflows. *Remote Sens.*, 10(7):1–42.

Adão, T., J. Hruška, L. Pádua, J. Bessa, E. Peres, R. Morais, and J. J. Sousa
2017. Hyperspectral imaging: A review on UAV-based sensors, data processing and applications for agriculture and forestry. *Remote Sens.*, 9(11).

Adelabu, S., O. Mutanga, E. Adam, and R. Sebego
2014. Spectral discrimination of insect defoliation levels in mopane woodland using hyperspectral data. *IEEE J. Sel. Top. Appl. Earth Obs. Remote Sens.*, 7(1):177–186.

Adeline, K. R., M. Chen, X. Briottet, S. K. Pang, and N. Paparoditis
2013. Shadow detection in very high spatial resolution aerial images: A comparative study. *ISPRS J. Photogramm. Remote Sens.*, 80:21–38.

Agisoft
2018a. *Agisoft PhotoScan User Manual: Professional Edition, Version 1.4*. Agisoft LCC, St. Petersburg, Russia.

Agisoft
2018b. *Tutorial Intermediate Level: Radiometric calibration using reflectance panels in PhotoScan: Professional Edition, Version 1.4*. Agisoft LLC, St. Petersburg, Russia.

Allen, T. R. and J. A. Kupfer
2001. Spectral response and spatial pattern of Fraser fir mortality and regeneration, Great Smoky Mountains, USA. *Plant Ecol.*, 156(1):59–74.

Allison, P. D.
2014. Measures of Fit for Logistic Regression. *SAS Glob. Forum 2014*, 2(1970):1–12.

Alonso, C., T. Vuorisalo, B. Wilsey, and T. Honkanen
2000. Yponomeuta evonymellus outbreaks in southern Finland: Spatial synchrony but different local magnitudes. *Ann. Zool. Fennici*, 37(3):179–188.

Anderegg, W. R., J. A. Hicke, R. A. Fisher, C. D. Allen, J. Aukema, B. Bentz, S. Hood, J. W. Lichstein, A. K. Macalady, N. Mcdowell, Y. Pan, K. Raffa, A. Sala,

J. D. Shaw, N. L. Stephenson, C. Tague, and M. Zeppel
2015. Tree mortality from drought, insects, and their interactions in a changing climate. *New Phytol.*, 208(3):674–683.

Arnaldo, P. S., S. Chacim, and D. Lopes
2010. Effects of defoliation by the pine processionary moth Thaumetopoea pityocampa on biomass growth of young stands of Pinus pinaster in northern Portugal. *iForest - Biogeosciences and Forestry*, 3(6):159–162.

Aronoff, S.
2005. *Remote sensing for GIS managers*. Redlands, Calif.: ESRI Press.

Augustin, S., S. Guichard, A. Svatoš, and M. Gilbert
2009. Monitoring the Regional Spread of the Invasive Leafminer *Cameraria ohridella* (Lepidoptera: Gracillariidae) by Damage Assessment and Pheromone Trapping. *Environ. Entomol.*, 33(6):1584–1592.

Aurenhammer, F.
1991. Voronoi Diagrams - A Survey of a Fundamental Data Structure. *ACM Comput. Surv.*, 23(3):345–405.

Avcí, M. and S. Carus
2005. The impact of cedar processionary moth [Traumatocampa ispartaensis (Doğanlar & Avcí) (Lepidoptera: Notodontidae)] outbreaks on radial growth of Lebanon cedar (Cedrus libani A. Rich.) trees in Turkey. *J. Pest Sci. (2004).*, 78(2):91–98.

Babst, F., J. Esper, and E. Parlow
2010. Landsat TM/ETM+ and tree-ring based assessment of spatiotemporal patterns of the autumnal moth (Epirrita autumnata) in northernmost Fennoscandia. *Remote Sens. Environ.*, 114(3):637–646.

Baena, S., J. Moat, O. Whaley, and D. S. Boyd
2017. Identifying species from the air: UAVs and the very high resolution challenge for plant conservation. *PLoS One*, 12(11):1–21.

Baldridge, A. M., S. J. Hook, C. I. Grove, and G. Rivera
2009. Remote Sensing of Environment The ASTER spectral library version 2 . 0. *Remote Sens. Environ.*, 113(4):711–715.

Barbedo, J. G. A.
2019. A Review on the Use of Unmanned Aerial Vehicles and Imaging Sensors for Monitoring and Assessing Plant Stresses. *Drones*, 3(2):40.

Barbosa, P., J. Hines, I. Kaplan, H. Martinson, A. Szczepaniec, and Z. Szendrei
2009. Associational Resistance and Associational Susceptibility: Having Right or Wrong Neighbors. *Annu. Rev. Ecol. Evol. Syst.*, 40(1):1–20.

Barron, E. S. and W. A. Patterson
2008. Monitoring the effects of gypsy moth defoliation on forest stand dynamics on Cape Cod, Massachusetts: Sampling intervals and appropriate interpretations. *For. Ecol. Manage.*, 256(12):2092–2100.

Battisti, A.
2008. Forests and climate change - Lessons from insects. *iForest - Biogeosciences and Forestry*, 1(1):1–5.

Battisti, A. and S. Larsson
2015. Climate Change and Insect Pest Distribution Range. In *Clim. Chang. Insect Pests*, C. Björkman and P. Niemelä, eds., chapter 1, Pp. 1–15. Oxfordshire, UK and Boston, USA: CAB International.

Battisti, A., S. Larsson, and A. Roques
2016. Processionary Moths and Associated Urtication Risk: Global Change–Driven Effects. *Annu. Rev. Entomol.*, 62(1):323–342.

Battisti, A. and M. Rodeghiero
1998. Monitoring spruce web-spinning sawflies Cephalcia spp.: The correlation between trap catches and soil sampling. *Entomol. Exp. Appl.*, 88(3):211–217.

Battisti, A., M. Stastny, S. Netherer, C. Robinet, A. Schopf, A. Roques, and S. Larsson
2005. Expansion of geographic range in the pine processionary moth caused by increased winter temperatures. *Ecol. Appl.*, 15(6):2084–2096.

Blaschke, T.
2010. Object based image analysis for remote sensing. *ISPRS J. Photogramm. Remote Sens.*, 65(1):2–16.

Bognounou, F., L. De Grandprè, D. S. Pureswaran, and D. Kneeshaw
2017. Temporal variation in plant neighborhood effects on the defoliation of primary and secondary hosts by an insect pest. *Ecosphere*, 8(3):e01759.

Bouchard, M. and D. Pothier
2010. Spatiotemporal variability in tree and stand mortality caused by spruce budworm outbreaks in eastern Quebec. *Can. J. For. Res.*, 40(1):86–94.

Boyd, I. L., P. H. Freer-Smith, C. A. Gilligan, and H. C. Godfray
2013. The consequence of tree pests and diseases for ecosystem services. *Science*, 342(6160).

Brandt, J. P., H. F. Cerezke, K. I. Mallett, W. J. Volney, and J. D. Weber
2003. Factors affecting trembling aspen (Populus tremuloides Michx.) health in the boreal forest of Alberta, Saskatchewan, and Manitoba, Canada. *For. Ecol. Manage.*, 178(3):287–300.

Brockerhoff, E. G., J. Bain, M. Kimberley, and M. Knížek
2006. Interception frequency of exotic bark and ambrosia beetles (Coleoptera: Scolytinae) and relationship with establishment in New Zealand and worldwide. *Can. J. For. Res.*, 36(2):289–298.

Brovkina, O., E. Cienciala, P. Surový, and P. Janata
2018. Unmanned aerial vehicles (UAV) for assessment of qualitative classification of Norway spruce in temperate forest stands. *Geo-Spatial Inf. Sci.*, 21(1):12–20.

Büntgen, U., D. Frank, A. Liebhold, D. Johnson, M. Carrer, C. Urbinati, M. Grabner, K. Nicolussi, T. Levanic, and J. Esper
2009. Three centuries of insect outbreaks across the European Alps. *New Phytol.*, 182(4):929–941.

Cabello, A., J. E. Frieyro, L. Granado, A. Hayas, E. Méndez, G. Montoya, and I. Pino
2011. Estudio de afecciones por plagas y decaimiento forestal en masas de coníferas mediante imágenes procedentes de sensores hiperespectrales. *XIV Congr. la Asoc. Española Teledetección*, Pp. 2–5.

Candau, J. N. and R. A. Fleming
2005. Landscape-scale spatial distribution of spruce budworm defoliation in relation to bioclimatic conditions. *Can. J. For. Res.*, 35(9):2218–2232.

Cardil, A., C. S. Eastaugh, and D. M. Molina
2015. Extreme temperature conditions and wildland fires in Spain. *Theor. Appl. Climatol.*, 122(1-2):219–228.

Cardil, A., D. M. Molina, and L. N. Kobziar
2014. Extreme temperature days and their potential impacts on southern Europe. *Nat. Hazards Earth Syst. Sci.*, 14(11):3005–3014.

Cardil, A., K. Otsu, M. Pla, C. A. Silva, and L. Brotons
2019. Quantifying pine processionary moth defoliation in a pine-oak mixed forest using unmanned aerial systems and multispectral imagery. *PLoS One*, 14(3):1–19.

Cardil, A., U. Vepakomma, and L. Brotons
2017. Assessing pine processionary moth defoliation using unmanned aerial systems. *Forests*, 8(10):402.

Carus, S. and M. Avci
2005. Growth loss of Lebanon cedar (Cedrus libani) stands as related to periodic outbreaks of the cedar shoot moth (Dichelia cedricola). *Phytoparasitica*, 33(1):33–48.

Catal, Y.
2011. The effects of pine processionary moth (PPM) defoliation degree on radial growth of brutian pine (Pinus brutia). *African J. Agric. Res.*, 6(21):4931–4936.

Cayuela, L., R. Hernández, J. A. Hódar, G. Sánchez, and R. Zamora
2014. Tree damage and population density relationships for the pine processionary moth: Prospects for ecological research and pest management. *For. Ecol. Manage.*, 328:319–325.

Cayuela, L., J. A. Hódar, and R. Zamora
2011. Is insecticide spraying a viable and cost-efficient management practice to control pine processionary moth in Mediterranean woodlands? *For. Ecol. Manage.*, 261(11):1732–1737.

Chen, Y., D. Wen, L. Jing, and P. Shi
2007. Shadow information recovery in urban areas from very high resolution satellite imagery. *Int. J. Remote Sens.*, 28(15):3249–3254.

Chenchouni, H., K. Zanati, A. Rezougui, A. Briki, and A. Arar
2010. Population Monitoring of Pine Processionary Moth (Thaumetopoea pityocampa) by Pheromone Trapping at the Southern Limit of Distribution of Pinus halepensis in Eastern Algeria. *Forest Sci. Technol.*, 6(2):67–79.

Chevrel, S., R. Belocky, and K. Grösel
2002. Monitoring and Assessing the Environmental Impact of Mining in Europe Using Advanced Earth Observation Techniques - MINEO. *Environ. Commun. Inf. Soc. - Proc. 16th Conf.*, Pp. 519–526.

Cocco, A., A. Q. Cossu, P. Erre, G. Nieddu, and P. Luciano
2010. Spatial analysis of gypsy moth populations in Sardinia using geostatistical and climate models. *Agric. For. Entomol.*, 12(4):417–426.

Coelho, I. and P. Campos
2009. *Mixed cork oak and stone pine woodlands in the Alentejo region of Portugal.* New York: Island Press.

Coli, W. M., C. S. Hollingsworth, and T. A. Hosmer
1997. Seasonal and vertical variation in activity of pear thrips (Thysanoptera: Thripidae) within stands of sugar maple. *Can. J. For. Res.*, 27(5):667–673.

Collins, M., R. Knutti, J. Arblaster, J.-L. Dufresne, T. Fichefet, P. Friedlingstein, X. Gao, W. Gutowski, T. Johns, G. Krinner, M. Shongwe, C. Tebaldi, A. Weaver, and M. Wehner
2013. Long-term Climate Change: Projections, Commitments and Irreversibility. In *Clim. Chang. 2013 Phys. Sci. Basis. Contrib. n Work. Gr. I to Fifth Assess. Rep. Intergov. Panel Clim. Chang.*, V. B. Stocker, T.F., D. Qin, G.-K. Plattner, M. Tignor, S.K. Allen, J. Boschung, A. Nauels, Y. Xia and P. Midgley, eds., chapter 12, Pp. 1029–1136. Cambridge, UK and New York, USA: Cambridge University Press.

Cook, B. D., P. V. Bolstad, J. G. Martin, F. A. Heinsch, K. J. Davis, W. Wang, A. R. Desai, and R. M. Teclaw
2008. Using light-use and production efficiency models to predict photosynthesis and net carbon exchange during forest canopy disturbance. *Ecosystems*, 11(1):26–44.

Cooke, B. J., V. G. Nealis, and J. Régnière
2007. as Periodic Northern Forest Ecosystems. *Plant Disturb. Ecol. Process Response*, Pp. 487–525.

Cooke, B. J. and J. Roland
2007. Trembling aspen responses to drought and defoliation by forest tent caterpillar and reconstruction of recent outbreaks in Ontario. *Can. J. For. Res.*, 37(9):1586–1598.

Damien, M., H. Jactel, C. Meredieu, M. Régolini, I. van Halder, and B. Castagneyrol
2016. Pest damage in mixed forests: Disentangling the effects of neighbor identity, host density and host apparency at different spatial scales. *For. Ecol. Manage.*, 378:103–110.

Dandois, J. P. and E. C. Ellis
2013. High spatial resolution three-dimensional mapping of vegetation spectral dynamics using computer vision. *Remote Sens. Environ.*, 136:259–276.

Dare, P. M.
2005. Shadow Analysis in High-Resolution Satellite Imagery of Urban Areas. *Photogramm. Eng. Remote Sens.*, 71(2):169–177.

Dash, J. P., G. D. Pearse, and M. S. Watt
2018. UAV multispectral imagery can complement satellite data for monitoring forest health. *Remote Sens.*, 10(8):1–22.

Dash, J. P., M. S. Watt, G. D. Pearse, M. Heaphy, and H. S. Dungey
2017. Assessing very high resolution UAV imagery for monitoring forest health during a simulated disease outbreak. *ISPRS J. Photogramm. Remote Sens.*, 131:1–14.

De Beurs, K. M. and P. A. Townsend
2008. Estimating the effect of gypsy moth defoliation using MODIS. *Remote Sens. Environ.*, 112(10):3983–3990.

Dennison, P. E., P. L. Nagler, K. R. Hultine, E. P. Glenn, and J. R. Ehleringer
2009. Remote monitoring of tamarisk defoliation and evapotranspiration following saltcedar leaf beetle attack. *Remote Sens. Environ.*, 113(7):1462–1472.

Deshayes, M., D. Guyon, H. Jeanjean, N. Stach, A. Jolly, and O. Hagolle
2006. The contribution of remote sensing to the assessment of drought effects in forest ecosystems. *Ann. For. Sci.*, 63(6):579–595.

DJI
2015. *Phantom 2 Vision+ User Manual V1.8*. DJI, Shenzhen, China.

Duning, J. B.
1995. Spatially explicit population models: current forms and future uses. *Ecol. Appl.*, 5(1):3–11.

Duro, D. C., S. E. Franklin, and M. G. Dubé
2012. A comparison of pixel-based and object-based image analysis with selected machine learning algorithms for the classification of agricultural landscapes using SPOT-5 HRG imagery. *Remote Sens. Environ.*, 118:259–272.

Dymond, C. C., E. T. Neilson, G. Stinson, K. Porter, D. A. MacLean, D. R. Gray, M. Campagna, and W. A. Kurz
2010. Future spruce budworm outbreak may create a carbon source in Eastern Canadian forests. *Ecosystems*, 13(6):917–931.

Eisenbies, M. H., C. Davidson, J. Johnson, R. Amateis, and K. Gottschalk
2007. Tree mortality in mixed pine-hardwood stands defoliated by the European gypsy moth (Lymantria dispar L.). *For. Sci.*, 53(6):683–691.

Eklundh, L., T. Johansson, and S. Solberg
2009. Mapping insect defoliation in Scots pine with MODIS time-series data. *Remote Sens. Environ.*, 113(7):1566–1573.

ESA
2015. *Sentinel -2 User Handbook*. European Space Agency.

Eshleman, K. N., D. A. Fiscus, N. M. Castro, J. R. Webb, and A. T. Herlihy
2004. Regionalization of disturbance-induced nitrogen leakage from mid-Appalachian forests using a linear systems model. *Hydrol. Process.*, 18(14):2713–2725.

Eshleman, K. N., R. H. Gardner, S. W. Seagle, N. M. Castro, D. A. Fiscus, J. R. Webb, J. N. Galloway, F. A. Deviney, and A. T. Herlihy
2000. Effects of Disturbance on Nitrogen Export from Forested Lands of the Chesapeake Bay Watershed. *Environ. Monit. Assess.*, 63(1):187–197.

FAO
2009. Global review of forest pests and diseases. Technical report, Food and Agriculture Organization of the United Nations, Rome.

FAO
2018. State of Mediterranean forests 2018. Technical report, Food and Agriculture Organization of the United Nations and Plan Bleu, Rome and Marseille.

Feng, Q., J. Liu, and J. Gong
2015. UAV Remote sensing for urban vegetation mapping using random forest and texture analysis. *Remote Sens.*, 7(1):1074–1094.

Fernández, C., J. A. Vega, T. Fonturbel, J. M. Gras, and E. Jiménez
2011. Absence of effects on nutrient budgets after insect defoliation. *For. Syst.*, 20(2):228–234.

Fernández-Guisuraga, J. M., E. Sanz-Ablanedo, S. Suárez-Seoane, and L. Calvo
2018. Using unmanned aerial vehicles in postfire vegetation survey campaigns through large and heterogeneous areas: Opportunities and challenges. *Sensors (Switzerland)*, 18(2):586.

Filho, W. L., M. Mandel, A. Q. Al-Amin, A. Feher, and C. J. C. Jabbour
2017. An assessment of the causes and consequences of agricultural land abandonment in Europe. *Int. J. Sustain. Dev. World Ecol.*, 24(6):554–560.

Fischer, R., V. Mues, E. Ulrich, G. Becher, and M. Lorenz
2007. Monitoring of atmospheric deposition in European forests and an overview on its implication on forest condition. *Appl. Geochemistry*, 22(6):1129–1139.

Fisichelli, N. A., S. R. Abella, M. Peters, and F. J. Krist
2014. Climate, trees, pests, and weeds: Change, uncertainty, and biotic stressors in eastern U.S. national park forests. *For. Ecol. Manage.*, 327:31–39.

Flower, C. and M. Gonzalez-Meler
2015. Responses of Temperate Forest Productivity to Insect and Pathogen Disturbances. *Annu. Rev. Plant Biol.*, 66:547–569.

Fraser, R. H., J. van der Sluijs, and R. J. Hall
2017. Calibrating satellite-based indices of burn severity from UAV-derived metrics of a burned boreal forest in NWT, Canada. *Remote Sens.*, 9(3):279.

García, M. J. L. and V. Caselles
1991. Mapping burns and natural reforestation using thematic mapper data. *Geocarto Int.*, 6(1):31–37.

Garcia-Ruiz, F., S. Sankaran, J. M. Maja, W. S. Lee, J. Rasmussen, and R. Ehsani
2013. Comparison of two aerial imaging platforms for identification of Huanglongbing-infected citrus trees. *Comput. Electron. Agric.*, 91:106–115.

Gilichinsky, M., H. Olsson, and S. Solberg
2013. Reflectance changes due to pine sawfly attack detected using multitemporal SPOT satellite data. *Remote Sens. Lett.*, 4(1):10–18.

Gini, R., D. Passoni, L. Pinto, and G. Sona
2014. Use of unmanned aerial systems for multispectral survey and tree classification: A test in a park area of northern Italy. *Eur. J. Remote Sens.*, 47(1):251–269.

Gitelson, A. A., Y. J. Kaufman, and M. N. Merzlyak
1996. Use of a green channel in remote sensing of global vegetation from EOS-MODIS. *Remote Sens. Environ.*, 58(3):289–298.

Gómez, S., L. Gonda-King, C. M. Orians, D. A. Orwig, R. Panko, L. Radville, N. Soltis, C. S. Thornber, and E. L. Preisser
2015. Interactions between invasive herbivores and their long-term impact on New England hemlock forests. *Biol. Invasions*, 17(2):661–673.

Guyot, V., B. Castagneyrol, A. Vialatte, M. Deconchat, and H. Jactel
2016. Tree diversity reduces pest damage in mature forests across Europe. *Biol. Lett.*, 12(4):0–4.

Haase, J., B. Castagneyrol, J. H. C. Cornelissen, J. Ghazoul, J. Kattge, J. Koricheva, M. Scherer-Lorenzen, S. Morath, and H. Jactel
2015. Contrasting effects of tree diversity on young tree growth and resistance to insect herbivores across three biodiversity experiments. *Oikos*, 124(12):1674–1685.

Haines-Young, R. and M. B. Potschin
2018. Common International Classification of Ecosystem Services (CICES) V5.1 and Guidance on the Application of the Revised Structure. *Eur. Environ. Agency*, (January):53.

Hall, R. J., G. Castilla, J. C. White, B. J. Cooke, and R. S. Skakun
2016. Remote sensing of forest pest damage: a review and lessons learned from a Canadian perspective. *Can. Entomol.*, 148(S1):S296–S356.

Hall, R. J., R. A. Fernandes, E. H. Hogg, J. P. Brandt, C. Butson, B. S. Case, and S. G. Leblanc
2003. Relating aspen defoliation to changes in leaf area derived from field and satellite remote sensing data. *Can. J. Remote Sens.*, 29(3):299–313.

Hall, R. J. and R. S. Skakun
2006. Remotely Sensed Data in the Mapping of Insect Defoliation. *Underst. For. Disturb. Spat. Pattern Remote Sens. GIS Approaches*, Pp. 85–111.

Halldórsson, G., T. Benedikz, Ó. Eggertsson, E. S. Oddsdóttir, and H. Óskarsson
2003. The impact of the green spruce aphid Elatobium abietinum (Walker) on long-term growth of Sitka spruce in Iceland. *For. Ecol. Manage.*, 181(3):281–287.

Hanssen, K. H. and S. Solberg
2007. Assessment of defoliation during a pine sawfly outbreak: Calibration of airborne laser scanning data with hemispherical photography. *For. Ecol. Manage.*, 250(1-2):9–16.

Hantson, S. and E. Chuvieco
2011. Evaluation of different topographic correction methods for landsat imagery. *Int. J. Appl. Earth Obs. Geoinf.*, 13(5):691–700.

Harwin, S. and A. Lucieer
2012. Assessing the Accuracy of Georeferenced Point Clouds Produced via Multi-View Stereopsis from Unmanned Aerial Vehicle (UAV) Imagery. *Remote Sens.*, 4(6):1573–1599.

Haynes, K. J., A. J. Allstadt, and D. Klimetzek
2014. Forest defoliator outbreaks under climate change: Effects on the frequency and severity of outbreaks of five pine insect pests. *Glob. Chang. Biol.*, 20(6):2004–2018.

Hentschel, R., K. Möller, A. Wenning, A. Degenhardt, and J. Schröder
2018. Importance of ecological variables in explaining population dynamics of three important pine pest insects. *Front. Plant Sci.*, 871(November):1–17.

Hentz, A. M. K. and M. P. Strager
2017. Cicada damage detection based on UAV spectral and 3D data. *Silvilaser 2017*, 10(1):95–96.

Hicke, J. A., C. D. Allen, A. R. Desai, M. C. Dietze, R. J. Hall, E. H. Hogg, D. M. Kashian, D. Moore, K. F. Raffa, R. N. Sturrock, and J. Vogelmann
2012. Effects of biotic disturbances on forest carbon cycling in the United States and Canada. *Glob. Chang. Biol.*, 18(1):7–34.

Hódar, J. A., J. Castro, and R. Zamora
2003. Pine processionary caterpillar Thaumetopoea pityocampa as a new threat for relict Mediterranean Scots pine forests under climatic warming. *Biol. Conserv.*, 110(1):123–129.

Hódar, J. A., R. Zamora, J. Castro, and E. Baraza
2004. Feast and famine: Previous defoliation limiting survival of pine processionary caterpillar Thaumetopoea pityocampa in Scots pine Pinus sylvestris. *Acta Oecologica*, 26(3):203–210.

Holmes, R. L.
1983. Computer-Assisted Quality Control in Tree-Ring Dating and Measurement. volume 43, Pp. 51–67. Tree-Ring Society.

Hossain, M. D. and D. Chen
2019. Segmentation for Object-Based Image Analysis (OBIA): A review of algorithms and challenges from remote sensing perspective. *ISPRS J. Photogramm. Remote Sens.*, 150(November 2018):115–134.

Huberty, A. F. and R. F. Denno
2004. Plant Water Stress and Its Consequences for Herbivorous Insects : A New Synthesis. *Ecology*, 85(5):1383–1398.

Hung, C., Z. Xu, and S. Sukkarieh
2014. Feature learning based approach for weed classification using high resolution aerial images from a digital camera mounted on a UAV. *Remote Sens.*, 6(12):12037–12054.

Hunt Jr, E. R. and B. N. Rock
1989. Detection of changes in leaf water content using Near- and Middle-Infrared reflectances. *Remote Sens. Environ.*, 30(1):43–54.

Hyvonen, R., G. I. Agren, S. Linder, T. Persson, M. F. Cotrufo, A. Ekblad, M. Freeman, A. Grelle, I. A. Janssens, P. G. Jarvis, S. Kellomaki, A. Lindroth, D. Loustau, T. Lundmark, R. J. Norby, R. Oren, K. Pilegaard, M. G. Ryan, B. D. Sigurdsson, M. Stromgren, M. van Oijen, and G. Wallin
2007. The likely impact of elevated [CO2], nitrogen deposition, increased temperature and management on carbon sequestration in temperate and boreal forest ecosystems: a literature review. *New Phytol*, 173(3):463–480.

ICGC
2018. *Orthophoto in colour of Catalonia 25cm (OF-25C) V4.0.* Institut Cartogràfic i Geològic de Catalunya.

Inbar, M., H. Doostdar, D. Gerling, and R. T. Mayer
2001. Induction of systemic acquired resistance in cotton by BTH has a negligible effect on phytophagous insects. *Entomol. Exp. Appl.*, 99(1):65–70.

Isenburg, M.
2015. *LAStools: efficient tools for LiDAR processing V1.3.* rapidlasso GmbH, Gilching, Germany.

Jaafar, W. S. W. M., I. H. Woodhouse, C. A. Silva, H. Omar, K. N. A. Maulud, A. T. Hudak, C. Klauberg, A. Cardil, and M. Mohan
2018. Improving individual tree crown delineation and attributes estimation of tropical forests using airborne LiDAR data. *Forests*, 9(12):1–23.

Jactel, H. and E. G. Brockerhoff
2007. Tree diversity reduces herbivory by forest insects. *Ecol. Lett.*, 10(9):835–848.

Jactel, H., P. Menassieu, F. Vétillard, B. Barthélémy, D. Piou, B. Frérot, J. Rousselet, F. Goussard, M. Branco, and A. Battisti
2006. Population monitoring of the pine processionary moth (Lepidoptera: Thaumetopoeidae) with pheromone-baited traps. *For. Ecol. Manage.*, 235(1-3):96–106.

Jactel, H., J. Petit, M. L. Desprez-Loustau, S. Delzon, D. Piou, A. Battisti, and J. Koricheva
2012. Drought effects on damage by forest insects and pathogens: A meta-analysis. *Glob. Chang. Biol.*, 18(1):267–276.

James, P. M., R. A. Fleming, and M. J. Fortin
2010. Identifying significant scale-specific spatial boundaries using wavelets and null models: Spruce budworm defoliation in Ontario, Canada as a case study. *Landsc. Ecol.*, 25(6):873–887.

Jan-Chang C, Yi-Ta H, C.-T. C. S.-T. W.
2016. Evaluation of Automatic Shadow Detection Approaches Using ADS-40 High Radiometric Resolution Aerial Images at High Mountainous Region. *Journal of Remote Sensing GIS*, 5(2):1–5.

Jönsson, P. and L. Eklundh
2002. Seasonality extraction by function fitting to time-series of satellite sensor data. *IEEE Trans. Geosci. Remote Sens.*, 40(8):1824–1832.

Kanat, M., M. H. Alma, and F. Sivrikaya
2005. Effect of defoliation by Thaumetopoea pityocampa (Den. & Schiff.) (Lepidoptera: Thaumetopoeidae) on annual diameter increment of Pinus brutia Ten. in Turkey. *Ann. For. Sci.*, 62(1):91–94.

Kantola, T., M. Vastaranta, P. Lyytikäinen-Saarenmaa, M. Holopainen, V. Kankare, M. Talvitie, and J. Hyyppä
2013. Classification of needle loss of individual scots pine trees by means of airborne laser scanning. *Forests*, 4(2):386–403.

Kantola, T., M. Vastaranta, X. Yu, P. Lyytikainen-Saarenmaa, M. Holopainen, M. Talvitie, S. Kaasalainen, S. Solberg, and J. Hyyppa
2010. Classification of defoliated trees using tree-level airborne laser scanning data combined with aerial images. *Remote Sens.*, 2(12):2665–2679.

Kapeller, S., H. Schroeder, and S. Schueler
2011. Modelling the spatial population dynamics of the green oak leaf roller (Tortrix viridana) using density dependent competitive interactions: Effects of herbivore mortality and varying host-plant quality. *Ecol. Modell.*, 222(7):1293–1302.

Kattenborn, T., M. Sperlich, K. Bataua, and B. Koch
2014. Automatic single palm tree detection in plantations using UAV-based photogrammetric point clouds. *Int. Arch. Photogramm. Remote Sens. Spat. Inf. Sci. - ISPRS Arch.*, 40(3):139–144.

Kautz, M., A. J. H. Meddens, R. J. Hall, and A. Arneth
2017. Biotic disturbances in Northern Hemisphere forests – a synthesis of recent data , uncertainties and implications for forest monitoring and modelling. *Global Ecology and Biogeography*, 26(5):533–552.

Kirschbaum, A. A., E. Pfaff, and U. B. Gafvert
2016. Are U.S. national parks in the Upper Midwest acting as refugia? Inside vs. outside park disturbance regimes. *Ecosphere*, 7(9):1–15.

Koricheva, J., S. Larsson, and E. Haukioja
2002. Insect Performance on Experimentally Stressed Woody Plants: A Meta-Analysis. *Annu. Rev. Entomol.*, 43(1):195–216.

Koukl, J., D. G. McCullough, and L. D. Marshall
1997. Effect of forest stand and edge characteristics on the vulnerability of jack pine stands to jack pine budworm (Choristoneura pinus pinus) damage. *Can. J. For. Res.*, 27(11):1765–1772.

Kozlov, M. V.
2008. Losses of birch foliage due to insect herbivory along geographical gradients in Europe: A climate-driven pattern? *Clim. Change*, 87(1-2):107–117.

Kramer, P. J. and T. T. Kozlowski
1979. Physiology of Woody Plants. In *Acad. Press*, P. 826. New York, USA: Academic Press.

Kraus, K. and N. Pfeifer
1998. Determination of terrain models in wooded areas with airborne laser scanner data. *ISPRS J. Photogramm. Remote Sens.*, 53(4):193–203.

Krause, C., B. Luszczynski, H. Morin, S. Rossi, and P. Y. Plourde
2012. Timing of growth reductions in black spruce stem and branches during the 1970s spruce budworm outbreak. *Can. J. For. Res.*, 42(7):1220–1227.

Kretchun, A. M., R. M. Scheller, M. S. Lucash, K. L. Clark, J. Hom, and S. Van Tuyl
2014. Predicted effects of gypsy moth defoliation and climate change on forest carbon dynamics in the New Jersey Pine Barrens. *PLoS One*, 9(8).

Lasanta, T., J. Arnáez, N. Pascual, P. Ruiz-Flaño, M. P. Errea, and N. Lana-Renault
2017. Space–time process and drivers of land abandonment in Europe. *Catena*, 149:810–823.

Legendre, P. and L. Legendre
1998. Numerical Ecology. In *Dev. Environ. Model.*, volume 24, P. 852. Elsevier Science.

Lehmann, J. R. K., F. Nieberding, T. Prinz, and C. Knoth
2015. Analysis of unmanned aerial system-based CIR images in forestry-a new perspective to monitor pest infestation levels. *Forests*, 6(3):594–612.

Leland, C., J. Hom, N. Skowronski, F. T. Ledig, P. J. Krusic, E. R. Cook, D. Martin-Benito, J. Martin-Fernandez, and N. Pederson
2016. Missing rings, synchronous growth, and ecological disturbance in a 36-year pitch pine (pinus rigida) provenance study. *PLoS One*, 11(5):1–18.

Li, S., J. J. Daudin, D. Piou, C. Robinet, and H. Jactel
2015. Periodicity and synchrony of pine processionary moth outbreaks in France. *For. Ecol. Manage.*, 354:309–317.

Liang, Q., I. S. Otvos, and G. E. Bradfield
1998. Pupal sampling of the western hemlock looper,. 122:85–88.

Liebhold, A., E. Luzader, R. Reardon, A. Roberts, W. F. Ravlin, A. Sharov, and G. Zhou
1998. Forecasting Gypsy Moth (Lepidoptera: Lymantriidae) Defoliation with a Geographical Information System. *J. Econ. Entomol.*, 91(2):464–472.

Linnakoski, R., R. Kasanen, A. Dounavi, and K. M. Forbes
2019. Editorial: Forest Health Under Climate Change: Effects on Tree Resilience, and Pest and Pathogen Dynamics. *Front. Plant Sci.*, 10(October):1–3.

Lisein, J., A. Michez, H. Claessens, and P. Lejeune
2015. Discrimination of deciduous tree species from time series of unmanned aerial system imagery. *PLoS One*, 10(11):1–20.

Lottes, P., R. Khanna, J. Pfeifer, R. Siegwart, and C. Stachniss
2017. UAV-based crop and weed classification for smart farming. *Proc. - IEEE Int. Conf. Robot. Autom.*, Pp. 3024–3031.

Lu, D.
2007. Detection and substitution of clouds/hazes and their cast shadows on IKONOS images. *Int. J. Remote Sens.*, 28(18):4027–4035.

Lu, D., P. Mausel, E. Brondizio, and E. Moran
2004. Change detection techniques. *Int. J. Remote Sens.*, 25(March):2365–2407.

Lucieer, A., D. Turner, D. H. King, and S. A. Robinson
2014. Using an unmanned aerial vehicle (UAV) to capture micro-topography of antarctic moss beds. *Int. J. Appl. Earth Obs. Geoinf.*, 27(PARTA):53–62.

Luyssaert, S., P. Ciais, S. L. Piao, E. D. Schulze, M. Jung, S. Zaehle, M. J. Schelhaas, M. Reichstein, G. Churkina, D. Papale, G. Abril, C. Beer, J. Grace, D. Loustau, G. Matteucci, F. Magnani, G. J. Nabuurs, H. Verbeeck, M. Sulkava, G. R. van der Werf, and I. A. Janssens
2010. The European carbon balance. Part 3: Forests. *Glob. Chang. Biol.*, 16(5):1429–1450.

Lyytikäinen-saarenmaa, P., M. Varama, and O. Anderbrant
2001. Predicting Pine Sawfly Population Densities and Subsequent Defoliation with Pheromone Traps. *Integr. Manag. Dyn. For. desfoliating insects*, (Tiihonen 1970):108–116.

Lyytikäinen-Saarenmaa, P., M. Varama, O. Anderbrant, M. Kukkola, A. M. Kokkonen, E. Hedenström, and H. E. Högberg
2006. Monitoring the European pine sawfly with pheromone traps in maturing Scots pine stands. *Agric. For. Entomol.*, 8(1):7–15.

MacLean, D. A., W. E. MacKinnon, K. B. Porter, K. P. Beaton, G. Cormier, and S. Morehouse
2000. Use of forest inventory and monitoring data in the spruce budworm decision support system. *Comput. Electron. Agric.*, 28(2):101–118.

Man, R., G. J. Kayahara, J. A. Rice, and G. B. MacDonald
2008. Response of trembling aspen to partial cutting and subsequent forest tent caterpillar defoliation in a boreal mixedwood stand in northeastern Ontario, Canada. *Can. J. For. Res.*, 38(6):1349–1356.

Manfreda, S., M. F. McCabe, P. E. Miller, R. Lucas, V. P. Madrigal, G. Mallinis, E. B. Dor, D. Helman, L. Estes, G. Ciraolo, J. Müllerová, F. Tauro, M. I. de Lima, J. L. de Lima, A. Maltese, F. Frances, K. Caylor, M. Kohv, M. Perks, G. Ruiz-Pérez, Z. Su, G. Vico, and B. Toth
2018. On the use of unmanned aerial systems for environmental monitoring. *Remote Sens.*, 10(4):641.

Martin, M. E., L. C. Plourde, S. V. Ollinger, M. L. Smith, and B. E. McNeil
2008. A generalizable method for remote sensing of canopy nitrogen across a wide range of forest ecosystems. *Remote Sens. Environ.*, 112(9):3511–3519.

Martinuzzi, S., W. A. Gould, and O. M. Ramos González
2007. Creating Cloud-Free Landsat ETM+ Data Sets in Tropical Landscapes: Cloud and Cloud-Shadow Removal IITF-32. Technical report, U.S. Department of Agriculture, Forest Service, International Institute of Tropical Forestry, Rio Piedras, PR.

Masaitis, G., G. Mozgeris, and A. Augustaitis
2013. Spectral reflectance properties of healthy and stressed coniferous trees. *iForest - Biogeosciences and Forestry*, 6:30–36.

Mason, R. R.
1996. Dynamic behavior of Douglas-fir tussock moth populations in the pacific northwest. *For. Sci.*, 42(2):182–191.

Mathews, A. J. and J. L. Jensen
2013. Visualizing and quantifying vineyard canopy LAI using an unmanned aerial vehicle (UAV) collected high density structure from motion point cloud. *Remote Sens.*, 5(5):2164–2183.

McFadden, D.
1973. *Conditional logit analysis of qualitative choice behavior*. New York, USA: Academic Press.

McNeil, B. E., K. M. De Beurs, K. N. Eshleman, J. R. Foster, and P. A. Townsend
2007. Maintenance of ecosystem nitrogen limitation by ephemeral forest disturbance: An assessment using MODIS, Hyperion, and Landsat ETM+. *Geophys. Res. Lett.*, 34(19):1–5.

Meigs, G. W., R. E. Kennedy, and W. B. Cohen
2011. A Landsat time series approach to characterize bark beetle and defoliator impacts on tree mortality and surface fuels in conifer forests. *Remote Sens. Environ.*, 115(12):3707–3718.

Michez, A., H. Piégay, J. Lisein, H. Claessens, and P. Lejeune
2016. Classification of riparian forest species and health condition using multi-temporal and hyperspatial imagery from unmanned aerial system. *Environ. Monit. Assess.*, 188(3):1–19.

Miller, J. D. and A. E. Thode
2007. Quantifying burn severity in a heterogeneous landscape with a relative version of the delta Normalized Burn Ratio (dNBR). *Remote Sens. Environ.*, 109(1):66–80.

Miura, H. and S. Midorikawa
2013. Detection of Slope Failure Areas due to the 2004 Niigata-ken Chuetsu Earthquake Using High-Resolution Satellite Images and Digital Elevation Model. *J. JAEEJournal Japan Assoc. Earthq. Eng.*, 7(5):1–14.

Mohan, M., C. A. Silva, C. Klauberg, P. Jat, G. Catts, A. Cardil, A. T. Hudak, and M. Dia
2017. Individual tree detection from unmanned aerial vehicle (UAV) derived canopy height model in an open canopy mixed conifer forest. *Forests*, 8(9):1–17.

Moore, B. and G. Allard
2008. Climate change impacts on forest health: Forest health and biosecurity working papers FBS/34E. Technical report, U.S. Department of Agriculture, Forest Service, Forestry Department, Rome, Italy.

Morán-Ordóñez, A., J. V. Roces-Díaz, K. Otsu, A. Ameztegui, F. Lefevre, J. Retana, L. Coll, and L. Brotons
2018. The use of scenarios and models to evaluate the future of nature values and ecosystem services in Mediterranean forests. *Reg. Environ. Chang.*, 19(2):415–428.

Motohka, T., K. N. Nasahara, H. Oguma, and S. Tsuchida
2010. Applicability of Green-Red Vegetation Index for remote sensing of vegetation phenology. *Remote Sens.*, 2(10):2369–2387.

Muller, E. U., A. V. Kushlin, T. Linhares-Juvenal, D. Muchoney, S. Wertz-Kanounnikoff, and D. Henderson-Howat
2018. The state of the world's forests: forest pathways to sustainable development. Technical report, Food and Agriculture Organization of the United Nations, Rome, Italy.

Murtha, P. A.
1972. *A guide to air photo interpretation of forest damage in Canada*. Ottawa: Information Canada.

Nakajima, H.
2015. Defoliation by gypsy moths negatively affects the production of acorns by two Japanese oak species. *Trees - Struct. Funct.*, 29(5):1559–1566.

NASA
2019. *Landsat 8 Data Users Handbook V5.0*. National Aeronautics and Space Administration.

Näsi, R., E. Honkavaara, P. Lyytikäinen-Saarenmaa, M. Blomqvist, P. Litkey, T. Hakala, N. Viljanen, T. Kantola, T. Tanhuanpää, and M. Holopainen
2015. Using UAV-based photogrammetry and hyperspectral imaging for mapping bark beetle damage at tree-level. *Remote Sens.*, 7(11):15467–15493.

Netherer, S. and A. Schopf
2010. Potential effects of climate change on insect herbivores in European forests-General aspects and the pine processionary moth as specific example. *For. Ecol. Manage.*, 259(4):831–838.

Nevalainen, S., M. Lindgren, A. Pouttu, J. Heinonen, M. Hongisto, and S. Neuvonen
2010. Extensive tree health monitoring networks are useful in revealing the impacts of widespread biotic damage in boreal forests. *Environ. Monit. Assess.*, 168(1-4):159–171.

Noi, P. T. and M. Kappas
2018. Comparison of random forest, k-nearest neighbor, and support vector machine classifiers for land cover classification using sentinel-2 imagery. *Sensors*, 18(1).

Oberhuber, W., G. Thomaser, S. Mayr, and H. Bauer
1999. Radial growth of Norway spruce infected by Chrysomyxa rhododendri. *Phyt. - Ann. Rei Bot.*, 39(4):147–154.

Olsson, P. O., M. Heliasz, H. Jin, and L. Eklundh
2017. Mapping the reduction in gross primary productivity in subarctic birch forests due to insect outbreaks. *Biogeosciences*, 14(6):1703–1719.

O'Neill, G. A., A. Hamann, and T. Wang
2008. Accounting for population variation improves estimates of the impact of climate change on species' growth and distribution. *J. Appl. Ecol.*, 45(4):1040–1049.

Ortiz, S. M., J. Breidenbach, and G. Kändler
2013. Early detection of bark beetle green attack using terraSAR-X and rapideye data. *Remote Sens.*, 5(4):1912–1931.

Otsu, K., M. Pla, A. Duane, A. Cardil, and L. Brotons
2019. Estimating the Threshold of Detection on Tree Crown Defoliation Using Vegetation Indices from UAS Multispectral Imagery. *Drones*, 3(4).

Otsu, K., M. Pla, J. Vayreda, and L. Brotons
2018. Calibrating the severity of forest defoliation by pine processionary moth with landsat and UAV imagery. *Sensors*, 18(10):1–14.

Otsu, N.
1979. A Threshold Selection Method from Gray-Level Histograms. *IEEE Trans. Syst. Man. Cybern.*, 9(1):62–66.

Paine, T. D. and F. Lieutier
2016. *Insects and Diseases of Mediterranean Forest Systems*. Cham, Switzerland: Springer International Publishing.

Pajares, G.
2015. Overview and Current Status of Remote Sensing Applications Based on Unmanned Aerial Vehicles (UAVs). *Photogramm. Eng. Remote Sens.*, 81(4):281–330.

Paritsis, J., T. T. Veblen, and T. Kitzberger
2009. Assessing dendroecological methods to reconstruct defoliator outbreaks on Nothofagus pumilio in northwestern Patagonia, Argentina. *Can. J. For. Res.*, 39(9):1617–1629.

Parks, S. A., G. K. Dillon, and C. Miller
2014. A new metric for quantifying burn severity: The relativized burn ratio. *Remote Sens.*, 6(3):1827–1844.

Peltonen, M., A. M. Liebhold, O. N. Bjørnstad, and D. W. Williams
2002. Spatial synchrony in forest insect outbreaks: Roles of regional stochasticity and dispersal. *Ecology*, 83(11):3120–3129.

Pitman, R. M., E. I. Vanguelova, and S. E. Benham
2010. The effects of phytophagous insects on water and soil nutrient concentrations and fluxes through forest stands of the Level II monitoring network in the UK. *Sci. Total Environ.*, 409(1):169–181.

Pla, M., G. Bota, A. Duane, J. Balagu, A. Curc, and R. Guti
2019. Calibrating Sentinel-2 Imagery with Multispectral UAV Derived Information to Quantify Damages in Mediterranean Rice Crops Caused by Western Swamphen (Porphyrio porphyrio). *Drones*, 3(2):1–17.

Pla, M., A. Duane, and L. Brotons
2017. Potencial de las imágenes UAV como datos de verdad terreno para la clasificación de la severidad de quema de imágenes landsat: Aproximaciones a un producto útil para la gestión post incendio. *Rev. Teledetec.*, 2017(49 Special Issue):91–102.

Popa, I., O. Badea, and D. Silaghi
2017. Influence of climate on tree health evaluated by defoliation in the ICP level I network (Romania). *iForest - Biogeosciences For.*, 10:554–560.

Post, E.
2003. Population cycles: The case for trophic interactions. edited by alan berryman. *The Quarterly Review of Biology*, 78(4):483–484.

Puliti, S., L. T. Ene, T. Gobakken, and E. Næsset
2017. Use of partial-coverage UAV data in sampling for large scale forest inventories. *Remote Sens. Environ.*, 194:115–126.

Puliti, S., H. O. Ørka, T. Gobakken, and E. Næsset
2015. Inventory of small forest areas using an unmanned aerial system. *Remote Sens.*, 7(8):9632–9654.

Qian, Y., W. Zhou, J. Yan, W. Li, and L. Han
2015. Comparing machine learning classifiers for object-based land cover classification using very high resolution imagery. *Remote Sens.*, 7(1):153–168.

R Core Team
2016. *R: 3.2.4 for Windows*. R Foundation for Statistical Computing, Vienna, Austria.

Radeloff, V. C., D. J. Mladenoff, and M. S. Boyce
2000. Effects of interacting disturbances on landscape patterns: Budworm defoliation and salvage logging. *Ecol. Appl.*, 10(1):233–247.

Ramsfield, T. D., B. J. Bentz, M. Faccoli, H. Jactel, and E. G. Brockerhoff
2016. Forest health in a changing world: Effects of globalization and climate change on forest insect and pathogen impacts. *Forestry*, 89(3):245–252.

Resco De Dios, V., C. Fischer, and C. Colinas
2007. Climate change effects on mediterranean forests and preventive measures. *New For.*, 33(1):29–40.

Richter, R. and A. Müller
2005. De-shadowing of satellite/airborne imagery. *Int. J. Remote Sens.*, 26(15):3137–3148.

Riemann Hershey, R. and W. A. Befort
1995. Aerial photo guide to New England forest cover types NE-195. Technical report, U.S. Department of Agriculture, Forest Service, Northeastern Forest Experiment Station, Radnor, PA.

Robinet, C., P. Baier, J. Pennerstorfer, A. Schopf, and A. Roques
2007. Modelling the effects of climate change on the potential feeding activity of Thaumetopoea pityocampa (Den. & Schiff.) (Lep., Notodontidae) in France. *Glob. Ecol. Biogeogr.*, 16(4):460–471.

Robinet, C. and A. Roques
2010. Direct impacts of recent climate warming on insect populations. *Integr. Zool.*, 5(2):132–142.

Robinet, C., J. Rousselet, and A. Roques
2014. Potential spread of the pine processionary moth in France: Preliminary results from a simulation model and future challenges. *Ann. For. Sci.*, 71(2):149–160.

Rock, B. N., J. E. Vogelmann, D. L. Williams, A. F. Vogelmann, and T. Hoshizaki
1986. Remote Detection of Forest DamagePlant responses to stress may have spectral "signatures" that could be used to map, monitor, and measure forest damage. *Bioscience*, 36(7):439–445.

Roncat, A., F. Morsdorf, C. Briese, W. Wagner, and N. Pfeifer
2014. Laser Pulse Interaction with Forest Canopy: Geometric and Radiometric Issues. In *For. Appl. Airborne Laser Scanning Concepts Case Stud.*, M. Maltamo, E. Næsset, and J. Vauhkonen, eds., volume 27, chapter 2, Pp. 19–41. Dordrecht: Springer.

Roques, A.
2015. *Processionary moths and climate change: An update*. Cham, The Netherlands: Springer.

Rosenzweig, C., G. Casassa, D. Karoly, A. Imeson, C. Liu, A. Menzel, S. Rawlins, T. Root, B. Seguin, and P. Tryjanowski
2007. *Assessment of observed changes and responses in natural and managed systems*. Cambridge, UK: Cambridge University Press.

Rouse, J. W., R. H. Hass, J. Schell, and D. Deering
1973. Monitoring vegetation systems in the great plains with ERTS. *Third Earth Resour. Technol. Satell. Symp.*, 1:309–317.

Royle, D. D. and R. G. Lathrop
2002. Discriminating Tsuga canadensis Hemlock Forest Defoliation Using Remotely Sensed Change Detection. *J. Nematol.*, 34(3):213–221.

Rozendaal, D. M. and R. K. Kobe
2014. Competitive balance among tree species altered by forest tent caterpillar defoliation. *For. Ecol. Manage.*, 327:18–25.

Rullan-Silva, C., A. Olthoff, J. Delgado de la Mata, and J. Pajares-Alonso
2013. Remote Monitoring of Forest Insect Defoliation -A Review-. *For. Syst.*, 22(3):377.

Rullán-Silva, C., A. E. Olthoff, V. Pando, J. A. Pajares, and J. A. Delgado
2015. Remote monitoring of defoliation by the beech leaf-mining weevil Rhynchaenus fagi in northern Spain. *For. Ecol. Manage.*, 347:200–208.

Ryerson, D. E., T. W. Swetnam, and A. M. Lynch
2003. A tree-ring reconstruction of western spruce budworm outbreaks in the San Juan Mountains, Colorado, U.S.A. *Can. J. For. Res.*, 33(6):1010–1028.

Sangüesa-Barreda, G., J. J. Camarero, A. García-Martín, R. Hernández, and J. De la Riva
2014. Remote-sensing and tree-ring based characterization of forest defoliation and growth loss due to the Mediterranean pine processionary moth. *For. Ecol. Manage.*, 320:171–181.

Scanlon, T. M., S. M. Ingram, and A. L. Riscassi
2010. Terrestrial and in-stream influences on the spatial variability of nitrate in a forested headwater catchment. *J. Geophys. Res. Biogeosciences*, 115(G2).

Schläpfer, D., R. Richter, and T. Kellenberger
2012. Atmospheric and Topographic Correction of Photogrammetric Airborne Digital Scanner Data (Atcor-Ads). In *EuroSDR - EUROCOW*, P. 5, Barcelona, Spain.

Schuldt, A., M. Baruffol, M. Böhnke, H. Bruelheide, W. Härdtle, A. C. Lang, K. Nadrowski, G. von Oheimb, W. Voigt, H. Zhou, and T. Assmann
2010. Tree diversity promotes insect herbivory in subtropical forests of south-east China. *J. Ecol.*, 98(4):917–926.

Senf, C., R. Seidl, and P. Hostert
2017. Remote sensing of forest insect disturbances: Current state and future directions. *Int. J. Appl. Earth Obs. Geoinf.*, 60(February):49–60.

Shahtahmassebi, A., N. Yang, K. Wang, N. Moore, and Z. Shen
2013. Review of shadow detection and de-shadowing methods in remote sensing. *Chinese Geogr. Sci.*, 23(4):403–420.

Shahtahmassebi, A. R., K. Wang, Z. Shen, J. Deng, W. Zhu, N. Han, F. Lin, and N. Moore
2011. Evaluation on the two filling functions for the recovery of forest information in mountainous shadows on Landsat ETM + Image. *J. Mt. Sci.*, 8(3):414–426.

Sharov, A., A. Liebhold, and A. Roberts
1996. Spatial Variation Ainong Counts of Gypsy Moths (Lepidoptera: Lymantriidae) in Pheromone-Baited Traps at Expanding Population Fronts. *Environ. Entomol.*, 25(6):1312–1320.

Sikström, U., S. Jacobson, F. Pettersson, and J. Weslien
2011. Crown transparency, tree mortality and stem growth of Pinus sylvestris, and colonization of Tomicus piniperda after an outbreak of Gremmeniella abietina. *For. Ecol. Manage.*, 262(12):2108–2119.

Silva, C., N. Crookston, A. Hudak, and L. Vierling
2017. rLiDAR: LiDAR Data Processing and Visualization.

Simmons, M. J., T. D. Lee, M. J. Ducey, J. S. Elkinton, G. H. Boettner, and K. J. Dodds
2014. Effects of invasive winter moth defoliation on tree radial growth in Eastern Massachusetts, USA. *Insects*, 5(2):301–318.

Smigaj, M., R. Gaulton, S. L. Barr, and J. C. Suárez
2015. Uav-Borne Thermal Imaging for Forest Health Monitoring: Detection of Disease-Induced Canopy Temperature Increase. *ISPRS - Int. Arch. Photogramm. Remote Sens. Spat. Inf. Sci.*, XL-3/W3:349–354.

Solberg, S.
2010. Mapping gap fraction, LAI and defoliation using various ALS penetration variables. *Int. J. Remote Sens.*, 31(5):1227–1244.

Solberg, S., E. Næsset, K. H. Hanssen, and E. Christiansen
2006. Mapping defoliation during a severe insect attack on Scots pine using airborne laser scanning. *Remote Sens. Environ.*, 102(3-4):364–376.

Sperlich, M., T. Kattenborn, B. Koch, and G. Kattenborn
2014. Potential of Unmanned Aerial Vehicle Based Photogrammetric Point Clouds for Automatic Single Tree Detection. volume 24, Pp. 1–6, Hamburg, Germany. Proceedings of the joint meeting of DGfK, DGPF, GfGI and GiN.

Tamburini, G., L. Marini, K. Hellrigl, C. Salvadori, and A. Battisti
2013. Effects of climate and density-dependent factors on population dynamics of the pine processionary moth in the Southern Alps. *Clim. Change*, 121(4):701–712.

Tang, L. and G. Shao
2015. Drone remote sensing for forestry research and practices. *J. For. Res.*, 26(4):791–797.

Thayn, J. B.
2013. Using a remotely sensed optimized Disturbance Index to detect insect defoliation in the Apostle Islands, Wisconsin, USA. *Remote Sens. Environ.*, 136:210–217.

Thompson, D. J., C. Hassall, C. D. Lowe, and P. C. Watts
2011. Field estimates of reproductive success in a model insect: Behavioural surrogates are poor predictors of fitness. *Ecol. Lett.*, 14(9):905–913.

Tian, J., L. Wang, X. Li, H. Gong, C. Shi, R. Zhong, and X. Liu
2017. Comparison of UAV and WorldView-2 imagery for mapping leaf area index of mangrove forest. *Int. J. Appl. Earth Obs. Geoinf.*, 61(May):22–31.

Tiberi, R., M. Branco, M. Bracalini, F. Croci, and T. Panzavolta
2016. Cork oak pests: a review of insect damage and management. *Ann. For. Sci.*, 73(2):219–232.

Tobin, P. C. and S. L. Whitmire
2009. Spread of Gypsy Moth (Lepidoptera: Lymantriidae) and Its Relationship to Defoliation. *Environ. Entomol.*, 34(6):1448–1455.

Torres-Sánchez, J., F. López-Granados, and J. M. Peña
2015. An automatic object-based method for optimal thresholding in UAV images: Application for vegetation detection in herbaceous crops. *Comput. Electron. Agric.*, 114:43–52.

Torresan, C., A. Berton, F. Carotenuto, S. Filippo, D. Gennaro, B. Gioli, A. Matese, F. Miglietta, C. Vagnoli, A. Zaldei, and L. Wallace
2017. International Journal of Remote Sensing Forestry applications of UAVs in Europe: a review Forestry applications of UAVs in Europe: a review. *Int. J. Remote Sens.*, 38(June):8–10.

Townsend, P. A., A. Singh, J. R. Foster, N. J. Rehberg, C. C. Kingdon, K. N. Eshleman, and S. W. Seagle
2012. A general Landsat model to predict canopy defoliation in broadleaf deciduous forests. *Remote Sens. Environ.*, 119:255–265.

Van Der Sanden, J. J., A. Deschamps, S. J. Thomas, R. Landry, and R. J. Hall
2006. Using MERIS to assess insect defoliation in Canadian aspen forests. *Int. Geosci. Remote Sens. Symp.*, Pp. 4149–4152.

Vastaranta, M., T. Kantola, P. Lyytikäinen-Saarenmaa, M. Holopainen, V. Kankare, M. A. Wulder, J. Hyyppä, and H. Hyyppä
2013. Area-based mapping of defoliation of scots pine stands using airborne scanning LiDAR. *Remote Sens.*, 5(3):1220–1234.

Villemant, C. and M. C. Andreï-Ruiz
1999. Life-cycles and biological features of eggs predators of Lymantria dispar (Lepidoptera: Lymantriidae) in the Mamora cork oak forest, Morocco. *Eur. J. Entomol.*, 96(1):29–36.

Vogelmann, J. E.
1990. Comparison between two vegetation indices for measuring different types of forest damage in the north-eastern united states. *Int. J. Remote Sens.*, 11(12):2281–2297.

Vogelmann, J. E., B. Tolk, and Z. Zhu
2009. Monitoring forest changes in the southwestern United States using multitemporal Landsat data. *Remote Sens. Environ.*, 113(8):1739–1748.

Wallace, L., A. Lucieer, Z. Malenovsk, D. Turner, and P. Vopěnka
2016. Assessment of forest structure using two UAV techniques: A comparison of airborne laser scanning and structure from motion (SfM) point clouds. *Forests*, 7(3):1–16.

Walter, J. A., F. T. Finch, and D. M. Johnson
2016. Re-evaluating fall cankerworm management thresholds for urban and suburban forests. *Agric. For. Entomol.*, 18(2):145–150.

Wang, F., J. Huang, Y. Tang, and X. Wang
2007. New Vegetation Index and Its Application in Estimating Leaf Area Index of Rice. *Rice Sci.*, 14(3):195–203.

Wang, J., T. W. Sammis, V. P. Gutschick, M. Gebremichael, S. O. Dennis, R. E. Harrison, E. Sciences, and P. O. Box
2010. Review of Satellite Remote Sensing Use in Forest Health Studies. *Open Geogr. J.*, 3(1):28–42.

Weih, R. C. and N. D. Riggan
2010. Object-based classification vs. pixel-based classification: Comparitive importance of multi-resolution imagery. *Int. Arch. Photogramm. Remote Sens. Spat. Inf. S41*, XXXVIII:1–6.

Weiskittel, A. R. and D. A. Maguire
2007. Response of Douglas-fir leaf area index and litterfall dynamics to Swiss needle cast in north coastal Oregon, USA. *Ann. For. Sci.*, 64(2):121–132.

Whipple, A. V., N. S. Cobb, C. A. Gehring, S. Mopper, L. Flores-Rentería, and T. G. Whitham
2019. Long-term studies reveal differential responses to climate change for trees under soil- Or herbivore-related stress. *Front. Plant Sci.*, 10(February):1–14.

Whitehead, K. and C. H. Hugenholtz
2014. Remote sensing of the environment with small unmanned aircraft systems (UASs), part 1: a review of progress and challenges. *J. Unmanned Veh. Syst.*, 02(03):69–85.

Wingfield, M. J., E. G. Brockerhoff, B. D. Wingfield, and B. Slippers
2015. Planted forest health: The need for a global strategy. *Science*, 349(6250):832–836.

Wolter, P. T., P. A. Townsend, and B. R. Sturtevant
2009. Estimation of forest structural parameters using 5 and 10 meter SPOT-5 satellite data. *Remote Sens. Environ.*, 113(9):2019–2036.

Wulder, M. A., C. C. Dymond, J. C. White, D. G. Leckie, and A. L. Carroll
2006. Surveying mountain pine beetle damage of forests: A review of remote sensing opportunities. *For. Ecol. Manage.*, 221(1-3):27–41.

Wulder, M. A., J. G. Masek, W. B. Cohen, T. R. Loveland, and C. E. Woodcock
2012. Opening the archive: How free data has enabled the science and monitoring promise of Landsat. *Remote Sens. Environ.*, 122:2–10.

Xiao, Q. and E. G. McPherson
2005. Tree health mapping with multispectral remote sensing data at UC Davis, California. *Urban Ecosyst.*, 8(3-4):349–361.

Yoder, B. J. and R. H. Waring
1994. The normalized difference vegetation index of small Douglas-fir canopies with varying chlorophyll concentrations. *Remote Sens. Environ.*, 49(1):81–91.

Zhang, J., J. Hu, J. Lian, Z. Fan, X. Ouyang, and W. Ye
2016. Seeing the forest from drones: Testing the potential of lightweight drones as a tool for long-term forest monitoring. *Biol. Conserv.*, 198:60–69.

Zhen, Z., Y. Zhao, Y. Hao, and Q. Wei
2016. Development of accuracy assessment tool of individual tree crown delineation. *Int. Geosci. Remote Sens. Symp.*, 2016-Novem(26):3186–3189.

Zhu, C., X. Zhang, N. Zhang, M. A. Hassan, and L. Zhao
2018. Assessing the defoliation of pine forests in a long time-series and spatiotemporal prediction of the defoliation using Landsat data. *Remote Sens.*, 10(3).